LBL-12626

Lawrence Berkeley Laboratory
UNIVERSITY OF CALIFORNIA

Materials & Molecular Research Division

MULTIPHOTON DISSOCIATION AND THERMAL UNIMOLECULAR REACTIONS INDUCED BY INFRARED LASERS

Hai-Lung Dai
(Ph.D. thesis)

MASTER

April 1981

Prepared for the U.S. Department of Energy under Contract W-7405-ENG-48

DISTRIBUTION OF THIS DOCUMENT IS UNLIMITED

MULTIPHOTON DISSOCIATION AND THERMAL UNIMOLECULAR REACTIONS INDUCED BY INFRARED LASERS

Hai-Lung Dai

Abstract

Multiphoton dissociation (MPD) of ethyl chloride was studied using a tunable 3.3 μm laser to excite CH stretches. The absorbed energy increases almost linearly with fluence, while for 10 μm excitation there is substantial saturation. Much higher dissociation yields were observed for 3.3 μm excitation than for 10 μm excitation, reflecting bottlenecking in the discrete region of 10 μm excitation. Resonances in MPD yields vs frequency in the 3.3 μm region match the position and shape of peaks in the fundamental, as narrow as 0.4 cm^{-1}, and first and second overtone absorption spectra. Transitions through the discrete levels are all at or nearly resonant. Anharmonicity is compensated by the presence of five CH stretch modes. Overtone spectra show that line broadening already occurs at the $v_{CH} = 2$ level and that $v_{CH} = 3$ is clearly in the quasi-continuum. The resonant nature of the excitation allows the rate equations description for transitions in the quasicontinuum and continuum to be extended to the discrete levels. Absorption cross sections are estimated from ordinary ir spectra. A set of cross sections which is constant or slowly decreasing with increasing vibrational excitation gives good fits to both absorption and dissociation yield data. When the strong collision assumption is made for vibrational quenching and RRKM dissociation rates are used, the calculated excitation distribution gives a pressure dependence of dissociation similar to the experiments.

The rate equations model was also used to quantitatively calculate the pressure dependence of the MPD yield of SF_6 caused by vibrational self-quenching. Between 1000-3000 cm^{-1} of energy is removed from SF_6 excited to $\gtrsim$60 kcal/mole by collision with a cold SF_6 molecule at gas kinetic rate. Calculation showed the fluence dependence of dissociation varies strongly with the gas pressure.

Infrared multiphoton excitation was applied to study thermal unimolecular reactions. With SiF_4 as absorbing gas for the CO_2 laser pulse, transient high temperature pulses were generated in a gas mixture. IR fluorescence from the medium reflected the decay of the temperature. C_2H_5Cl which has known Arrhenius parameters for its dissociation was used as an internal standard. From the ratio of the dissociation of the reactant and that of C_2H_5Cl, the activation energy and the preexponential factor of the reactant dissociation were obtained from a phenomenological model calculation. The rate constant of the overall dissociation of CCl_3CH_3 is $k = 10^{13.0 \pm 0.3} \exp(-49{,}000 \pm 2000/RT)$. For $CHCl_2CH_2Cl$ dissociation, the rate constants for the molecular elimination reactions producing trans- and cis-$C_2H_2Cl_2$ are $k_{trans} = 10^{13.6 \pm 0.4} \exp(-57{,}000 \pm 2000/RT)$ and $k_{cis} = 10^{14.0 \pm 0.4} \exp(-60{,}000 \pm 2000/RT)$. CCl_2CH_2 is produced from molecular elimination, radical reactions and even surface reactions. The rate constant for the production of C_2H_3Cl is very close to that for C-Cl bond fission.

學而不思則罔
思而不學則殆

論語

Learning without thought is vain.

Thought without learning is perilous.

- The Analects of Confucius

Dedicated to

my grandparents and parents

ACKNOWLEDGMENTS

It is not a common practice for the more timid Chinese to write a section to acknowledge the people they appreciate and respect. However, my experiences in the past several years in Berkeley have led me to do this with full heartedness.

I was very fortunate to have Professor C. Bradley Moore as my research director. I have learned a great deal from him, especially the attitude of pursuing both perfection and complete understanding of scientific research, and I have benefited and been inspired by his many suggestions and ideas. In addition to the many conferences together planning and interpreting experiments, he also spent lengthy hours patiently correcting my English composition. I also enjoyed his friendship and concern toward his students.

Dr. Andy Kung has provided valuable assistance especially during my early less-confident years as a graduate student. He constructed the optical parametric oscillator and participated in the 3.3 μm multiphoton dissociation work. Much of my practical knowledge in lasers was gained through working and discussion with Andy.

I enjoyed working with a talented group of fellow students - graduate and undergraduate, past and present. Jim Wong helped me greatly in using the microcomputer and in the intracavity dye laser optoacoustic spectroscopy of high vibrational overtones, though the later work was not included in this thesis. Mike Berman set up the CO_2 laser and provided helpful assistance in the sensitized laser

pyrolysis work. I also thank Linda Young for helping me gather and prepare experimental equipment on many occasions, Pauline Ho for her interest in efficient GC performance, and Wes Natzle for many interesting discussions on intramolecular vibrational relaxation. In addition, they and many other group members have helped me overcome many linguistic difficulties. I appreciate Jackie Denney for her endeavors in keeping the group in a warm and pleasant atmosphere and fighting some inevitable (?) bureaucratic procedures.

I thank Peter Schulz for providing the original computer program for the rate equations calculation and many useful discussions on the program. Suggestions and criticisms of Professors Y. T. Lee and Y. R. Shen are gratefully acknowledged.

Ann Weightman's skillful and efficient typing of this thesis and her patient cooperation during the process are gratefully appreciated.

I am grateful to the University of California for predoctoral fellowships. This work was supported by the Division of Advanced Systems Materials Production, Office of Advanced Isotope Separation, U.S. Department of Energy under Contract No. W-7405-ENG-48.

I would like to take this opportunity to thank my undergraduate advisor, Professor K. C. Lin, at Taiwan University. If not for his guidance, I may not have studied in Berkeley. Finally, I want to thank my wife for bearing to be a graduate student's wife while being a graduate student herself.

Table of Contents

Chapter		Page
I.	INTRODUCTION TO IR MULTIPHOTON DISSOCIATION	1
II.	IR MULTIPHOTON DISSOCIATION AT 3.3 μm	9
	A. HCl Elimination Reaction of Chlorinated Hydrocarbons	9
	B. Experimental	14
	1. Nd:YAG Laser	14
	2. $LiNbO_3$ Optical Parametric Oscillator	14
	3. CO_2 Laser	23
	4. Photolysis and Absorption Measurements	23
	5. Data Analysis	29
	C. Results	32
	D. Vibrational Spectroscopy	53
	E. Excitation Mechanism	64
	F. A Rate Equations Model for MPD	71
	1. The Model	71
	2. Evaluation of Parameters	76
	G. Absorption Cross Section and Excitation Distribution	81
	H. 3.3 μm vs 10 μm Excitation	94
	I. Collisional Deactivation	98
	J. Concluding Remarks	102

Chapter Page

III. RATE EQUATIONS ANALYSIS OF VIBRATIONAL SELF-QUENCHING IN IR MULTIPHOTON DISSOCIATION OF SF_6 109

A. Introduction 109

B. The Model and the Determination of Parameters 114

C. Results and Discussion 119

D. Conclusion 133

IV. DETERMINATION OF THE ARRHENIUS PARAMETERS FOR UNIMOLECULAR REACTIONS BY SENSITIZED LASER PYROLYSIS 134

A. Introduction 134

B. Experimental 138

1. Pyrolysis 138

2. IR Fluorescence 143

3. Determination of the Irradiation Volume and the Product Yield 145

C. The Model Calculation 148

D. Results and Discussion 151

1. Pyrolysis 151

2. IR Fluorescence 165

3. Model Calculation and the Extraction of E_a and A 176

4. 1,1,1-Trichloroethane Dissociation 187

5. 1,1,2-Trichloroethane Dissociation 190

E. Concluding Remarks 202

CHAPTER I. INTRODUCTION TO IR MULTIPHOTON DISSOCIATION

It would not be too much an exaggeration to say that infrared multiphoton dissociation (IRMPD) is the most well studied phenomenon in chemical physics during the 70's. However, when it was first suggested that a polyatomic molecule in an intense infrared field might absorb tens of photons to account for the observed luminescence from photofragments,[1] the response from scientific field was far from enthusiastic. It was laser isotope separation[2] that later revived peoples' interests and rapidly many experimentalists and theoreticians joined the efforts to reveal the secrets and to exploit the usefulness of IRMPD.

To a student of interaction between light and molecules, the first question is naturally "how can a molecule absorb so many ir photons within a short and intense laser pulse."

The average energy content of an harmonic oscillator in resonance with a 100 ns laser pulse ($h\nu$) can easily exceed 100 $h\nu$ if the Rabi frequency of the electric dipole transition, $\omega_R = \mu \cdot F/\hbar$, is 0.1 cm^{-1}.[3] For an oscillator with oscillator strength similar to the ν_3 mode of SF_6 it requires only a laser fluence of 0.01 J/cm^2 to achieve such an excitation. However, in a molecule, the laser pulse in resonance with the 0→1 transition of a vibrational mode will be out of resonance with the 1→2 transition by the amount of vibrational anharmonicity. The effect of anharmonicity on the transition probability may be easily appreciated from the strong interaction limit of perturbation theory,

in which $P=2^{-1}(\omega_R^2/(\Delta\omega^2+\omega_R^2))$ for a two-level system.[4] $\Delta\omega$ is the off-resonance. The anharmonicity of the SF_6 ν_3 mode is 2.9 cm^{-1}. So even at intensities (~10 MW/cm^2) for which $\omega_R \sim 1$ cm^{-1} the probability of reaching v=30 will be as small as 10^{-60} for a laser tuned to 0→1 resonance. In some early experiments MPD of SF_6 was observed at intensities as low as 30 kW/cm^2.[5] At 500 MW/cm^2 a dissociation yield near 100% was reported.[6] SF_6 needs more than 30 CO_2 laser photons for dissociation. Apparently some factors that may overcome the off-resonance effect by anharmonicity were overlooked in the simple discussion above.

Among the many excitation mechanisms that were suggested, the most important one is the concept of "quasicontinuum" brought up by Bloembergen.[3] He suggested that after the molecule absorbs the first several photons, the next transitions will be in an energy range where the large vibrational level density (~1000 level/cm^{-1} at 5000 cm^{-1} for SF_6) and the interaction among the levels considerably broaden the transition lines so that at every step a transition can be on resonance with the laser. Due to anharmonicity, the center of the broadened absorption may shift to the red as the molecule absorbs more photons. Intramolecular energy transfer among vibrational modes occurs on a time scale faster than the optical pumping rate so that there is no coherence induced by the strong laser field. The transitions may be described by a set of rate equations and the excitation rate will depend on laser fluence rather than on intensity.[7]

The molecule may reach the quasicontinuum (QC) by simultaneously absorbing several CO_2 laser photons. It was calculated that at a properly detuned frequency $(\omega_{0\to1}-\omega_R)$ through such a n-photon absorption the

probability of reaching v=3 is unity at 1 GW/cm^2.[3] The vibrational levels below the QC are sharp and discrete. Therefore transitions in this regime will be coherent and isotope selective. The excitation rate would depend strongly on intensity. Furthermore, these transitions may be resonantly enhanced by a sequence of rotational transitions[8] and by anharmonic splitting of degenerate levels.[9] A most recent study showed that such a resonant scheme exists for SF_6 up to v=6.[10] Power broadening of the discrete level transitions would include more rotational states in resonance with the laser.

There is abundant experimental evidence indirectly supporting the above picture for IRMPD. Typical MPD spectra at 10 μm region are red-shifted from the fundamental reflecting both the shifts of the QC absorption and the preference of discrete level excitation at P and Q branches and at frequencies for n-photon absorption. The smeared and broadened structure of MPD spectra then indicates the effect of power broadening and of the complicate excitation schemes in the discrete region.[11] The resemblance between the small signal spectra at high temperature and MPD spectra[12] as well as the observation of dissociation of ions with excess internal energy by a cw CO_2 laser in an ion cyclotron[13] further strengthen the argument for the QC absorption. MPD with two CO_2 laser frequencies, one tuned for discrete level excitation at medium intensity to avoid too large a power broadening and the other at lower frequency with larger fluence meant for QC absorption, showed that the change of isotope selectivity and dissociation yield when tuning the two frequencies can be explained by this two-region excitation scheme.[14] While there were

attempts to accurately calculate the excitation rate and spectra in the discrete region of SF_6,[15] the characterization of the QC remains a difficult task. The intramolecular vibrational relaxation rate for SF_6 at ~5000 cm^{-1} was measured to be faster than 30 ps,[16] which corresponds to a linewidth of >0.9 cm^{-1}. Broadened linewidths were also reported for high CH stretching overtones of many polyatomic molecules in optoacoustic spectroscopy.[17,18] The dependence of excitation on fluence rather than on intensity in the QC was verified by using various length laser pulses.[6]

In addition to the excitation mechanism of IRMPD, there are many other important questions and issues that have been intensively studied and need further exploration. Some of them are listed as following.

1. Molecular Dynamics of Excitation and Dissociation

The origin of the observed visible fluorescence in MPD remained as one of the unsolved mysteries. Is it the result of "inverse electronic relaxation", the fluorescence of photofragments, or something else?[19,20] MPD product energy distribution poses another interesting question. Several laser induced fluorescence experiments showed that each of the internal degrees of freedom of dissociation products can usually be described by a certain temperature, yet these temperatures differ from each other.[21]

Probably the most important issue regarding molecular dynamics is whether nonstatistical unimolecular reaction can be induced by multiphoton excitation (MPE). It was argued that a short enough laser pulse may

excite certain vibrational modes with a rate faster than the relaxation rate; unimolecular reactions can then be mode-selective.[22] Although such a short ir pulse laser was never constructed, many experiments with CO_2 TEA lasers prompted early claims of nonstatistical dissociation. It was later shown that these results were either due to secondary MPD of products or due to lack of knowledge of the excitation distribution.[20,77,78] The statistical RRKM theory agreed well with the molecular beam measurement of MPD product translational energy distribution[23] and the relationship between the dissociation yield and the absorbed energy.[24]

2. Characterization of the Quasicontinuum

The QC may be defined as an energy range in which the molecular linewidth, $\Delta\omega_{mol.}$, is much greater than the optical transition rate and this rate is in turn much larger than the inverse level densities.[25] $\Delta\omega_{mol.} >> \omega_R >> \rho^{-1}_{vib.}$. Therefore the rigorous Schroedinger equation describing the excitation can be reduced to a set of rate equations.[26] Notably the energy range that satisfies these conditions varies with molecular properties as well as laser intensities.[27] Molecular properties vary drastically from molecule to molecule. While the linewidth of the CH stretching overtone of benzene may be as high as 100 cm^{-1} at 16000 cm^{-1}, C_2H_2 shows $\Delta\omega_{mol.}$ smaller than Doppler width.[28] For each individual molecule, where the QC starts and how to qualitatively describe the transition from the discrete region to the QC are still unclear. Although these questions are not necessarily resolvable by direct MPD experiments, the studies of collisionless MPD of smaller molecules may aid our

understanding of intramolecular vibrational relaxation. The magnitude and the trend of absorption cross section, the width of optical resonances, and the intramolecular vibrational relaxation rate are of great importance for the characterization of the QC.

3. The Excitation Distribution

It is essential to know the excitation distribution during and after the laser pulse if IRMPD is to have greater applications in kinetic studies. A thermal distribution was suggested to be a good approximation.[7] The distribution calculated by rate equations may be closer to reality.[23] Yet in order to make these calculations at all significant, knowledge of the absorption cross sections, both in the QC and in the discrete region, is indispensable.

4. The Effects of Collisions

MPE requires no collisions. Collisionless MPD has been demonstrated in molecular beams.[29] However, collisions are difficult to eliminate in many studies and applications of MPD. Some studies showed that collisions may aid in the excitation of small molecules to the QC through vibration-vibration up-pumping.[30] Collision-induced rotational relaxation may put more molecules in resonance with the laser during the pulse and therefore increase the yield.[31] Collisional deactivation is a very important process in MPD. The magnitude of energy loss and the rate of deactivation for highly vibrationally excited molecules, especially their dependence on energy content and collision partner, need further exploration.

The majority of the MPD experiments and theoretical works are done for SF_6 under 10 μm radiation. Imagining the variety of molecular structure and properties and of excitation sources, there might be abundant different MPD phenomena to be explored.

Only recently have laser sources other than CO_2 laser been used for MPD. Formic acid[32] and methanol[33] have been dissociated by HF lasers and cyclopropane[34] by an optical parametric oscillator pumping CH stretching modes. These cases provide a qualitatively different situation from that of SF_6 dissociated by CO_2 lasers. The anharmonicity of the hydrogen stretches is too large to be significantly compensated by the mechanisms operative in SF_6. The photon energy is a much larger fraction of the dissociation energy and fewer photons are needed to reach the QC. How does MPD occur in these cases? Can the established models for SF_6 10 μm MPD be used to describe these MPD results?

The much smaller number of higher frequency photons required for dissociation is a great advantage for quantitative modelling of the MPD processes. Furthermore, due to the relative isolation of CH stretching modes from the rest of the modes all at lower frequency, unimolecular reactions involving CH bond rupture induced by exciting the CH stretching modes constitute a test example for "mode-selective" chemistry. Chapter II contains a detailed report of the results of MPD and MPE experiments at 3.3 μm. The unimolecular reaction studied is HCl elimination from chlorinated hydrocarbons. A model was established to account for all the MPD and MPE observations.

The fact that MPD by CO_2 laser is a statistical process makes it a useful tool to identify the lowest activation energy channel of homogeneous gas phase unimolecular reactions. To avoid ambiguity caused by not knowing the exact excitation distribution, IRMPE can be used simply as a heating method. Inert absorbing gas can be added to the unimolecular reactant, which does not absorb laser pulse, and collisional energy transfer heats up the reactant.[35,36] Chapter IV describes an attempt to extract activation energy and preexponential factor of unimolecular reaction from pyrolysis induced by IRMPE heating. IRMPD also has great potential in other kinetic studies. It has been used as a way to generate radicals for radical reaction rate measurements.[37]

Isotope separation has been one of the most important applications of IRMPD. Enrichments of about a dozen elements have been achieved. The most impressive one is the separation of deuterium where the enrichment factor is as large as 10^4.[38] A pilot plant is in operation for ^{13}C separation by CF_3X (X=Br, I) MPD.[39] Recently enrichment of U isotopes was reported.[40] To achieve more efficient separation, better understanding of the many previously stated questions is required.

CHAPTER II. IR MULTIPHOTON DISSOCIATION AT 3.3 μm

A. HCl Elimination Reaction of Chlorinated Hydrocarbons

There are two major reasons for choosing the molecular elimination reactions of halogenated hydrocarbons for MPD studies at 3.3 μm; their low activation energies require a relatively small number of photons for reactions to occur and the dissociation involves rupture of the CH bonds.

$C_2H_5Cl \rightarrow HCl + C_2H_4$ (ΔH = 16 kcal/mole) is probably the most thoroughly studied reaction for halogenated hydrocarbons.[41,42] From many static pyrolysis, shock tube, and chemical activation studies, the dissociation of ethyl chloride (EtCl) was shown to be a homogenous molecular elimination process. Its activation energy in the high pressure limit was determined to be 57.4 ± 1.0 kcal/mole and the preexponential factor to be $10^{13.8\pm0.2}$ sec^{-1}.

It is now widely accepted that the relatively low activation energy comparing with the bond dissociation energies, is due to a 4-centered activated complex,[42]

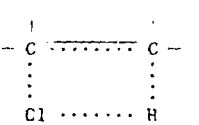

The simultaneous formation of the H-Cl and C=C bonds at the time of the rupture of the C-Cl and C-H bonds stabilizes the potential energy of the activated complex.

The most detailed calculation with the RRKM theory on the rate constant of EtCl dissociation was done by Setser and coworkers.[43] Several different models for the activated complex were used for the

tests of the rate constants measured both by thermal pyrolysis and chemical activation, the fall-off pressure, and the isotope effect (D vs H) for the rate constant. The most successful model depicts the activated complex as a 4-centered ring with asymmetric bond orders for C-H and C-Cl bonds. The internal rotation was treated as a torsional motion, therefore the reaction path degeneracy was set as 2, and the overall rotations were treated as being inactive. A 50 cm^{-1} ring distortion motion was taken as the reaction coordinate. The characteristics of the activated complex are listed in Table II-1.

Figure II-1 shows the RRKM rate constant for EtCl calculated with the above activated complex. In these calculations, the experimental value of 58 kcal/mole was taken for the activation energy in the high pressure limit; this gave the value 56.5 kcal/mole for the reaction barrier height. The calculation was done with a computer program by Hase and Bunker.[44] In the program, the vibrational level densities were calculated using the Whitten-Rabinovitch approximation.[42]

Table II.1. Models for ethyl chloride and its activated complex in RRKM calculation.[a]

Molecule[b]		Complex[c]	
Frequencies (cm^{-1})	Moment of inertia (amu $Å^2$)	Frequencies (cm^{-1})	Moment of inertia (amu $Å^2$)
3014			
2986	16.13	3054(4)[d]	18.77
2967	92.22	1393(2)	75.55
2946	102.00	1117	87.51
2887		987(4)	
1470		920	
1448(2)		890(2)	
1385		854	
1289		576	
1251		400	
1081			
1036			
974			
785			
677			
336			
250			

a. Critical energy is 56.5 kcal/mole. Reaction-path degeneracy is set as 2.
b. Taken from Ref. 45.
c. Taken from Ref. 43.
d. Numbers in the parentheses indicate numbers of vibrational modes at that frequency.

Fig. II-1. Unimolecular dissociation rate constant of ethyl chloride calculated by RRKM theory as a function of vibrational energy in excess of the dissociation barrier height.

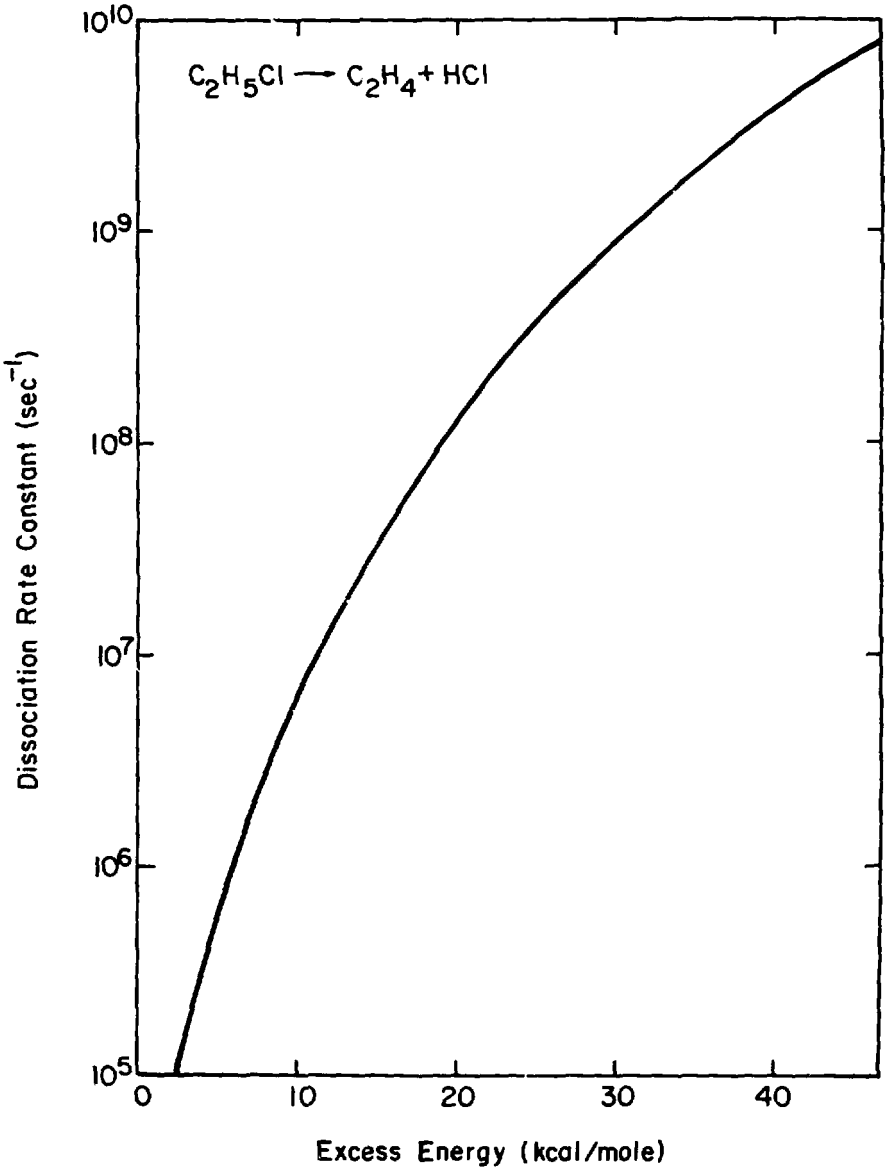
$C_2H_5Cl \longrightarrow C_2H_4 + HCl$
10^{10}
10^9
10^8
10^7
10^6
10^5
Dissociation Rate Constant (sec^{-1})
0
10
20
30
40
Excess Energy (kcal/mole)

Fig. II-1

B. Experimental

1. Nd:YAG Laser

An angle phase-matched tunable $LiNbO_3$ optical parametric oscillator (OPO) pumped by a Raytheon model SS404 Nd:YAG oscillator-amplifier system was used as a 3.3 μm laser source. The Nd:YAG laser contains a master oscillator, 3 amplifiers, and 2 Faraday rotators each placed after the 2nd and 3rd amplifiers. The pair of Faraday rotators are to prevent self-oscillation among the amplifiers and to eliminate beams specularly reflected from outside the system. A more detailed description of the construction and the elements of the laser can be found in Ref. 46. The Q-switched pulse from the flashlamp-pumped master oscillator of 5 mJ can usually be amplified up to more than 200 mJ after the 3rd amplifier. The maximum output of 1.064 μm is about 300 mJ. A fused silica lens with 2 m focal length is placed between the oscillator and the first amplifier to produce a collimated beam at the output. The horizontally polarized output beam has a diameter (FWHM) of 4 mm in cross section and a divergence of 1 mrad. Its radial profile is nearly Gaussian. The bandwidth (FWHM) is ~0.4 cm^{-1} with an etalon placed in the oscillator. The pulse duration is about 15 ns (FWHM) as examined by a Si photodiode.

2. $LiNbO_3$ Optical Parametric Oscillator

Optical parametric oscillation has long been recognized as an important source for visible and infrared tunable coherent radiation

because of its tunability, high conversion efficiency and low pump threshold. Its theory and working principles can be found in several review articles.[47,48] For 3.3 μm radiation generation the best pump-OPO combination at present is the Nd:YAG laser pumped $LiNbO_3$ OPO, from which 1.4 to 4.0 μm radiation can be obtained.

The design of the OPO built in this laboratory follows closely that given by Byer and Herbst.[48] It consists of an L-shaped cavity as shown in Fig. II-2. On the input is a 45° incidence mirror dielectric coated for high reflection centered at 1.7 μm and high transmission (>85%) at 1.06 μm for the horizontal polarization. A CaF_2 flat substrate coated for high reflection at 1.06 μm and 30% reflection from 1.4 μm to 2.0 μm is used as the output coupler. A Bausch and Lomb grating of 300 l/mm and blazed at 1.8 μm completes the optics of the OPO. The $LiNbO_3$ crystal is cut for phase-matching at 47° vs the optical axis, and is 1.5 cm in diameter and 5 cm long. It is polished and antireflection coated with SiO_2 at both end surfaces. Since the crystal cross section is large enough, angle variation rather than temperature variation is used for phase matching of the desired frequency. Tuning is achieved by rotating the grating angle and the phase matching angle simultaneously. The distance between beamsplitter and output mirror is about 12 cm and between beamsplitter and grating 6 cm. A CaF_2 plate high-reflection coated for 1.06 μm and antireflection coated for the signal and idler was placed in front of the output coupler to reflect the 1.06 μm back through the crystal to aid the oscillation. The 1.06

Fig. II-2. Schematic of the 1.06 μm pumped, angle tuned $LiNbO_3$ singly resonant parametric oscillator.

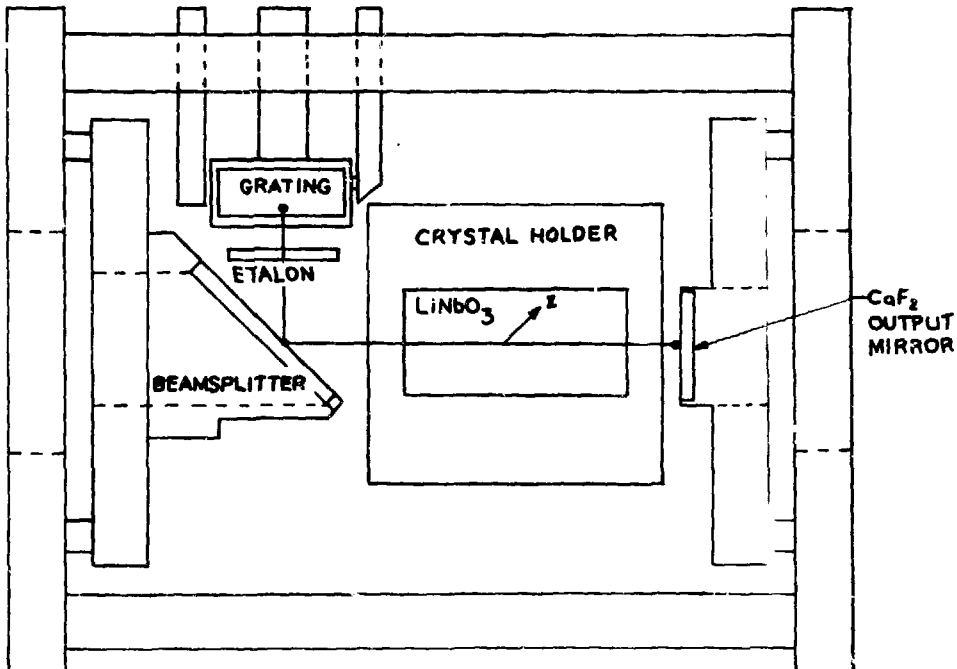
GRATING
ETALON
CRYSTAL HOLDER
LiNbO3
z
BEAMSPLITTER
CaF2
OUTPUT
MIRROR

Fig. 11-2

μm pulse makes a double pass through the crystal for parametric generation.

The alignment of the OPO is done as follows.

1. The optical elements of the OPO are centered against the green second harmonic of the Nd:YAG pulses. The second harmonic is generated by a KDP crystal placed between the Nd:YAG laser and the OPO.
2. The reflection of the green light off the output mirror (O/P) is used to crudely align the O/P normal to the 1.06 μm beam.
3. Precise alignment of the O/P is achieved by obtaining the 1.06 μm lasing between the rear reflection mirror of the Nd:YAG master oscillator and the O/P. In obtaining the lasing, all the amplifiers, except the master oscillator, of the Nd:YAG laser are pumped by flashlamps at full capacity.
4. A He-Ne laser was set in front of the O/P and the red beam was aligned normal to the O/P. By rotating the grating in its own plane, the reflection of the He-Ne from the grating at different orders was set on a straight line crossing with the He-Ne. Then the 3rd order He-Ne reflection was centered in coincidence with the beam.
5. The OPO was then pumped with 1.06 μm pulses. The crystal angle was rotated to obtain the 1.9 μm signal and the 2.4 μm idler beams.

The OPO is generally operated at several times above threshold. The threshold intensity was experimentally observed (limited by the pulse energy detection sensitivity) to be around 40 MW/cm^2, in rough agreement with the calculated value. The energy conversion efficiency is about 20% when the pump pulse energy is 180-200 mJ. The OPO output pulse energy, determined by a factory calibrated Scientech model 3600-01 surface absorbing thermopile, was typically 30-40 mJ total (signal plus idler). After filtering the unwanted wavelength with an AR coated Ge flat, up to 7 mJ at 3.3 μm was available for experiments. The OPO pulse energy can be adjusted by varying the energy of the 1.06 μm beam and quartz flats can be used for attenuating the 3.3 μm energy. The temporal pulse shape was measured using a PEM InSb detector and a Tektronix 7704 oscilloscope. The system response time was <3 ns. The OPO pulse rose in ~8 ns, and fell less rapidly. The FWHM was 10 ns and time between 5% points was 20 ns. Pulse-to-pulse intensity variation was ±15%. Long-term energy stability was usually better than 10%. The output bandwidth of the grating-tuned OPO was 2-3 cm^{-1}. There were 6 distinct peaks with a peak-to-valley ratio of 1.8 separated by 0.6 cm^{-1}, Fig. II-3(a), due to the 30 sec wedged output coupler functioning as a low finesse etalon at 3.3 μm. The breadth of the OPO pulse may be caused by 1). The small laser spot covers only a small number of grating lines; 2). There is a thermal gradient in the crystal; 3). The laser spot size is large enough for the phase matching condition to be satisfied for a wide frequency range. The broad bandwidth was narrowed to 0.15 ± 0.03 cm^{-1} (Fig. II-3(b)) with a 20-30% loss in energy by a

1 mm thick quartz etalon (finesse, free spectral range/HWHM, of 7). Tilting the etalon alone allowed tuning over at least 1.5 cm^{-1}.

The OPO beam, which has a diameter of 5 mm and a divergence of about 10 mrad, was directed into a 3/4 m Spex monochromator for frequency measurements. The monochromator, with ~2 μm entrance and 5 μm exit slits, had a 0.1 cm^{-1} resolution and a 0.2 cm^{-1} resettability. The single Spex itself was calibrated by the reflection of a Spectra-Physics He-Ne laser off the grating at different orders. The frequency stability for the OPO without etalon was ±1 cm^{-1} only after a 15-30 min wait for thermal stabilization of the crystal. The frequency drift is believed to be caused by the combined effects of mechanical vibrations and laser heating of the $LiNbO_3$ crystal. With the grating and etalon, the frequency is stable to within ±0.08 cm^{-1} over an extended period of time (longer than the duration for photolysis). Damage to coatings and crystal surfaces occurs. While the exact cause of damage has not been determined, it is possibly due to occasional excessive laser intensity and/or dust or defective spots on the coating. Damages occur more often on the exit surface of the crystal than on the input surface. This problem of surface damage is mitigated by translating the damaged element to a clear aperture. Over the course of this experiment, two crystals were changed and repolished due to damage. At the operating level for photolysis in these experiments (nominally 100 MW/cm^2 at 1.06 μm) we estimate one damage spot is incurred for every 10 operating hours. If use of the OPO at 70% or less of the

Fig. II-3. Frequency distribution of the output of the optical parametric oscillator at 3.3 μm. a) Broadband pulse with gating only in the cavity. b) Narrow band pulse with both grating and etalon in the cavity.

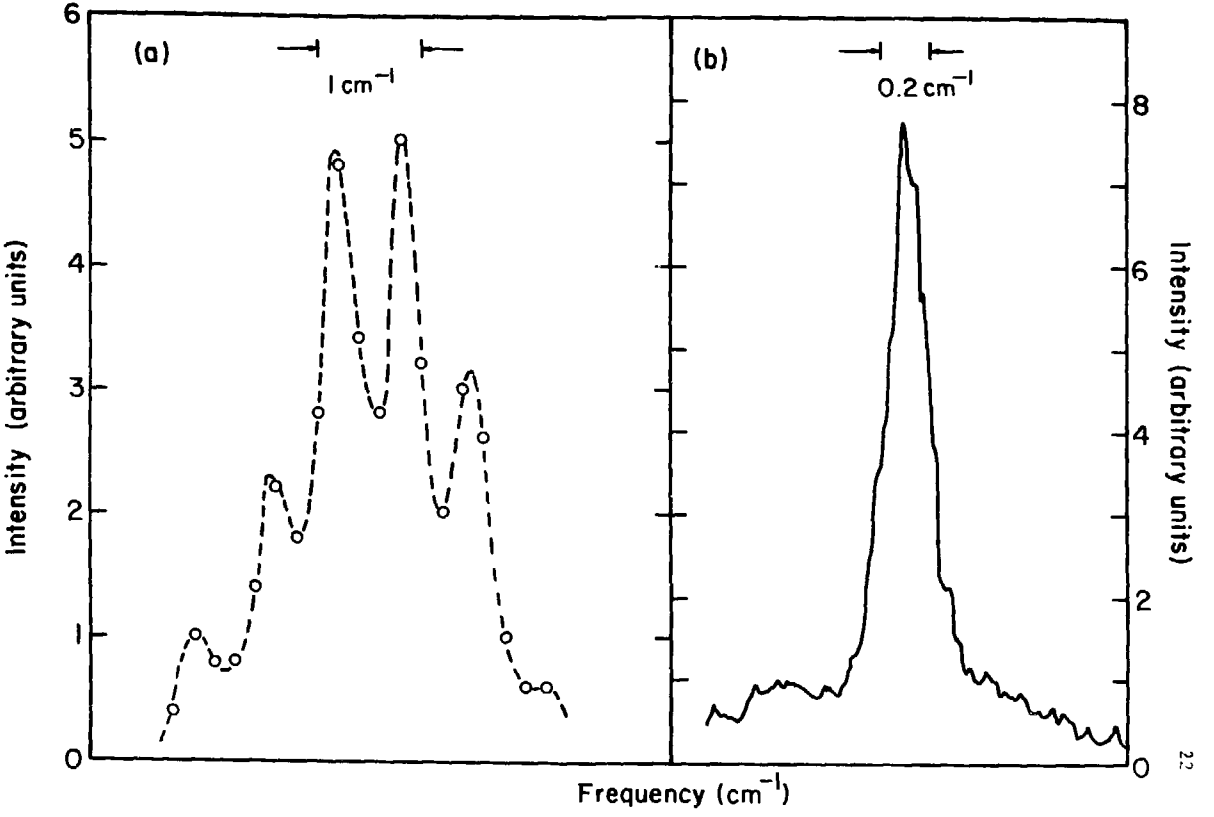
(a)
1 cm⁻¹
(b)
0.2 cm⁻¹
Intensity (arbitrary units)
Intensity (arbitrary units)
Frequency (cm⁻¹)
0
1
2
3
4
5
6
0
2
4
6
8

Fig. II-3

powers described can be tolerated, then damage-free operation should be possible.

3. CO_2 Laser

For 10 μm excitation, a grating-tuned Tachisto model 215 CO_2 transversely excited atmosphere (TEA) laser was used. The total multi-transverse mode output was typically 0.5 J. A 70 ns FWHM spike contained 0.2 J and 0.4 J were emitted in the first 600 ns. The total pulse duration was 1.3 μs. A detailed description of the design and the operation of the laser and the measurement of its output pulses can be found in Ref. 49.

4. Photolysis and Absorption Measurements

Ethyl chloride (Matheson Gas, Grade R) was purified by fractional distillation. Its purity was determined by gas chromatograph (GC) to be >99.9%; no ethylene was detected (<10 ppm C_2H_4). Gas pressure was measured by a calibrated variable-reluctance manometer (Validyne) with a 50 Torr range. The EtCl pressure ranged from 1.65 to 1.72 Torr except where specified otherwise. Gas transfer was done in a vacuum system with greaseless stopcocks. The vacuum system was pumped to 10^{-6} Torr before each experiment.

For photolysis at 3.3 μm, the several mJ OPO pulses were focused up to 2 J/cm^2 with a 5 cm focal length 5 cm diameter CaF_2 lens. The focusing parameters were measured by attaching a 20 μm diameter pinhole (diamond wire die) to a PbSe detector mounted on a 3-D translator.

After the measurements, the pinhole was examined by a microscope to ensure that no enlargement was caused by focused laser pulses. At the center of the focus the spot size is 0.6 mm FWHM and the beam diameter is less than 0.9 mm over a distance of 8 mm (Fig. II-4). Since the dissociation yield strongly depends on the laser fluence and intensity, the effect of the drastic fluence and intensity variation along the longitudinal axis caused by such a tight focus on the quantitative measurement of dissociation yield should be noted. Although the problem may be solved in principle by a deconvolution technique (see Data Analysis), a short path cell was designed to reduce intensity (and fluence) variation inside the cell and to reduce contributions to dissociation from low intensity zones. Several 14 mm (<2 focal parameters) long pyrex cells with parallel NaCl windows attached by Torr seal epoxy at Brewster's angle were used. The cells must be accurately placed around the beam focus to avoid damage to the cell windows. For each photolysis, between 3000 and 7200 pulses were used. The energy of the laser pulse is monitored continuously, and the frequency occasionally, during photolysis. For experiments performed at the 2944 cm^{-1} Q branch of EtCl, the signal from an optoacoustic cell filled with 2 Torr EtCl was used to fine tune the etalon angle. The method allowed setting of the OPO frequency to within 0.1 cm^{-1} of the peak absorption. In the measurement of dissociation yield as a function of frequency over the entire C-H stretching region, the optoacoustic cell with 2 Torr EtCl was irradiated with the unfocussed OPO beam.

Fig. II-4. Spatial profile of the OPO pulses measured in the focal plane with a 20 μm diameter pinhole. a) FWHM of transverse profile along the longitudinal axis z. z = 0 is 4.5 mm away from the center of the focal lense. Black points (•) are the FWHM on the horizontal axis and open circles (o) are those on the vertical axis. b) and c) Transverse intensity profiles at z = 2.5 and 8.9 respectively. Black points are horizontal scans at the vertical maxima. Open circles are vertical scans at the horizontal maxima.

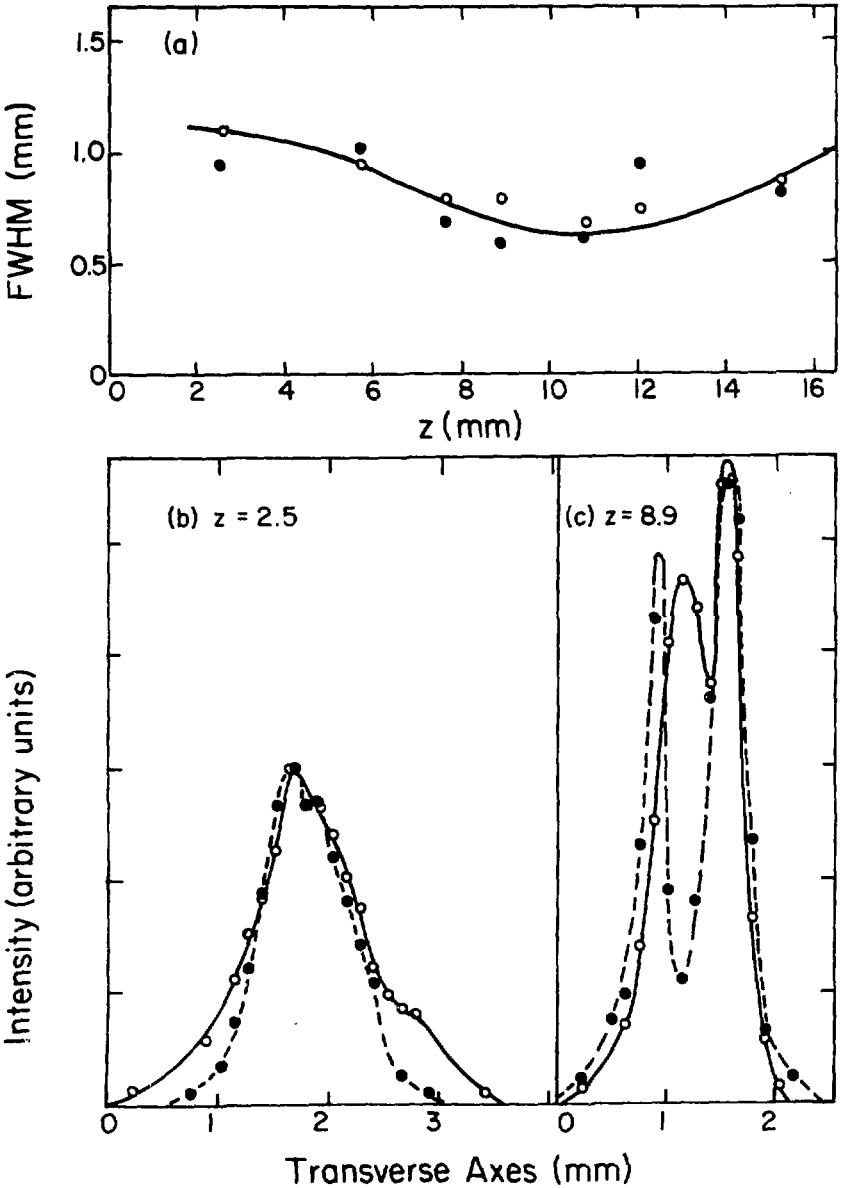
(a)
FWHM (mm)
1.5
1.0
0.5
0
0
2
4
6
8
10
12
14
16
z (mm)
(b) z = 2.5
(c) z = 8.9
Intensity (arbitrary units)
0
1
2
3
0
1
2
Transverse Axes (mm)

Fig. II-4

This made it possible to set the photolysis frequency at either the peak or the valley of the rotational structure.

For photolysis by the CO_2 laser, a 25 cm focal length 5 cm diameter NaCl lens was used for focusing and the photolysis cell was placed 13 cm away from the lens to obtain the desired energy fluence. An unfocused beam was used for optoacoustic measurements. The laser was attenuated by a 4 mm CaF_2 flat, a NaCl flat, or a 10 cm glass cell with NaCl windows containing 40 Torr SF_6. No change in the temporal or spatial profile of the beam was observed after attenuation.[49]

After photolysis, the sample in the cell was immediately condensed into an evacuated pyrex GC sample loop. Since ethylene has a vapor pressure of about 1 m Torr at liquid nitrogen temperature, a liquid helium bath was used for condensation. The sample was then analyzed by a Varian 3700 gas chromatograph with a flame ionization detector. For EtCl photolysis, ethylene was the only hydrocarbon product detected. Flame ionization is not sensitive to HCl. A 12 feet long Porapak S column (mesh size 100/120) in 1/8 inch diameter stainless steel tubing was used to separate the products from the reactant. At the conditions of 30 cm^3/min. He carrier gas flow rate and 105°C column temperature, the retention time for ethylene and EtCl are 3.4 min. and 12 min. respectively. The flame combustion gas mixture was composed of 30 cm^3/min. H_2 and 300 cm^3/min. air. The detector with such a flame would produce a 1 min. FWHM GC peak with 20 mvolt peak height at the most sensitive scale for a quantity of about 0.20 cm^3-Torr (11

nanomole) ethylene. The detection sensitivity for ethylene is about 11% higher than for EtCl. For each individual chemical, the detection response is linear over at least a few orders magnitude of quantity. The broad width of the GC peaks is primarily due to the large volume of the gas injection loop, which is about 5 c.c. A much smaller volume (preferably at μl level) would bring the width into the limit caused by column retention and therefore increase the sensitivity. Such a small volume is hardly obtainable for loops constructed with stopcocks. However, with current devices for detection, for all the photolyses, the worst GC peak S/N ratio is better than 10/1. A negative dip of the GC signal baseline occurred at the injection of the gas sample as the injection of the low pressure gas suddenly dropped the back pressure of the column. This dip recovered before the ethylene peak and therefore did not hinder a good quantitative measurement of the peak area.

Optoacoustic measurements were made with two types of stainless steel cells. One was 38 mm in length and 20 mm in diameter with CaF_2 windows and a Sony foil electret microphone placed at the center. The microphone signal was preamplified then averaged over 32 pulses using a Biomation Transient Recorder and a Northern NS-575A Digital Signal Analyzer. For 3.3 μm excitation a second cell 12 mm long and 40 x 14 mm cross section with NaCl windows was used to eliminate the low intensity region far from the focus. Several runs with both cells gave the same dependence of energy absorbed on laser wavelength and on laser intensity.

Standard single photon absorption spectra for the fundamental and first overtone were recorded with a Nicolet 7199 FTIR for which the highest resolution is 0.06 cm^{-1}. A 10 cm pyrex cell with NaCl windows was used to contain the gases. For the second overtone spectra, a Cary-17 spectrometer and a 12 cm pyrex cell with quartz windows were used.

For photolysis of $CHClF_2$, a Varian 1800 FID GC was used to detect the product C_2F_4 after 12,000 to 18,000 laser pulses. The gas (Matheson Gas, Grade R) was fractionally distilled and its purity shown by GC to be >99.9%.

5. Data Analysis

The dissociation yield, W_d, is the fraction dissociation for those molecules in the volume irradiated by the laser. W_d is given by the ratio of the ethylene and EtCl GC peak areas (A), normalized by the GC detection sensitivity (S), the number of pulses n, and an effective focal volume V_f in the cell.

$$W_d = \frac{A_{C_2H_4}}{A_{EtCl}} \cdot \frac{S_{EtCl}}{S_{C_2H_4}} \cdot \frac{V_{cell}}{V_f} \cdot \frac{1}{n} \quad . \qquad \text{(II-1)}$$

Since the total fraction of molecules dissociated in the entire cell was less than 2% for any photolysis, normalization by the number of laser pulses was linear. The yields as a function of pressure and of wavelength should also be normalized by multiplying a fluence factor (pulse energy/4.1 mJ)$^{3.5}$ for pressure dependence and (pulse energy/3.3 mJ)$^{3.5}$ for wavelength dependence, to obtain the true functional dependence at

a single laser fluence. The value 3.5 was obtained from the fluence dependence study of yield (see Section C). The combined deviation of the GC calibration and the pressure measurement is ±4% for larger yields and higher pressures and is ±9% for smaller values. The long term drift of laser energy, ±5%, during the photolysis is responsible for the major uncertainty, ±18%, in the precision of the dissication yield. The effective focal volume is defined as

$$\int_{\text{cell}} \frac{W_d(\text{fluence})}{W_d(\text{focal point fluence})}\, dV,$$

and was approximated as

$$\int_{\text{cell}} \left[\frac{\text{Fluence}}{\text{Focal point fluence}}\right]^{3.5} dV$$

for dissociations at 3.3 μm (Fig. II-4). However, even such an integration can not be meaningfully carried out without a complete knowledge of the 3-D fluence distribution within the cell. By using the FWHM of the focused beam to calculate the average fluence, (pulse energy/π(FWHM/2)^2), an integration along the longitudinal axis was carried out using Fig. II-4(a). The value 1.6 x 10^{-3} cm^3 was obtained for the effective focal volume in a 14 mm path cell. The upper limit on the error that might be caused by neglect of the transverse deconvolution on the focal volume can be established by comparing the two areas π(FWHM/2)^2 and

$$\int_{\text{focal plane}} \frac{W_d(\text{fluence})}{W_d(\text{average fluence})} dA.$$

This error limit combined with other uncertainties discussed above sets the limit of uncertainty for the dissociation yield to be $^{+150}_{-50}$% for dissociations with higher fluences. For dissociations with fluence ~0.1 J/cm^2 and at frequencies where the yield is relatively low, the uncertainty is about twice larger. The magnitude of the optoacoustic signal was measured as the height of the first peak vs the first valley in each series of acoustic waves. For the wavelength dependence of absorption of focused OPO pulses, a linear normalization was used to correct the optoacoustic signal for the variation of the averaged pulse energy (see Section C for the linear fluence dependence of absorption at 3.3 μm). The ±15% pulse-to-pulse energy fluctuation was reduced to a ±3% uncertainty of laser fluence after 32 pulse average.

C. Results

For the convenience of later discussion, the experimental results of MPD and optoacoustic measurements are summarized and presented in this section. All the results presented here are for EtCl unless specified otherwise. Other spectroscopic and kinetic measurements will be presented and discussed in Sections D and H.

Optoacoustic signal vs 3.3 μm laser fluence is shown in Fig. II-5. Data points between 0.04 and 0.2 J/cm^2 constitute a straight line with slope slightly larger than unity. Points begin to deviate from the line only at fluences for which a significant fraction of EtCl molecules is dissociated. The linear saturation fluence is estimated as $h\nu/2\sigma$ as for a non-degenerate two-level system. At this fluence the upper level population is $(1 - \frac{1}{e})$ times the lower level population. In Section F, σ, the absorption cross section for broadband OPO pulses at 2992 cm^{-1}, is calculated as 2.4×10^{-19} cm^2. Because of the small energy of the laser pulses and the small total absorption of low pressure EtCl, an accurate and absolute calibration of the vertical scale is difficult to obtain. However, since saturation is not possible much below $E_{sat.linear}$, the number of photons absorbed per absorbing molecule, $\langle n \rangle_{real}$, at $E_{sat.linear}$, is on the order of 0.4 and is about 3 at 1.1 J/cm^2. When the laser was tuned 50 cm^{-1} to the blue of the EtCl C-H fundamental absorptions, no acoustic signal (electronic or window-induced) was observed.

Fig. II-5. Dependence of absorbed energy on focal point fluence for 0.32 Torr ethyl chloride irradiated by broadband OPO pulses at 2992 cm^{-1}. Optoacoustic measurements are shown by black points. $\langle n \rangle$ is the number of photons absorbed per molecule under irradiation. The solid and dotted lines are calculated by rate equations analysis with $\sigma^a_{01} = 2.4 \times 10^{-19}$ cm^2, $\sigma^a_{12} = 5 \times 10^{-19}$ cm^2 and $P_{12} = 0.5$. $\sigma^a_{\ell,\ell+1}$, $\ell \geq 2$, for the solid line is set (3) of Table II-7 and for the dotted line is set (4).

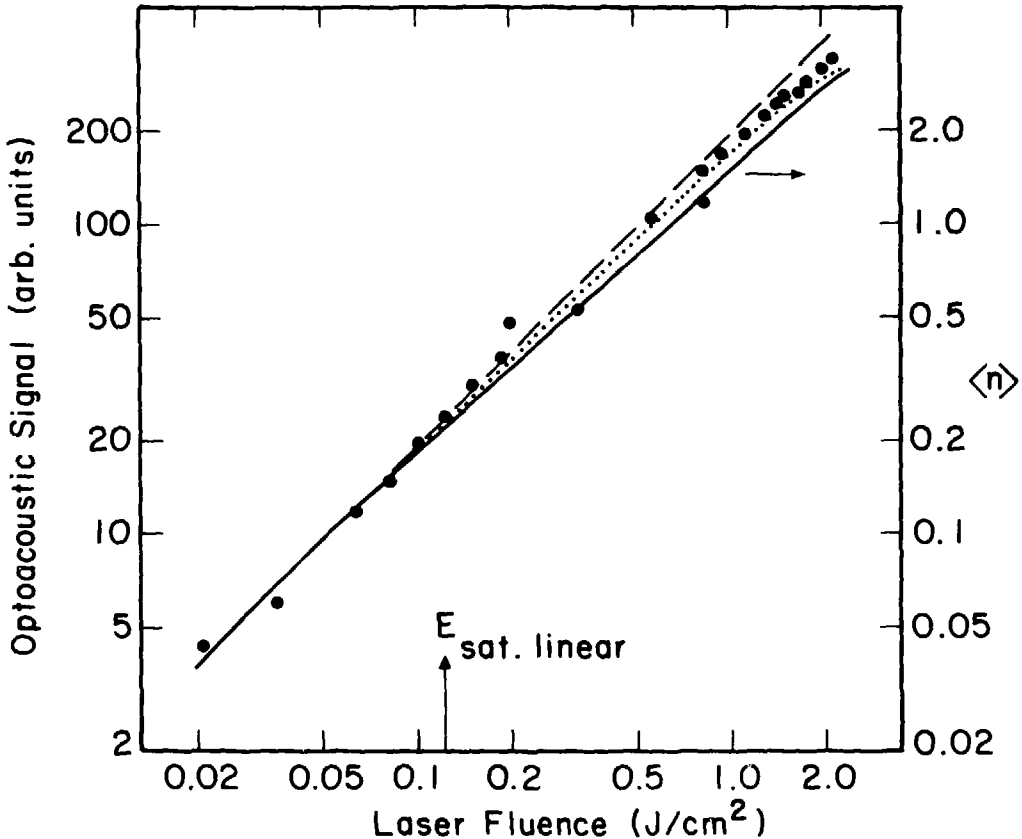
Optoacoustic Signal (arb. units)
200
100
50
20
10
5
2
2.0
1.0
0.5
⟨η⟩
0.2
0.1
0.05
0.02
E sat. linear
0.02
0.05
0.1
0.2
0.5
1.0
2.0
Laser Fluence (J/cm²)

Fig. II-5

Fig. II-6. Dependence of absorbed energy on fluence for 0.85 Torr ethyl chloride for the R(8) line of the CO_2 laser at 967.7 cm^{-1}. The line (---) has a slope of one.

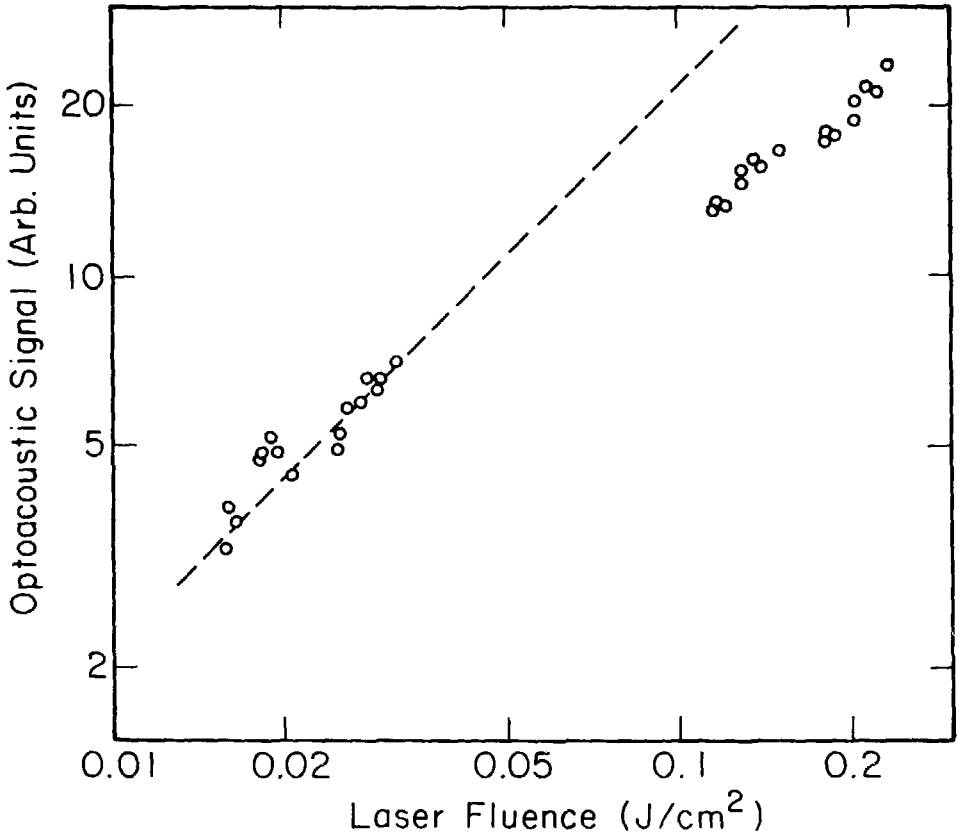
Optoacoustic Signal (Arb. Units)
20
10
5
2
0.01
0.02
0.05
0.1
0.2
Laser Fluence (J/cm^2)

Fig. II 6

The dependence of the optoacoustic signal on the fluence of the CO_2 laser R(8) line is shown in Fig. II-6. The absorption is linear below 0.03 J/cm^2 and exhibits saturation in the higher fluence range. The line with unity slope drawn through the lower fluence points lies at least a factor of two above the higher fluence points. The possibility of instrumental saturation at high energy fluences was excluded by the reproducibility of the curvature at the lower EtCl pressure of 0.17 Torr. Although CaF_2 absorbs significantly at 10 μm, the contribution of window absorption to the acoustic signal with 2 Torr Ar gas in the spectrophone cell was less than 1%. Thus energy absorbed increases with fluence throughout the range but is substantially saturated above 0.1 J/cm^2.

The optoacoustic spectra of absorption with narrowband (FWHM 0.15 cm^{-1}) OPO pulses at 0.90 ± 0.02 J/cm^2 showed a striking resemblance to the fundamental over the entire CH stretching region (Fig. II-7). The fluence used was well above the linear saturation fluences for the narrowband laser at all the CH stretching bands. Although these optoacoustic spectra showed a slight overall enhancement of absorption for the lower frequency CH bands, they contrast strongly with the usual 10 μm MPA spectra. In these 10 μm optoacoustic measurements, the spectral features are usually broad, smeared and red-shifted vs the fundamental. The optoacoustic technique monitors the total absorption in the gas medium. It does not discriminate between absorption to very high vibrational levels and excitation at low levels. Therefore,

hypothetically, if a major fraction of the molecules can only absorb the first photon due to vibrational anharmonicity, the optoacoustic signal does not represent the true MPA spectra even though a significant portion of molecules undergo MPA. Since only molecules excited above the reaction barrier may dissociate, dissociation may be used to obtain the multiphoton excitation spectrum.

MPD occurs throughout the entire spectral range for the five C-H stretching fundamentals, Fig. II-8. The dissociation yield spectrum, taken with 1.1 J/cm^2 narrowband OPO pulses at 1.7 Torr EtCl pressure, follows approximately the same shape as the ordinary linear absorption spectrum $A_{01}(\nu)$. The relative yields are somewhat enhanced at longer wavelengths. The peak yields near 2944 and 2977 cm^{-1} are about 2%. The band center frequency and band shape of the sharp peak in W_d at 2943.8 cm^{-1} match those of the fundamental Q branch almost exactly. In addition, a W_d peak near 2913 cm^{-1} was found. It does not correspond to any peak of $A_{01}(\nu)$. However, it coincides with half the frequency of a strong, sharp Q branch in the first overtone spectrum. When W_d is divided by $A_{01}(\nu)$ a good correlation with the overtone spectrum is found, Fig. II-9. Finally, far in the red end of the spectrum where the yield is low, W_d/A_{01} shows a broader resonance, Fig. II-10, which corresponds to one-third the frequency of the strong resonance in the second overtone spectrum. For the first time in MPD experiments, resonances in MPD yield were found to match the position and shape of peaks in the fundamental, as narrow as 0.4 cm^{-1}, and first- and second-overtone absorption spectra.

Fig. II-7. Frequency dependence of absorption for 0.65 Torr EtCl irradiated by 0.9 J/cm^2 narrowband OPO pulses, (●). The linear absorption spectrum was taken for 27 Torr EtCl in 10 cm cell by FTIR with 1 cm^{-1} resolution.

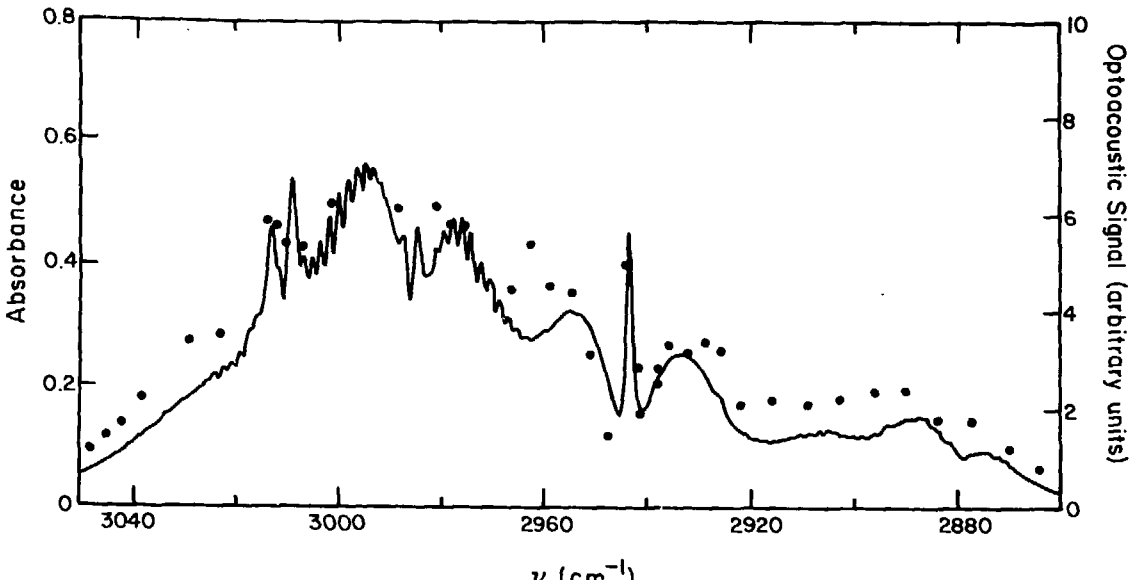
0.8
0.6
0.4
0.2
0
Absorbance
10
8
6
4
2
0
Optoacoustic Signal (arbitrary units)
3040
3000
2960
2920
2880
ν (cm⁻¹)

Fig. II-7

Fig. II-8. Dissociation yield, W_d, and linear absorption spectrum, A_{01} vs frequency. On the relative scale for dissociation yield, 10 = 2.0%. All points (●) were measured at the peaks of absorption lines. Two points (▼) were taken in valleys. A sharp resonance (○) is shown enlarged with an absorption spectrum at 0.24 cm^{-1} resolution. Two points near 2977 cm^{-1} show sharp structure in a P branch. The conditions for the absorption spectrum are the same as in Fig. IV-7.

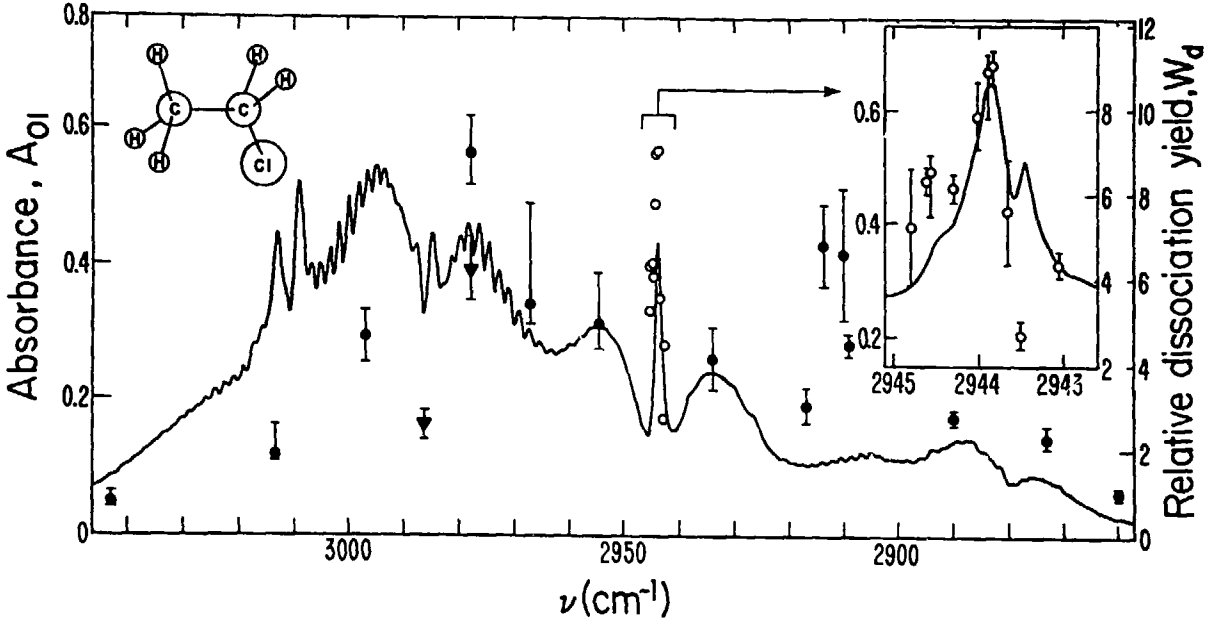
Absorbance, A_{01}
Relative dissociation yield, W_d
ν (cm^{-1})
3000
2950
2900
2945
2944
2943
0.8
0.6
0.4
0.2
0
12
10
8
6
4
2
H
C
Cl

Fig. II-8

Fig. II-9. Relative dissociation yield, W_d $(\nu/2)$, divided by the absorbance, $A_{01}(\nu/2)$ at 0.24 cm^{-1} resolution, from (●) in Fig. II-8. The first overtone absorption spectrum, $A_{02}(\nu)$, is also plotted at 1 cm^{-1} resolution (FTIR).

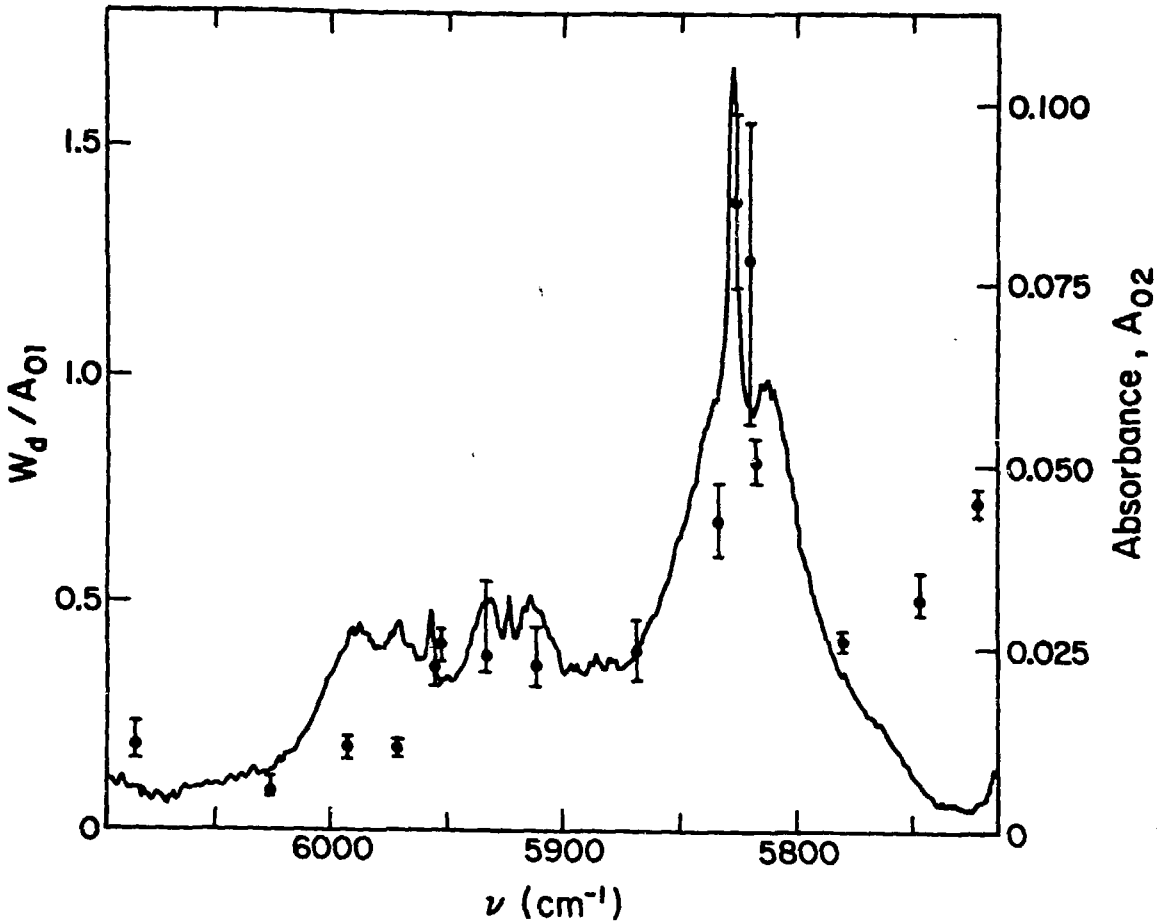
1.5
1.0
0.5
0
W_d / A_{01}
0.100
0.075
0.050
0.025
0
Absorbance, A_{02}
6000
5900
5800
ν (cm^{-1})

Fig. II-9

Fig. II-10. (a) Relative dissociation yield $W_d(\nu/3)$ and second overtone spectrum $A_{03}(\nu)$ (1.5 cm^{-1} resolution, Cary 17). $A_{01}(\nu/3)$ ····· and $A_{02}(2\nu/3)$ --- are also shown. (b) $W_d/A_{01}(\nu/3)$ and the second overtone spectrum. The monotonic decrease of W_d in (a) becomes a broad resonance matching the second overtone spectrum when normalized.

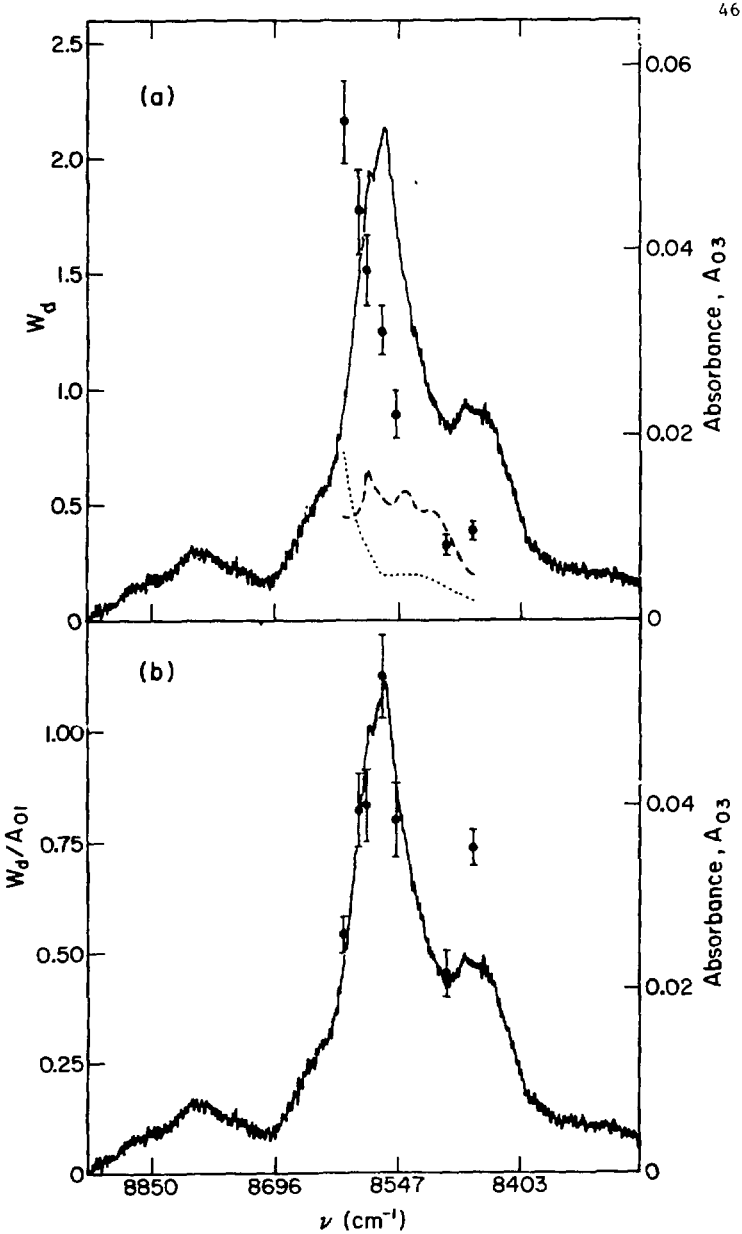
(a)
(b)
W_d
W_d/A_{01}
Absorbance, A_{03}
2.5
2.0
1.5
1.0
0.5
0
1.00
0.75
0.50
0.25
0.06
0.04
0.02
8850
8696
8547
8403
ν (cm^{-1})

Fig. II-10

The dependence of MPD yield on energy fluence was studied for broadband OPO pulses at 2977 cm^{-1}, Fig. II-11. In the range from 0.5 to 2 J/cm^2 a straight line with slope 3.5 can be drawn through the data on a log-log plot, although the experimental points are better fit by a curved line with decreasing slope at higher fluences. The shape of the yield vs fluence curve may vary with wavelength and laser bandwidth. The effect of bandwidth on yield is illustrated by the data near 2977 cm^{-1} in Table II-2. The factor $E_p^{3.5}$ has been used in correcting all wavelength dependence data to 1.1 J/cm^2. However since the observed yields are of the same order of magnitude and since the energy range is small, 0.94 to 1.2 J/cm^2, this approximate correction should not introduce significant errors. MPD yield decreases with increasing EtCl pressure, Fig. II-12. W_d decreases nearly a factor of two between 0.25 and 2 Torr. From 2 to 6.2 Torr the yield decreases by only about 10%.

The absolut dissociation yield at various frequencies around 3.3 μm is listed in Table II-2 along with a dissociation yield at one wavelength in the 10 μm CC stretching band. At even higher fluence, the yield at 10 μm is smaller than most of the 3.3 μm yields.

No MPD yield as C_2F_4 was detectable for broadband laser excitation of 2.5 Torr $CHClF_2$ at the 3010 cm^{-1} band center or 13 cm^{-1} to the red of band center at fluences of 2.2 J/cm^2. The detection limit corresponded to 0.01% dissociation.

Fig. II-11. Dependence of dissociation yield (Φ) on fluence for 1.7 Torr ethyl chloride irradiated by broadband OPO pulses at 2977 cm^{-1}. The slope of the line (---) is 3.5. The solid line and the dotted line are calculated by rate equations analysis with set (3) and set (4) $\sigma^a_{i,i+1}$ in Table II-7, respectively.

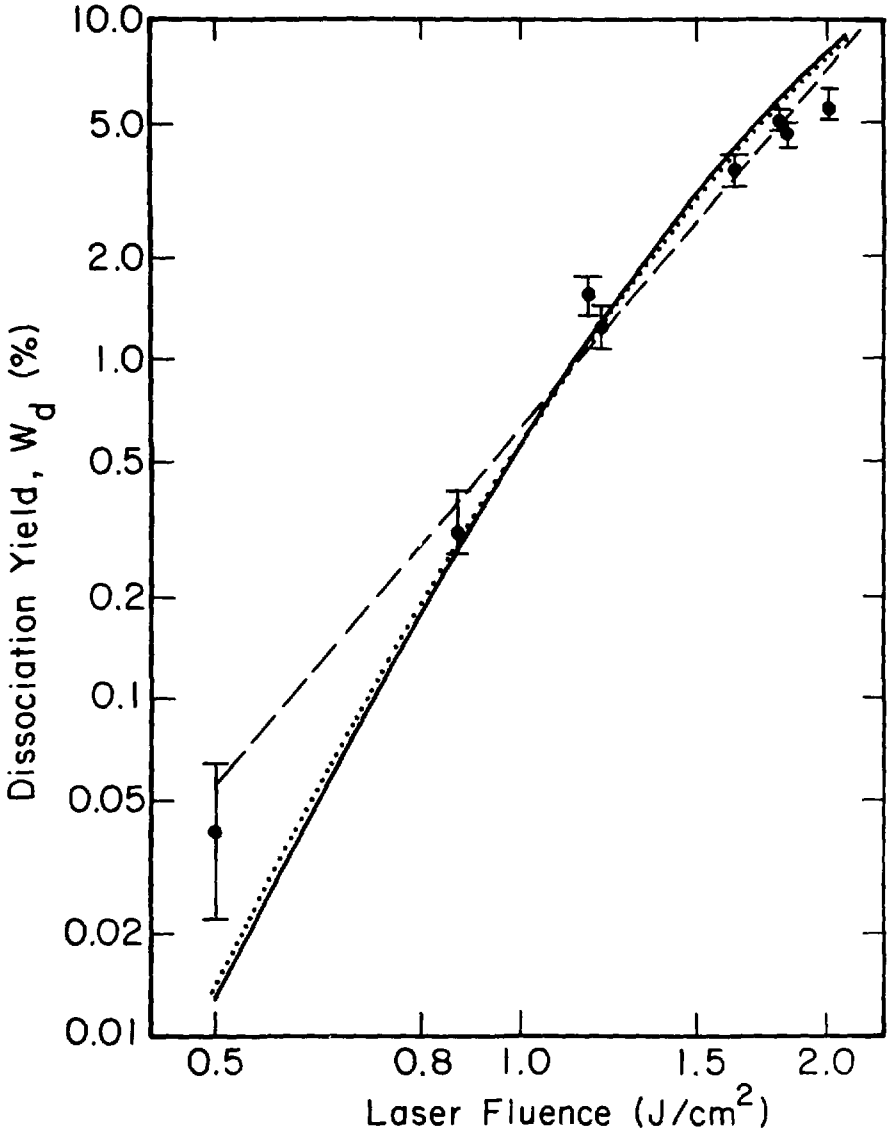
10.0
5.0
2.0
1.0
0.5
0.2
0.1
0.05
0.02
0.01
Dissociation Yield, W_d (%)
0.5
0.8
1.0
1.5
2.0
Laser Fluence (J/cm^2)

Fig. II-11

Table II-2. Measured and calculated ethyl chloride MPD yields for selected frequencies at 1.1 J/cm^2 fluence and 1.7 torr pressure.

ν (cm^{-1})	σ^a_{01} ($10^{-19} cm^2$)	σ^a_{01} ($10^{-19} cm^2$)	P_{12}	$\sigma^a_{\ell,\ell+1}$ ($\ell \geq 2$)[a] ($10^{-19} cm^2$)	$W_{d,cal}$[b] (%)	$W_{d,expt}$ (%)
3014	26	5	0.5	1.3-1.4	--	$0.36^{+0.04}_{-0.01}$
2976.6	30	5	0.5	2.4-2.7	1.7	1.8±0.2
2977[c]	1.8	5	0.5	1.9-2.3	1.6	0.9±0.3
2943.8	13	5	0.5	2.3-2.5	2.1	1.8±0.2
2913	11	5	1[d]	2.4-2.7	1.2	1.3±0.2
2829	2	5	0.5	1.8-1.9	--	0.065±0.005
967.7[e]	--	--	--	--	--	0.09±0.01

[a] The range of ℓ-independent quasicontinuum cross sections that matches the experimental yield range.

[b] Dissociation yields calculated with $\sigma^d_{\ell,\ell+1} = 2.5 \times 10^{-19}$ cm^2, $\ell \geq 2$.

[c] Photolysis with broadband laser. All the other 3.3 μm photolyses were with narrowband.

[d] There is a Q branch of an overtone band at 5826 cm^{-1}.

[e] CO_2 laser fluence at 6 J/cm^2.

Fig. II-12. Dependence of dissociation yield (Φ) on ethyl chloride pressure for 2979 cm^{-1} broadband photolysis at 1.4 J/cm^2 (4.1 mJ). The laser pulse energy varied from 3.8 to 4.6 mJ. Dissociation yields were normalized by (pulse energy/4.1 mJ)$^{3.5}$. The solid line and the dotted line are calculated by rate equations analysis with set (3) and set (4) $\sigma^a_{\ell,\ell+1}$ in Table II-7, resepctively. Collision rate, k_c = 7.7 μs^{-1} $Torr^{-1}$.

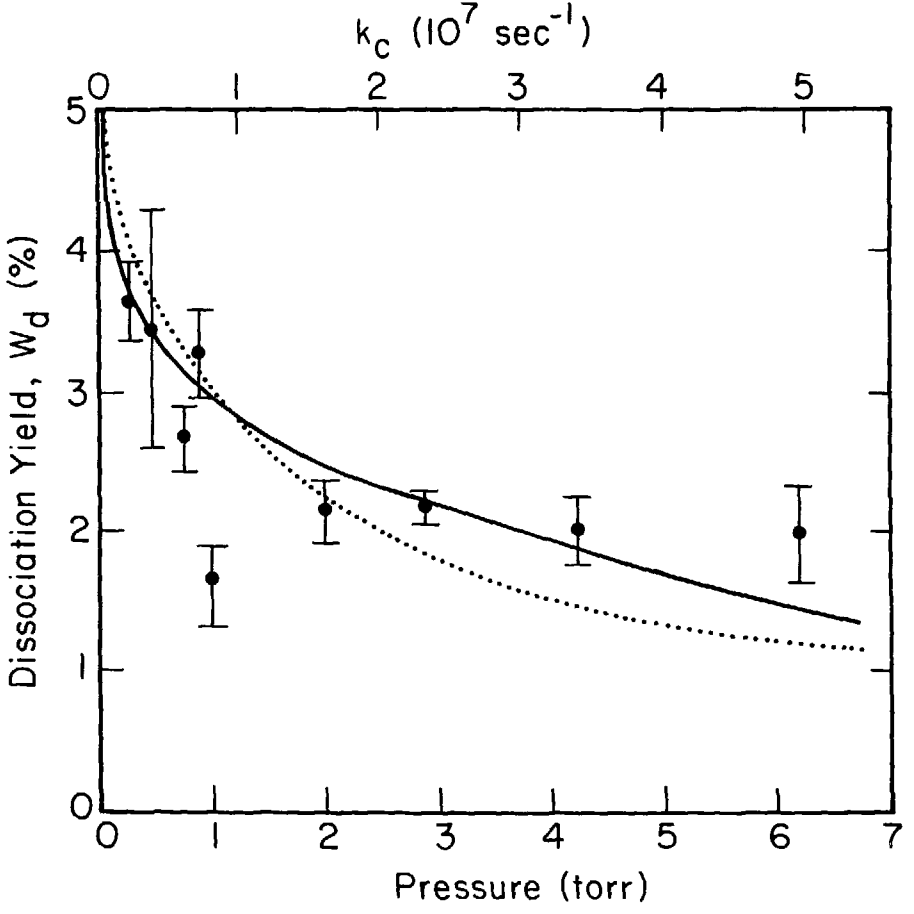
k_c (10^7 sec^{-1})
0
1
2
3
4
5
Dissociation Yield, W_d (%)
0
1
2
3
4
5
0
1
2
3
4
5
6
7
Pressure (torr)

Fig. II-12

D. Vibrational Spectroscopy

C_2H_5Cl is a small enough molecule so that its lowest vibrational energy levels may be studied in detail by ordinary ir absorption spectroscopy. This spectral data may then be used to help define the multiphoton excitation mechanism and to make quantitative estimates of excitation parameters.

The CH stretching fundamental region has been well studied.[45] The five fundamentals are listed in Table II-3. A sixth band is assigned to a CH_3 deformation overtone which probably borrows transition strength by Fermi resonance with the nearby CH_3 stretching levels. The integrated absorption cross section for the entire CH stretching range is approximately 1.5×10^{-17} cm/molecule. This value was obtained from the fundamental spectrum of 27 Torr EtCl in 406 Torr CF_3I at 0.06 cm^{-1} spectrometer resolution. The single vibration-rotation linewidth was broadened to be greater than the spectrometer resolution to assure that the true absorbance was recorded. Part of the pressure broadened spectrum is shown in Fig. II-13. All the peaks that are resolvable are broader than 0.06 cm^{-1} (c.f. Fig. II-14(a)). Data for the 974 cm^{-1} mode pumped by the CO_2 laser is also given in Table II-3.

The molecule belongs to the C_s point group and is nearly a prolate symmetric top with rotational constants A = 1.044, B = 0.183 and C = 0.165 cm^{-1}.[45] The $\|$ components of vibrational bands, $\Delta K = 0$ with $\Delta J = 0, \pm 1$, give typical PQR band shapes as for the band at 2944 cm^{-1}

Table II-3. Frequencies and assignments of the ethyl chloride vibrational bands excited.

$\nu(cm^{-1})$[a]	Assignment[b]	Symmetry, Band Type	Integrated Absorption (10^{-18} cm/molec.)
3011	CH_2 a.s.	a", ⊥	3.5
2987	CH_3 a.s.	a", ⊥	5.3
2967	CH_2 s.s.	a', ⊥, ∥	--
2944	CH_3 a.s.	a', ∥	3.5
2904	CH_3 v=2,d.	a', ⊥	1.0
2881	CH_3 s.s.	a', ⊥	1.1
974	C-C	a', ∥	2.5

[a]Band centers measured from FTIR spectra, except the very weak 2967 cm^{-1} band from Raman spectroscopy.

[b]From Ref. 45. Symbols: a.s. - asymmetric stretch; s.s. - symmetric stretch; d. - deformation.

Fig. II-13. Fundamental spectra of 27 Torr ethyl chloride pressure broadened by 406 Torr CF_3I in a 10 cm cell. Spectrometer resolution 0.06 cm^{-1}. Features shown here correspond to the ones in Fig. II-14(a).

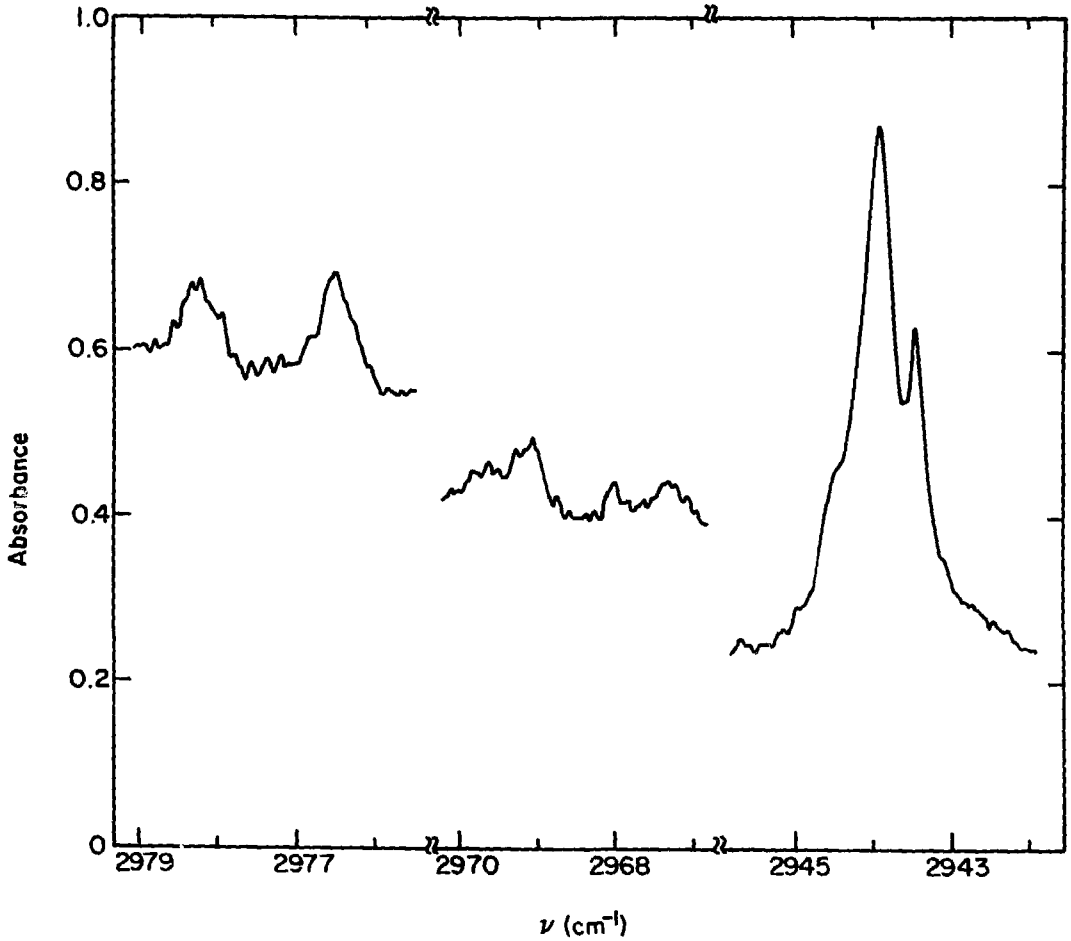

Fig. II-14

Fig. II-14. a) Ethyl chloride fundamental spectra from a Nicolet 7199 FTIR with a 10 cm cell and 27 Torr EtCl. Spectrometer resolution 0.06 cm^{-1}. Features from left to right are structure near 2977 cm^{-1} where most MPD experiments were performed, sharp peaks with 0.06 cm^{-1} width indicated by arrows, and the Q banch of a $\|$ band. b) EtCl first overtone spectrum at 0.06 cm^{-1} resolution (by Charles Anderson, Nicolet Inst. Corp., Madison, Wisconsin, using Nicolet 7199 FTIR). A 15 cm cell with 420 Torr EtCl was used. Only one band is shown here. c) EtCl second overtone spectrum at 1.5 cm^{-1} resolution from a Cary - 17 with a 12 cm cell containing 1100 Torr EtCl.

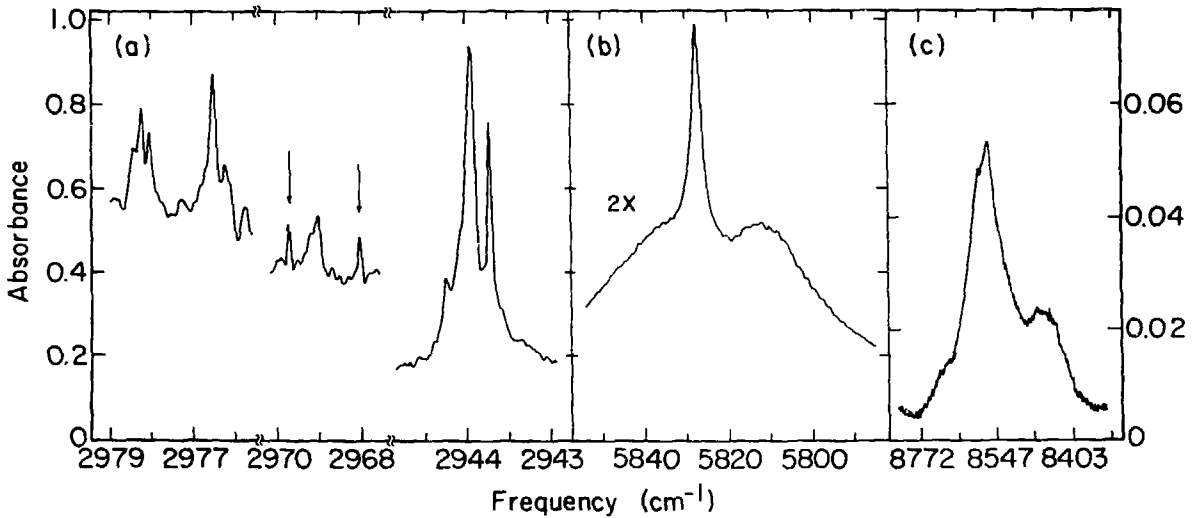
(a)
(b)
(c)
2X
Absorbance
1.0
0.8
0.6
0.4
0.2
0
0.06
0.04
0.02
0
2979 2977 2970 2968 2944 2943 5840 5820 5800 8772 8547 8403
Frequency (cm^{-1})

Fig. II-14

(Fig. II-8). The integrated intensity of the Q branch and hence the absorption cross section is about 3 to 6 times smaller than for P or R branches.[50] The ⊥ components show prominent series of Q branches with $\Delta J = 0$ and $\Delta K = \pm 1$. The accompanying series of P and R branches appear continuous at medium resolution. Thus each vibrational band consists of up to 9 vibration-rotation lines for each populated rotational state.

At high resolution, Q branches in the fundamental spectrum exhibit widths of a few tenths cm^{-1}, Fig. 14(a). At 0.06 cm^{-1} resolution individual rotational line structure is observed in the band wing near 2970 cm^{-1} with widths of ~0.06 cm^{-1}. Since for $v_{CH} = 1$ the density of vibrational levels (Table II-4), $\rho << 1/0.06$ cm^{-1}, the $v_{CH} = 1$ levels must be well-defined energy eigenstates with only limited coupling to a few CH bending overtones. Pressure broadening was measured for a weak band at 677 cm^{-1}. At 1100 Torr EtCl pressure, the FWHM of the rotational lines at around 645 cm^{-1} was broadened to 0.16 cm^{-1} from 0.09 cm^{-1} at 27 Torr. This corresponds to a pressure broadening of ~6 x 10^{-5} cm^{-1} $Torr^{-1}$.

Overtone transitions are forbidden in the harmonic oscillator approximation. Hence their spectra give only the positions of the most anharmonic $v_{CH} = 2$ levels. The observed intensities are not related to the $v_{CH} = 1 \rightarrow 2$ transitions. The sharpest rotational structures in the spectrum at 0.06 cm^{-1} resolution are the ∥-band Q branches. The widths are all greater than 2 cm^{-1}, Fig. 14(b), greater

Table II-4. Spectroscopic properties of the lowest CH stretching levels of ethyl chloride.

v_{CH}	ρ_{vib}[a] (levels/cm^{-1})	Linewidth (cm^{-1})	CH Stretch Mode Levels	Energy Range
1	<1	<0.06	5	3050~2850
2	70	1.2±0.4	15	6050~5650[b]
3	1300	30±15	35	9000~8300[b]

[a] ρ_{vib} calculated by direct count. See Chapter V of Ref. 42.

[b] Estimated from the most harmonic high frequency level to the least harmonic low frequency level consistent with the observed overtone spectra.

than can be expected from the change of rotational constants with vibrational excitation. By comparing with the Q-branch widths of the fundamental spectrum at different resolutions, 0.5, 1.0 and 2.0 cm^{-1}, the width of a vibration-rotation line was determined to be 1.2 ± 0.4 cm^{-1}. This broadening may be caused by coupling to lower frequency modes. The linewidth gives an effective rate of energy transfer from CH stretching to other modes. Since this requires many levels per linewidth and since no structure is seen with 0.06 cm^{-1} resolution, most, if not all, vibrations must be coupled (see densities in Table II-4).

Many general features of the $v_{CH} = 1 \rightarrow 2$ spectrum are known. There are 15 $v_{CH} = 2$ energy levels. For non-interacting harmonic oscillators there are 5 allowed transitions from any given $v_{CH} = 1$ level, the addition of one quantum in any one of the five modes. The total integrated intensity of these transitions should be slightly larger than that measured for the fundamental due to larger quantum number involved in some of these transitions. Since there is coupling among the CH stretching modes, all 15 transitions become allowed to some extent. In addition coupling with $v_{CH} = 1$, $v_{def} = 2$, and $v_{def} = 4$ levels will occur. Since coupling among CH_3 vibrations and among CH_2 vibrations should be stronger than coupling between groups perhaps 10-20 levels should share comparably in the intensity of the $v_{CH} = 1 \rightarrow 2$ spectrum. Thus, spread over 200-300 cm^{-1} are some fifteen vibrational transitions each with 3 to 9 rotational branches. For any given J, K level of

$v_{CH} = 1$ there are probably some 100-200 lines, each about 1 cm^{-1} broad. Thus even considering the non-random grouping of lines and variation in intensity, resonant transitions from $v_{CH} = 1 \rightarrow 2$ for a single rotational state should cover much of the spectral range.

The second overtone spectrum, Fig. 14(c), is so severely broadened that not even Q-branch structure is resolved. Each vibration appears with a FWHM of about 60 cm^{-1} compared to ~35 cm^{-1} for all fundamental bands. Thus linewidths for individual rotational states must be ~30 ± 15 cm^{-1}. For $v_{CH} = 2 \rightarrow 3$ there are even more individual lines than for $v_{CH} = 1 \rightarrow 2$. These lines are overlapped into a completely continuous though not uniformly intense spectrum. Table II-4 summarizes some relevant properties of these fundamentals.

In summary, the 5 C-H modes provide the dominant coupling between the molecule and the 3.3 μm radiation field. The $v_{CH} = 1$ states are sharp and perfectly discrete. The $v_{CH} = 2$ levels are broadened with widths being larger than the Q-branch width of a parallel band and smaller than the P- and R-branch widths. The $v_{CH} = 3$ levels are much broader and are clearly in the quasicontinuum for 3.3 μm transitions.

The CH stretching mode of $CHClF_2$ has a vibrational anharmonicity, $2\omega_e x_e$, of 116 cm^{-1}. The band centers and the linewidths of single vibration-rotation features are listed in Table II-V for the fundamental, first- and second-overtone spectra. The calculated vibrational level densities are also listed. The integrated absorption of the fundamental C-H band of $CHClF_2$ is ~4 x 10^{-18} cm/molecule, comparable to that of the strongest C-H band of EtCl.

Table II-5. Spectroscopic properties of the CH stretching mode of $CHClF_2$.

v_{CH}	0→v Transition Bandcenter (cm^{-1})	Linewidth, FWHM (cm^{-1})	ρ_{vib}[a] (levels/cm^{-1})
1	3022	<0.06	<<1
2	5928	<0.12	8
3	8720	~2	60

[a] ρ_{vib} calculated by Whitten-Rabinovitch approximation. See Chapter V of Ref. 42.

E. Excitation Mechanism

Since CH stretching anharmonicities, usually about 50 cm^{-1}, are larger than vibration-rotation bandwidths and much larger than Rabi frequencies at MPD intensities, the mechanism established for anharmonic compensation in SF_6 cannot operate for EtCl (see Table II-6). However, the existence of five CH stretching modes with similar frequencies provides a new type of nearly resonant pathway for excitation to the quasi-continuum. The resonant nature of the transitions through the discrete CH stretching levels is manifested clearly in the dissociation yield spectra.

The MPD spectrum, $W_d(\nu)$, exhibits the same sharp rotational structure as the fundamental absorption spectrum, $A_{01}(\nu)$. Thus excitation from $v_{CH} = 0$ to $v_{CH} = 1$ is only possible for molecules in rotational states which absorb resonantly for one of the CH stretching modes. Since there are many $v_{CH} = 2$ levels each broadened by about 1 cm^{-1}, there is a good probability that for a given $v_{CH} = 1$ level and rotational state a resonant excitation to $v_{CH} = 2$ will occur. The shape of the overtone spectrum $A_{02}(2\nu)$ is similar to that of $W_d(\nu)/A_{01}(\nu)$. A resonance in $W_d(\nu)$ occurs at 2913 cm^{-1} which matches a Q branch in the first overtone spectrum. At this frequency any molecule which is resonantly excited to $v_{CH} = 1$ is necessarily resonant for the $v_{CH} = 1 \rightarrow 2$ transition. At a few frequencies P-R rotational compensation of anharmonicity may occur for the highest thermally populated J and K values. In most cases compensation occurs by excitation of two

Table II-6. Relevant quantities for compensation of vibrational anharmonicity in MPD of EtCl and $CHClF_2$ at 3.3 μm region.

Physical Quantity (cm^{-1})	C_2H_5Cl[a]	$CHClF_2$
CH Stretching Anharmonicity ($2\omega_e X_e$)	(50)[b]	116
Rotational Branchwidth,[c] ω_{VB}	16	~20
Rotational Compensation,[d] $\Delta\omega_{PR}$	~20	~20
Rabi Frequency, ω_R(at 100 MW/cm^2)	0.36	0.3

[a]Properties listed are for the CH mode of the strongest fundamental at 2987 cm^{-1}.

[b]Without a definitive assignment of the first overtone spectrum, the value of the vibrational anharmonicity for each CH stretching mode can not be accurately obtained. However, in the first overtone spectrum, three strong Q branches can be identified at 5958, 5924 and 5826 cm^{-1}. By assigning them to the three strongest C-H fundamentals at 3011, 2987 and 2944 cm^{-1} respectively, anharmonicity of the three modes can be determined as 64, 50 and 62 cm^{-1}.

[c]Measured as the FWHM of the P and R branches.

[d]Estimated for the sequence $v = 0 \rightarrow 1$ (P branch) and $v = 1 \rightarrow 2$ (R branch) of transitions of J and K levels with maximum thermal population. Rotational compensation for J and K levels at the outer edge of the P and R branches is approximately $\omega_{VB} + \Delta\omega_{PR}$.

different modes. The $v_{CH} = 3$ levels are sufficiently broad that resonant excitation should always be possible. The matching of peaks in the second overtone spectrum, $A_{03}(\nu)$, with peaks in $W_d(\nu)/A_{01}(\nu)$ indicates higher transition rates at these frequencies. The overall broad shape of $W_d(\nu)$ is in fact red-shifted from $A_{01}(\nu)$. Since the overall effect of anharmonicity is to shift the absorption spectrum progressively to the red as excitation increases, resonances are more frequent and MPD more easily achieved in the red end of the fundamental band.

It might be argued that the enhancement of W_d at 2913 cm^{-1}, half the frequency of a first overtone Q branch, is due to a direct two-photon absorption. All $v_{CH} = 0$ molecules are in resonance for such a transition. For molecules in rotational states which are in resonance for the sequential absorption of two photons through a real $v_{CH} = 1$ state the sequential process is identical to the two-photon process with zero frequency difference for the intermediate level.[51] For molecules which become resonant on the $v_{CH} = 0 \rightarrow 1$ as a result of power broadening the two-photon and sequential processes are again equivalent. For the case of rotational states which are far from resonance on the $0 \rightarrow 1$ transition, such a two-photon transition would have a low probability. In the strong interaction limit of perturbation theory,[4] the probability of a transition with one step off-resonance $\Delta\omega$ is $(\omega_R^2/(\Delta\omega^2 + \omega_R^2))$ times that of a completely resonant transition. ω_R for EtCl CH stretching modes at 100 MW/cm^2 is 0.25 cm^{-1} on average.

For rotational states with $\Delta\omega = 6\ cm^{-1}$ (roughly half of the rotational bandwidth) on the 0→1 transition, the transition probability to v=2 would be 600 times smaller than that for the rotational states at resonance on the first transition. Only at very high intensities would such two-photon excitation contribute substantially to the dissociation yield.

The resonant excitation path exists for ethyl chloride excited at 3.3 μm because there are several fundamentals with overlapping rotational structures in the same frequency range and because the quasicontinuum is reached with the second or third photon.

Excitation of the CH stretch of $CHClF_2$ gave no dissociation yield. This is so despite the fact that its one CH stretching mode is as strong an absorber as the strongest modes of C_2H_5Cl. The activation energy for dissociation, $CHClF_2 \rightarrow CF_2 + HCl$, is 54 kcal/mole.[52] Since there was less than 0.01% dissociation at the fluences obtainable, there must not be a sufficiently resonant path through the discrete levels for the molecules to reach the quasicontinuum. In contrast, $CHClF_2$ is dissociated by 10 μm excitation at moderate fluences in a molecular beam.[52] The large anharmonicity of the CH mode rules out compensation mechanisms typical for 10 μm (Table II-6). The lack of any other modes of similar frequency eliminates the C_2H_5Cl mechanism. Thus the 3.3 μm laser is unable to excite $CHClF_2$ above the first or second vibrational energy level. The OH stretching vibrations of CH_3OH and HCOOH are similarly spectrally isolated. MPD was achieved by excitation of these absorptions with an HF laser only when collisions occurred during the laser pulse.[32,33]

The excitation mechanism deduced from the experiments is a modification of the established SF_6 model for the different spectroscopic and structural properties of EtCl. EtCl absorbs two photons at or near resonance with levels of the five C-H modes to reach $v_{CH} = 2$. Then sequential absorption of 5 or more photons excites the molecule to the continuum. Dissociation must then occur before collisions remove excitation energy. This nearly resonant scheme of multiphoton excitation of EtCl at 3.3 μm and the properties of the vibrational levels are shown in Fig. II-15. A specific excitation path is also shown as an example in the figure. The rotational states at resonance with the laser through the R-branch transition of the 2944 cm^{-1} band (| 01000 >) may absorb the second photon resonantly through the P-branch transition of the 2967 cm^{-1} band (| 01010 >) or be excited to the $v = 2$ states of the 2987 cm^{-1} band (| 00200 >). Sequentially, a variety of transitions exist for absorbing the third photon, since the $v_{CH} = 3$ states are broad and there are so many of them.

Fig. II-15. Vibrational level diagram and MPD excitation mechanism of EtCl. Only the pure CH stretching levels are sketched. Seven photons are required for dissociation. Anharmonicity is compensated by the spread of the 5 CH stretching modes. Excitation is resonant in the discrete region and in the quasicontinuum. A pathway $|00000\rangle \rightarrow |01000\rangle \rightarrow |01010\rangle$ or $|00200\rangle$ etc. $\rightarrow |01011\rangle$ etc. is indicated by arrows.

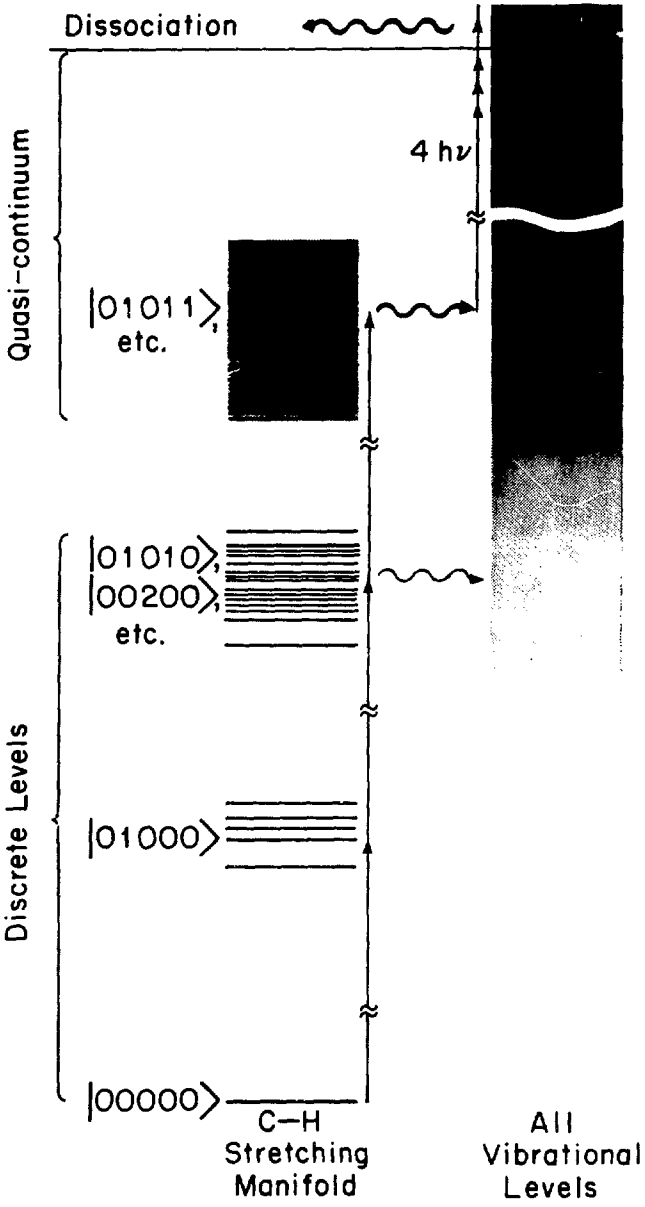
Dissociation
4 hν
Quasi-continuum
|01011⟩,
etc.
|01010⟩,
|00200⟩,
etc.
Discrete Levels
|01000⟩
|00000⟩
C—H
Stretching
Manifold
All
Vibrational
Levels

Fig. II-15

F. A Rate Equations Model for MPD

1. The Model

A rate equations approximation has frequently been used for dynamics in the quasicontinuum.[23,25,26,53-57] It has been shown that the rigorous Schrödinger equation can be reduced to a set of rate equations for transitions in the energy range for which the molecular linewidth, $\Delta\nu_{mol}$, is much greater than the optical transition rate and this rate is in turn much larger than the inverse level density.[25,26]

$$\Delta\omega_{mol} \gg \omega_R \gg \rho_{vib}^{-1} \qquad \text{(II-2)}$$

Thus rate equations may be safely applied to levels in the quasicontinuum and the continuum.

For ethyl chloride MPD rate equations can clearly be used to describe the transitions from $v_{CH} = 2$ upward. For the 2→3 transitions, the molecular linewidth of about 30 cm^{-1} and the inverse level density of 10^{-3} cm^{-1} at $v_{CH} = 3$ satisfy Equation (II-2) very well for a wide range of powers. At 100 MW/cm^2 (1.0 J/cm^2) the Rabi frequency is between 0.05 and 0.36 cm^{-1} depending on which mode is excited. For $v_{CH} = 2$ with $\Delta\omega_{mol} = 1.2$ cm^{-1} and $\rho_{vib}^{-1} = 0.02$ cm^{-1}, Equation (II-2) hold fairly well but with much smaller margins on the inequalities. It should be noted that the direct count of states used for ρ_{vib} underestimates the density to the extent that vibration-rotation interaction makes K a poor quantum number. Notice that even though Equation (II-2) may hold, that since

$\Delta\omega_{mol}$ is less than the spacing between absorption lines $v_{CH} = 1 \rightarrow 2$ for a single rotational state, a rotational bottleneck exists. Only for absorption to $v_{CH} = 3$ and higher where $\Delta\nu_{mol}$ is greater than an entire rotational branch width is the rotational bottleneck completely removed.

The $v_{CH} = 1$ level is clearly discrete and therefore the detailed time dependence of that level cannot be correctly described by rate equations under the conditions of these MPD experiments. However, since the Rabi frequencies are so much larger than the inverse pulse width, coherence effects on the dissociation yield should not be large and the use of rate equations for calculating quantities time integrated through the laser pulse should be reasonably accurate. For simplicity, the rate equation treatment is extended to the $0 \rightarrow 1$ transition. The usefulness of the model is limited more by an approximate knowledge of the optical cross sections than by neglect of coherent effects.

In the rate equations model, the absorption and reemission of single photons are treated as an harmonic oscillator incoherently driven by the radiation field. For those ethyl chloride molecules in resonance with the laser, the time evolution of the population fraction, N_ℓ, of molecules with ℓ photons of energy is given by the rate equation

$$\frac{dN_\ell}{dt} = (\sigma^a_{\ell-1,\ell} N_{\ell-1} + \sigma^e_{\ell+1,\ell} N_{\ell+1}) \frac{I}{h\nu}$$

$$- (\sigma^a_{\ell,\ell+1} + \sigma^e_{\ell,\ell-1}) \frac{I}{h\nu} N_\ell - k_\ell N_\ell, \qquad \text{(II-3)}$$

where I(t) is the laser intensity, $\sigma^e_{\ell+1,\ell}$ is the stimulated emission cross section from level $\ell+1$ to ℓ, $\sigma^a_{\ell,\ell+1}$ is the absorption cross section from ℓ to $\ell+1$, and k_ℓ is the unimolecular dissociation rate constant for molecules having energy $\ell h\nu$. Values of $\sigma^e_{\ell+1,\ell}$ were obtained from

$$\sigma^e_{\ell+1,\ell} = \sigma^a_{\ell,\ell+1} \, (g_\ell/g_{\ell+1}) \qquad \text{(II-4)}$$

where g_ℓ is the degeneracy of the ℓth level and the ratio $g_\ell/g_{\ell+1}$ in the quasicontinuum is the ratio of vibrational level densities. The ratio increases smoothly from $g_2/g_3 = 0.053$ to $g_{12}/g_{13} = 0.36$. Levels up through $\ell = 15$ were included in the calculation.

Only a fraction, Q_{01}, of the molecules in the irradiation zone is sufficiently resonant with the laser for transition to $v_{CH} = 1$ to be possible. Q_{01} depends on power broadening and thus varies during the pulse. For each time interval from t to t + dt during the pulse the fraction $\dot{Q}_{01}(t)dt$ of molecules starts to interact with the laser. Only a part, P_{12}, of those molecules which have been excited to $\ell=1$ will have a $1\rightarrow2$ transition in resonance with the laser. For molecules at $\ell\geq2$ no bottleneck exists. The dissociation probability, $P_d(t)$, for a molecule which start interacting with the laser from time t is obtained as

$$P_d(t) = \sum_{\ell\geq7} \int_t^{\tau_c} N_\ell k_\ell \, dt', \qquad \text{(II-5)}$$

where τ_c is the average time between collisions. Thus the dissociation yield is

$$W_d = P_{-?} \int_0^{\tau_{max}} P_d(t)\dot{Q}_{01}(t)dt. \qquad \text{(II-6)}$$

The integration was carried up to the time of maximum laser intensity, τ_{max}. Some molecules that come into resonance with the laser shortly before τ_{max} will be out of resonance shortly after τ_{max}. However, this does not cause an overestimate of W_d since the fraction of these molecules is small and since it is predominantly those molecules excited early in the pulse which dissociate. The experimental increase of W_d as $E_p^{3.5}$ shows that nearly all molecules which dissociate must be excited early in the pulse. Molecules excited beyond the midpoint must have a dissociation probability about $(0.5)^{3.5} = 0.09$ that of molecules at resonance from near the beginning of the pulse.

The same argument can be used to exclude the possible contribution to excitation from collision-induced rotational hole filling: as the population of those rotational states in resonance with the laser is depleted by optical excitation, collision-induced rotational relaxation puts more molecules into those resonant rotational states. Because the excitation pulse is short and the pressure relatively low there is little effect of rotational hole filling on excitation in the discrete range. The measured pressure broadening cross section of 84 $Å^2$ gives an upper limit on the rotational relaxation rate of 12 μs^{-1} $Torr^{-1}$.[58] Thus

during the rising portion of the laser pulse less than 16% of the molecules undergo rotationally inelastic collisions at the 1.7 Torr pressure of most experiments. Even at the maximum pressure of 6 Torr in Fig. II-12, the effect of rotational hole filling should be small; the pulse is still shorter than the minimum time between inelastic collisions. By contrast vibrational relaxation and quenching of dissociation depends on the ratio of inelastic collision rates to unimolecular dissociation rates.

There is much experimental evidence which indicates that highly vibrationally excited molecules lose several thousand cm^{-1} of vibrational energy per gas kinetic collision.[59] The step size for vibrational relaxation of $C_2H_4Cl_2$ was estimated to be about 10 kcal/mole or 3500 cm^{-1}.[43] Thus it is reasonable to expect that quenching of a full quantum from level ℓ to ℓ-1, $\ell \geq 7$, will occur with a hard sphere cross section of 53 $Å^2$. The hard sphere cross section was calculated from van der Waals b constant.[60] For 3000 cm^{-1} energy increments the rate of dissociation increases steeply with excitation level, Fig. II-1, so that if collisions compete with dissociation to deactivate level ℓ to ℓ-1 then level ℓ-1 will subsequently be quenched with almost unit efficiency to below the dissociation threshold. In the model calculation dissociation is simply terminated at an elapsed time equal to the inverse hard sphere collision rate of 7.7 μs^{-1} $Torr^{-1}$.

2. Evaluation of Parameters

The effective cross section, σ^a_{01}, for 0→1 excitation of a single vibration-rotation line is estimated from the integrated cross section measured for the entire branch divided by the laser linewidth, $\Delta\omega_\ell$, and the number of lines per initial rotational state in the branch.

$$\sigma^a_{01} = \frac{2.3 \cdot \int_{\text{rot. branch}} A \, d\omega}{nbN_t \Delta\omega_\ell} \qquad \text{(II-7)}$$

where N_t is the total number density of the molecule, b is the absorption cell length, and n is the number of lines for a single rotational state in the integrated rotational branch. For a parallel band and for the Q branch of a hybrid band n = 1, for perpendicular n = 3, and n = 4 for hybrid bands non-Q branches. In case the transition linewidth $\Delta\omega_{mol.}$ is broader than $\Delta\omega_\ell$, $\Delta\omega_\ell$ should be replaced with $\Delta\omega_{mol}$. in Equation (II-7). σ^a_{01} calculated for several selected frequencies are listed in Table II-2.

It is difficult to directly measure the absorption cross section in the QC. However, an average effective cross section for $\ell \to \ell+1$ transition, $\sigma^a_{\ell,\ell+1}$, can be estimated from the integrated absorption of the fundamental. In the case that the oscillator strength of the $\ell \to \ell+1$ transition is from a single vibrational mode,

$$\sigma^a_{\ell,\ell+1} = \frac{2.3 \cdot \int A_{01} d\omega \cdot \ell_{QC}}{bN_t n_r \Delta\omega_{mol.}} \cdot \frac{n_r \Delta\omega_{mol.}}{\omega_t (\ell \to \ell+1)} \qquad \text{(II-8)}$$

where $\omega_t(\ell\rightarrow\ell+1)$ is the overall bredth of the $\ell\rightarrow\ell+1$ transition, n_r is the total number of lines for a single rotational state in the vibrational band and ℓ_{QC} is the starting level of the QC. At ℓ_{QC} the intramolecular vibrational relaxation is much faster than the optical pumping rate that the absorption of photons can be viewed as going through the $\ell_{QC}-1\rightarrow\ell_{QC}$ transition. Even though ℓ increases as the molecule absorbs more photons, $v_{pump\ mode}$ should still be $\ell_{QC}-1$ since the excess energy, $\ell h\nu-(\ell_{QC}-1)h\nu$, is statistically distributed among other vibrational modes.[20,75,76] At levels $\ell \geq \ell_{QC}$, $\Delta\omega_{mol.}$ must be broad enough to form a smooth spectrum over the range of ω_t. The factor $n_r\Delta\omega_{mol.}/\omega_t$ simply depicts the number of rotational lines that would be in resonance with the laser. The absorption cross section integrated over the entire CH stretching range for sequential transitions to higher levels should be very close to that for the fundamental, 1.5×10^{-17} cm/molecule. It should increase slightly due to excitation of a mode already excited as ℓ increases. For $\ell>2$ individual transition lines with very broad linewidth form a single vibration-rotation state overlap to form a smooth spectrum, Sec. D. Therefore,

$$\sigma^a_{\ell,\ell+1} \approx \frac{2.3 \cdot \int_{\text{all C-H modes}} A\, d\omega}{bN_t\omega_t} \qquad \text{(II-9)}$$

where ω_t, the overall bredth of the CH stretching region, is about 150 cm^{-1} for the fundamental and should not greatly increase as ℓ increases through the quasicontinuum. Near the center of the CH stretching region

$\sigma^a_{\ell,\ell+1}$ may be twice the strength of the average value as indicated by the fundamental spectrum. All of these considered, σ^a_{23} is estimated to be $\geq 2 \times 10^{-19}$ cm^2 near the center of the CH stretching region. As ℓ increases, the slight increase of integrated absorption should be offset by the small increase of ω_t, therefore $\sigma^a_{\ell,\ell+1}$ are of the same magnitude as σ^a_{23}. Although the number of individual transitions sharing the CH oscillator strength increases with ℓ, these transitions all overlap and correspondingly more of them are resonant with the laser. Thus the effective cross section should remain approximately constant.

For the 1→2 transition the spectrum is quite complicated. At 2913 cm^{-1}, half the frequency of a Q branch in the 0→2 spectrum, it is guaranteed that a molecule which is excited from 0→1 will be in resonance at 1→2, i.e., P_{12} (2913 cm^{-1}) = 1. The yield at frequencies corresponding to the adjacent P and R branches of the overtone, Fig. II-8, is about half that at 2913 cm^{-1} and thus P_{12} is chosen to be 0.5. P_{12} can also be crudely estimated as $\Delta\omega_{mol.}$·(total number of transitions)/ω_t. Very roughly then the CH stretching region is about half covered by the lines of the 1→2 transition from a single rotational state as discussed in Sec. D. Therefore, the absorption cross sections should be about double those for 2→3. The value of 5×10^{-19} cm^2 was chosen since the laser wavelengths were closer to the stronger central part of the spectrum.

The fraction of molecules which can interact with the laser through the fundamental transition is

$$Q_{01}(t) \approx n\,[(a(t) + 1)\,\omega_R(t) + \Delta\omega_\ell]/\omega_{VB}, \qquad \text{(II-10)}$$

where ω_{VB} is the FWHM of the rotational branch excited. The power broadened molecular width $\omega_R(t)$ is $\mu \cdot E/\hbar$ for the narrow-band laser and is corrected for off-resonance for the broad-band laser by the formula $\sqrt{\omega_R^2(t) + (\text{off-resonance})^2}$ [4]. If the pulse energy up to time t, E(t), does not saturate the transition, the effective range for laser excitation is just $\Delta\omega_\ell + \omega_R(t)$. More often E(t) saturates transitions over a range for saturation $a\omega_R$ estimated to be

$$a(t) = [(E(t)/E_{sat})-1]^{1/2} \qquad \text{(II-11)}$$

with $E_{sat} = h\nu/2\sigma_{01}$ and σ_{01} the absorption cross section for a linewidth ω_R.

Equation (II-11) is derived in general for an absorption line with a Lorentzian lineshape

$$g(\nu) = (\frac{\Delta\nu}{2\Pi})[(\nu - \nu_o)^2 + (\frac{\Delta\nu}{2})^2]^{-1}, \qquad \text{(II-12)}$$

where $\Delta\nu$ is the FWHM and ν_o is the center frequency. If the absorption cross section at the line center is σ_o, then the absorption cross section at ν may be expressed as

$$(\nu) = \sigma_o\left[1 + \frac{4(\nu - \nu_o)^2}{\Delta\nu^2}\right]^{-1}. \qquad \text{(II-13)}$$

The laser fluence E can saturate a transition with absorption cross section $\sigma(\nu_{sat}) = h\nu/2E$. Therefore, the range for saturation of the

Lorentzian line is defined by the equation

$$\frac{h\nu}{2E} = \sigma_o \left[1 + \frac{4(\nu_{sat} - \nu_o)^2}{\Delta\nu^2} \right]^{-1} , \qquad \text{(II-14)}$$

and the range $a\Delta\nu$ is

$$a\Delta\nu = 2(\nu_{sat} - \nu_o) = \Delta\nu(\frac{2\sigma \cdot E}{h\nu} - 1)^{1/2}. \qquad \text{(II-15)}$$

RRKM theory was used to calculate the dissociation rate constants k_ℓ, Sec. A. The laser pulse shape I(t) was digitized into twenty 1 ns blocks matching the experimental pulse. The integration of the fifteen coupled Equations (II-3) and Equations (II-5) and (II-6) was done for each picosecond increment using a modified version of the program of Schulz et al.[61] The modified program in Fortran is listed in Appendix I.

G. Absorption Cross Section and Excitation Distribution

The experimental dissociation yields are compared with those calculated from the model described above, Table II-2. The discrete region parameters are fixed as described in the preceding section. A constant value of 2.5×10^{-19} cm^2 for $\sigma^a_{\ell,\ell+1}$ in the quasicontinuum, $\ell \geq 2$, matches the absolute magnitude and experimental trends of the data fairly well between 2910 and 2980 cm^{-1}. The ranges of quasicontinuum cross section values for an exact fit to the experimentally observed range of W_d are small and mostly overlapping. The magnitude of the cross section is only slightly larger than the average cross section estimated for the central part of the spectrum in the preceding subsection. For these wavelengths near the center, values larger than the average should be expected. Furthermore, anharmonicity will shift the peak absorbance to longer wavelength as ℓ increases. This expectation is born out by the quasicontinuum cross sections which fit the 3014 and 2829 cm^{-1} data at the blue and red ends of the spectrum. The quasicontinuum cross sections are smaller than the calculated average value for the central region and the value is smaller to the blue than to the red.

Since there are about six sequential absorptions in the quasicontinuum and the continuum before dissociation, the calculated yield varies as a strong function, third to fourth power, of this cross section (Table II-7, rows 1-3). The value of σ^a_{12} was fixed only roughly by knowledge of the spectrum. Fortunately, the yield is not a strong

Table II-7. Test calculations using different sets of absorption cross sections in the quasicontinuum for 1.7 Torr ethyl chloride excited by 1.1 J/cm^2 of broadband laser radiation at 2977 cm^{-1}.

Set	σ^a_{23} 10^{-19}cm^2)	σ^a_{78} (10^{-19}cm^2)	$\sigma^a_{11,12}$ (10^{-19}cm^2)	$W_{d,cal}$ (%)
(1)	1.0	1.0	1.0	0.04
(2)	4.2	4.2	4.2	6.6
(3)	2.1	2.1	2.1	0.9
(4)[a]	4.2	1.2	0.44	0.9
(5)[a]	8.4	0.8	0.12	0.9

[a] $\sigma^a_{\ell,\ell+1}$ decrease exponentially from σ^a_{23} to $\sigma^a_{14,15}$.

function of this parameter since it involves only a single excitation step. A factor of two increase in calculated yield results from a factor of four increase in σ^a_{12}. The yield is directly proportional to the factor P_{12}. Reasonable arguments can be made for P_{12} in the range 0.3 to 0.6. It should certainly vary somewhat with wavelength and may approach 1 at a few specific wavelengths in addition to 2913 cm^{-1}. A consistent spectroscopic model does require that when averaged over the CH stretching region $\sigma^a_{12} \cdot P_{12} \approx \sigma^a_{23}$. Thus the uncertainties of the discrete region parameters do not have a large effect on the quasicontinuum cross sections derived.

Owing to the effects of power broadening and saturation on Q_{01}, the calculated yield has a stronger dependence on σ^a_{01}, even though 0→1 is the lowest transition below dissociation. Among the many calculations performed, it is found that $W_{d,cal}$ is approximately proportional to σ^a_{01} for the rotational branches with similar ω_{VB}. It is obvious from Equation (II-10) that $W_{d,cal}$ is inversely proportional to ω_{VB}. Since $\sigma^a_{01}(\omega_\ell/\omega_{VB})$ is directly proportional to A_{01}, the measured integrated absorbance of the 0→1 transition, then $W_{d,cal}$ is proportional to A_{01}. In Figs. II-8, 9, and 10 it was shown experimentally that $W_d \propto A_{01}$. This is a strong support for the model treatment of resonant excitation in the discrete region.

The one effect on dissociation yield which is not treated well by the model is the factor of two decrease in W_d when broadband rather than narrowband excitation is used near 2977 cm^{-1}, Table II-2. The

larger cross section and larger power broadening for the narrow band laser outweight the increase in number of rotational levels with which the broadband laser can interact. The first two factors dominate by a modest amount in the model calculation and by a factor of two in the experiment. There is some deficiency in the treatment of this difference of excitation sources in the discrete range.

The dependences of energy absorbed and of dissociation yield on fluence are compared with the experimental results, Figs. II-5 and II-11. Calculations were made with constant cross sections and with cross sections which decreased exponentially with ℓ, Table II-7. The calculated dependence of W_d on fluence is in reasonable accord with the data both as to slope and magnitude. However, it seemed that as long as the set of $\sigma^a_{\ell,\ell+1}$ generates the correct magnitude for dissociation yield, the slopes of fluence dependence curves are rather insenitive to the variation of the trend of $\sigma^a_{\ell,\ell+1}$. The experimental values of W_d and their dependence on fluence could be fit even with such cross sections as set 5 but only by using values for σ^a_{23} which were unreasonably large by comparison to the observed fundamental spectrum. The optoacoustic signal increases almost linearly with fluence as shown by the dashed line of unit slope in Fig. II-5. The calculated curves show the same linearity at the low fluence end but start to deviate just slightly from the experimental points at higher fluences. Again, both the set 3 and set 4 cross sections gave reasonable fits.

It was experimentally observed that the fluence dependence of dissociation is a high power function and yet the dependence of absorption is almost linear. This is a very interesting phenomenon and an important characteristics for multiphoton processes. Such fluence dependences were also observed for the fluence range before reaching saturation for SF_6 under 10 μm radiation.[7,63] The reproduction of such fluence dependences by the rate equations calculation provides additional support for the model.

More inferences concerning the absorption cross sections can be drawn from the fluence dependence of absorption. Contributions to the optoacoustic signal mainly come from two groups of EtCl molecules that absorb under the 3.3 μm radiation. One group of molecules may undergo 0→1 transition but does not have a 1→2 transition in resonance with the laser (this group accounts for the portion of molecules, $Q_{01} \cdot P_{12}$). Their absorption certainly has a linear fluence dependence at very low fluences and saturates above $E_{sat.\ linear}$. The other group of molecules may find their way into the QC and their absorption contributes predominantly to the optoacoustic signal at higher fluences. The absorption of this group of molecules can be written analytical as

$$\text{Optoacoustic Signal} \propto \text{Total Energy Absorbed, } E_{abs.} = \sum_{\ell} \ell h\nu N_{\ell}, \qquad \text{(II-16)}$$

where N_{ℓ} is time dependent during the laser pulse. The time derivative of $E_{abs.}$ is

$$\frac{dE_{abs.}}{dt} = \sum_{\ell} \ell h\nu \frac{dN_{\ell}}{dt} \quad . \tag{II-17}$$

The rate equation expression for dN_{ℓ}/dt is used but the dissociation term, which is related to the "saturation" (level-off) of the absorption curve is neglected. Then

$$\frac{dE_{abs.}}{dt} = \sum_{\ell}(\sigma^{a}_{\ell,\ell+1} - \sigma^{e}_{\ell,\ell-1})I(t)N_{\ell} \cong \sum_{\ell} \sigma_{\ell} I(t)N_{\ell}(t). \tag{II-18}$$

Now it is clear that if σ_{ℓ} are constant or only approximately constant over a significant range of large ℓ values, after integration

$$E_{abs.} \cong \sigma_{\ell} \cdot (N_t \cdot P_{12} \cdot \int \dot{Q}_{01} dt)\ E_{laser}. \tag{II-19}$$

Therefore, the optoacoustic signal would be linearly proportional to the laser fluence E_{laser} if the absorption cross sections in the QC are approximately constant. On the other hand, any drastic change of absorption cross sections in the QC may cause the fluence dependence to deviate from linear. Any deviation could be used to monitor the variation of σ_{ℓ} in the QC.

The discrepancies between the experiments and the calculated curves in Figs. II-5 and II-11 might be partially caused by the approximate treatment of the laser spatial profile. In principle, the experimental fluence dependences should be deconvoluted from the spatial variation of fluence in the laser profile.[25,62] The effect of

deconvolution on the shape of the fluence dependence curve was estimated by integrating the calculated dissociation yield (solid curve of Fig. II-11) over the measured laser profile. The ratio, $W_d(1.1\ J/cm^2)/W_d(0.5\ J/cm^2)$, is reduced less than 5% by integration over the focal plane profile and reduced less than 20% by integration over the entire irradiation zone. Thus the tedious and uncertain deconvolution was not carried out. The fact that the magnitudes of dissociation yield and absorption are fit by the calculation means that the calculated distribution and assumed cross sections cannot be badly in error.

The excitation distribution calculated by rate equations for EtCl molecules at the end of the 1.4 J/cm^2 broadband 2977 cm^{-1} pulse is shown in Fig. II-16. Previously, a thermal distribution was suggested by Black et al. as a good approximation for an ensemble of molecules undergoing MPA.[70] A rate equations calculation by Grant et al., gave the excitation distributions which were narrower and differently shaped from thermal ones.[23] Certainly, the distribution calculated from rate equations depends heavily upon the set of cross sections used. In Fig. II-16 the distribution of the entire ensemble of molecules can hardly be characterized with a single temperature, since there are three distinct groups of EtCl molecules in the irradiation volume. One group, stuck in v = 0, contains molecules in the rotational states that do not have a 0→1 transition in resonance with the laser. The second group contains molecules excited to v = 1

Fig. II-16. Calculated population distribution at the end of the 1.4 J/cm^2 braodband 2977 cm^{-1} pulse is indicated by the blocks. a) and b) are calculated with the constant set (3) and the exponentially decreasing set (4) $\sigma^a_{\ell,\ell+1}$ of Table II-7, respectively. Molecules which have dissociated from the levels $\ell \geq 7$ are included in these levels. The curves are the best fitting thermal distributions at the designated temperatures.

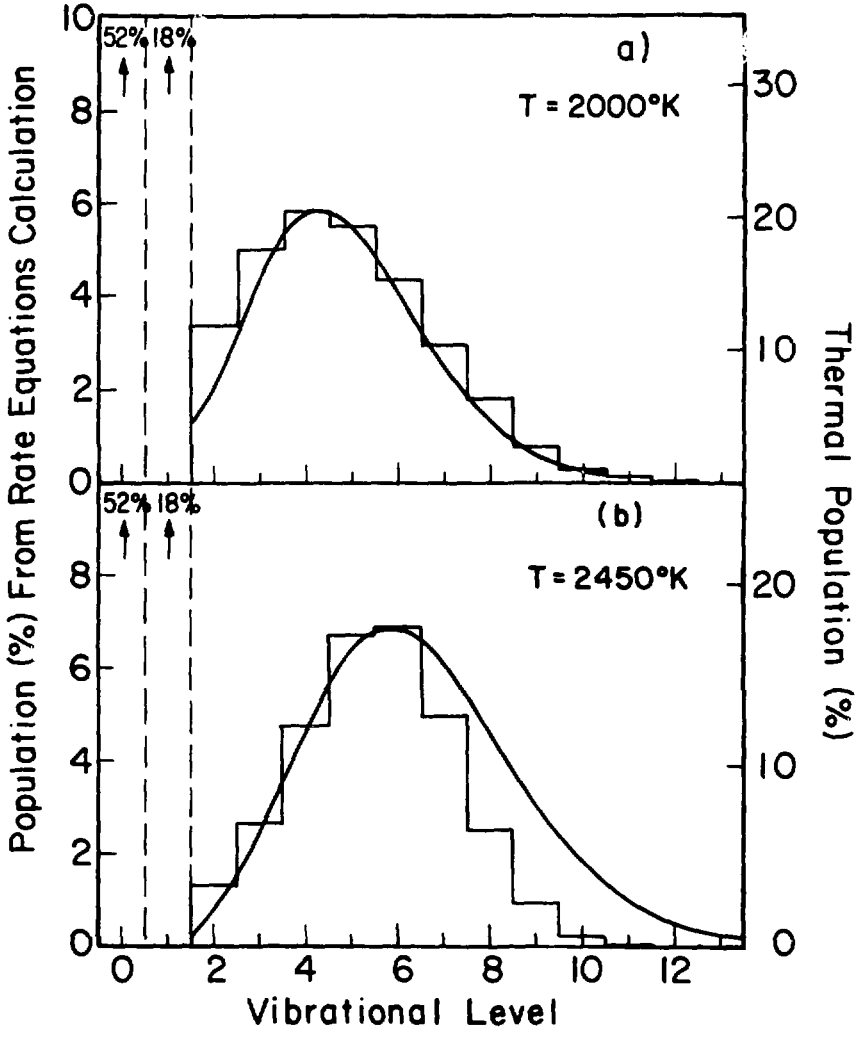
52%
18%
a)
T = 2000°K
52%
18%
(b)
T = 2450°K
Population (%) From Rate Equations Calculation
Thermal Population (%)
Vibrational Level
0
2
4
6
8
10
12
10
20
30

Fig. II-16

but do not have a 1→2 transition in resonance with the laser. Only for the third group, molecules which enter the QC, can a comparison between the calculated and thermal energy distributions be made.

The thermal distribution is

$$N_{\ell}(\text{thermal}) = \rho_{vib.} e^{-(E/kT)} / \sum_{\ell} \rho_{vib.} e^{-(E/kT)} . \qquad \text{(II-20)}$$

Thermal distributions at 100 K intervals were compared to the peak postion and the shape of the two rate equations calculations. The best fitting thermal distributions at the designated temperatures were plotted in Fig. II-16. Thermal curves for temperatures 100 K higher or lower were significantly different. The rate equations calculation with the set of exponentially decreasing cross sections produced a narrower and differently shaped 'istribution from the thermal one. The deviation is larger on the high energy side of the distribution. However, the calculation with constant absorption cross sections in the QC can be fitted well by a thermal distribution. This should not be surprising since it was stated that an incoherently driven harmonic oscillator reaches a Planck distribution function at a well-defined temperature determined by the total energy absorbed.[64] The deviation from a thermal distribution at the lower levels in Fig. II-16(a) is caused by the larger cross section 1→2 transitions than those for higher transitions.

The calculation also reproduced the general features of the pressure dependence of dissociation, i.e. a factor of two decrease in

yield from 0.2 to 2 Torr but a ~10% decrease from 2 to 6 Torr. The sensitivity of the pressure dependence to the assumed cross sections is shown in Fig. II-12. In this case, the dissociation yields calculated with constant $\sigma^a_{\ell,\ell+1}$ gives a better match with the measured pressure dependence.

Within the fluence range of Fig. II-5, the calculated <n> depends more strongly on the lower part of the quasicontinuum transition cross sections. In contrast, the pressure dependence of W_d depends on the excitation distribution above the dissociation threshold and therefore on the cross sections in the continuum. The facts that set 3 cross sections fit better with pressure dependence of W_d and that set 4 fits better with optoacoustic measurements suggest that $\sigma^a_{\ell,\ell+1}$ decreases slightly in the lower part of the quasicontinuum as ℓ increases and approaches a constant value near the continuum. In any case, a more complicated functional form is probably needed to describe the modest variation of $\sigma^a_{\ell,\ell+1}$ with ℓ.

Such complexity in describing the trend of absorption cross sections in the quasicontinuum was exhibited in a double resonance experiment measuring absorption cross sections of excited SF_6.[65] It was also qualitatively shown that different trends of $\sigma^a_{\ell,\ell+1}$ as ℓ increases may be expected depending on different pump mode anharmonicities and line broadening behaviors.[55] For SF_6[23] and $CHClF_2$[54] sets of decreasing quasicontinuum cross sections were assumed for MPD calculations. For these molecules a gradual but substantial line

broadening as ℓ increases might cause such a trend. For EtCl, however, the linewidth of a vibration-rotation state has been broadened to be comparable to the vibrational bandwidth of $v_{CH} = 3$. The many broadened C-H transitions overlap and cover a total range much larger than the broadening even at high ℓ. Therefore, the variation of $\sigma^a_{\ell,\ell+1}$ should be small. For SF_5NF_2, which has several strong absorption bands near 11 μm and a low molecular symmetry, excitation in the quasicontinuum by CO_2 laser is similar to that of EtCl at 3.3 μm. The phenomenological absorption cross section, $\sigma = \langle n \rangle h\nu/\text{fluence}$, of SF_5NF_2 was found to be nearly constant over five orders of magnitude of fluence.[66] Most recently, in a theoretical study with a series of Bloch equations for MPD of CF_2CFCl,[67] it was found that absorption cross sections which decrease sharply at the lower levels and approach a constant value at higher levels generated results in good agreement with the experimental dissociation dependence on laser intensity and on buffer gas pressure. The trend of the absorption cross section coincides well with the broadening of the assumed homogeneous linewidth as the transition goes upwards. From Equation (II-8) the relation $\sigma^a_{\ell,\ell+1} \cdot \omega_t(\ell \to \ell+1) \approx$ constant can be obtained. $\omega_t(\ell \to \ell+1)$ can be approximated by $\omega_t(0 \to 1) + \Delta\omega_{mol.}$. Since $\Delta\omega_{mol.}$ generally increases sharply for the lower transitions and less drastically for the higher ones,[17,18] it is reasonable to anticipate that $\sigma^a_{\ell,\ell+1}$ decreases more for lower transitions and less for higher ones.

Combined with the experimental wavelength dependence of dissociation, the success of the model calculation not only demonstrates the significance of the resonant excitation mechanism, but also indicates the usefulness of the absorption cross sections, both in the discrete region and in the quasicontinuum, calculated from the ordinary linear spectra. The excitation distribution strongly depends upon the magnitude and the trend of absorption cross sections in the QC. As these absorption cross sections approach a constant value, thermal distribution becomes a good approximation for the excitation distribution in the QC.

H. 3.3 μm vs 10 μm Excitation

The variety of molecular structures, of energy level patterns and of excitation wavelengths available in nature assures that there will be a great variety of multiphoton dissociation mechanisms and phenomena. The importance of vibrational spectroscopy to MPD was also stressed and discussed with more examples in a recent review article.[69] The sharp structure in the MPD spectrum of C_2H_5Cl at 3.3 μm contrasts with the broadened spectra exhibited by SF_6 at 10 μm. C_2H_5Cl is more easily dissociated by excitation of bands at 3.3 μm than at 10 μm; for $CHClF_2$ the reverse is found. The different MPD behaviors of these molecules may be understood in terms of their different discrete level structures. Furthermore, one can predict from ordinary absorption spectra whether, and at which frequencies, sharp resonances will be found in MPD yield spectra.

The most interesting new feature experimentally observed for EtCl MPD at 3.3 μm is the occurrence of sharp peaks in MPD yield (W_d and W_d/A_{01}) at frequencies given by ordinary spectra. This observation is a result of the small number of photons required to reach the QC and the existence of a resonant path for excitation. Since the vibrational level density is relatively high at $v_{CH} = 3$ and the 2→3 transition linewidth is very broad, the use of 3.3 μm radiation assures that the QC is reached at the absorption of the third photon. The sharp structure in the yield spectrum matches the fundamental spectrum because all levels $v_{CH} \geq 2$ are significantly

broadened. Anharmonicity is compensated by involving several nearly degenerate C-H modes in the discrete region. Power broadening is not necessarily required for anharmonicity compensation and only modest intensities are needed for excitation. Thus the sharp features of EtCl are preserved. In contrast, the more familiar 10 μm excitation requires up to three times as many photons to reach the QC. The 10 μm MPD spectrum is red shifted and broadened by the need to compensate for anharmonicity through the discrete levels, such as rotational compensation and power broadening. When several step-by-step resonances exist by coincidence, the MPD yield spectrum will be a convolution of the spectra of the several discrete steps.

Ethyl chloride may be dissociated at either 3.3 μm or 10 μm. The yield under comparable conditions is, however, much higher for the 3.3 μm excitation, Table II-2. The R(8) CO_2 laser line excites the center of the P branch of the 974 cm^{-1} band; it should be one of the most effective wavelengths for dissociation in that band. The rate equations model may be used to compare the rate excitation through the quasicontinuum for 3.3 and 10 μm excitation. Table II-8 compares the probabilities for excitation from an initial level of 6000 cm^{-1} to dissociation. The calculated probabilities for dissociation are actually smaller for 1.1 J/cm^2 at 2977 cm^{-1} than for 6 J/cm^2 at 968 cm^{-1}. Thus it is clear that the twenty times smaller dissociation yield for 10 μm excitation is caused by a severe bottleneck in the discrete region. This bottleneck is also responsible for the

Table II-8. Calculated probability for excitation through the quasicontinuum, 6,000-19,600 cm^{-1}.

ν (cm^{-1})	$\Delta\ell$[a]	$\sigma^a_{\ell,\ell+1}$ ($10^{-19} cm^2$)	Dissociation Probability[b] 1.1 J/cm^2	6 J/cm^2
2977	5	2.5	0.38	--
968	15	2.5[c]	0.09	0.99

[a]Number of photons needed to exceed the dissociation limit.

[b]The effects of collision were excluded in the calculation.

[c]$\sigma^a_{\ell,\ell+1}$ ($\ell \geq 6$) at this frequency can be estimated as 2.5×10^{-18}. $\ell_{QC}/\omega_t(\ell \rightarrow \ell+1)$ cm^2. (c.f. Table II-3 and Eq. (II-8)). ℓ_{QC} should be ~6-9. ω_t is ~40 cm^{-1} for the 0→1 transition and should increase as ℓ increases. Therefore it is reasonable to use the same value as in the 3.3 μm region.

saturation in the optoacoustic response to 10 μm excitation above 0.1 J/cm^2, Fig. II-6. No such saturation occurs at 3.3 μm, Fig. II-5, where the resonant excitation channel exists.

Resonances with widths of 5-20 cm^{-1} have been reported for multiphoton excitation and dissociation spectra. A peak about 10 cm^{-1} wide has been detected in the multiphoton excitation optoacoustic spectrum of cyclopropane at the 3102 cm^{-1} Q branch which has an 8 cm^{-1} width in the linear absorption spectrum.[34] The excitation mechanism for cyclopropane may be similar to that for ethyl chloride. For C_2H_4 at 10 μm an MPD resonance of 10 to 20 cm^{-1} width was observed.[68] The width of the resonance is much greater than the sharp Q branch near the CO_2 laser line. The quasicontinuum in this small molecule should begin only at a high energy; even though the mode pumped is relatively harmonic, powers in the GW/cm^2 range are required for substantial dissociation. The absorption spectrum is thus strongly power broadened. For the very large molecules such as $UO_2(fhacac)_2 \cdot THF$ MPD spectra are found to be coincident with ordinary absorption spectral features.[40] In this case rotational bandwidths are negligible compared to linewidths, $\lesssim 8$ cm^{-1}, caused by coupling to the dense background of low frequency modes. The molecule, with its substantial thermal vibrational excitation, starts in the quasicontinuum and its spectrum shifts very little as it is heated to dissociation.[40]

I. Collisional Deactivation

The effects of collisions in multiphoton processes can be multiple. However, for EtCl the effect of collision-induced rotational hole filling has been discounted in Sec. F. Because of the same reasons, the short laser pulse and the relatively low EtCl pressure, vibration-vibration up-pumping during the laser pulse needs not to be considered for any of the experiments performed with 3.3 μm radiation. Collision-induced vibrational deactivation for highly excited molecules must be the most important effect and is responsible for the observed dissociation yield pressure dependence.

As EtCl pressure is increased from 0.2 to 2 Torr the fraction dissociated decreases by nearly a factor of two. Only about 10% further decrease occurs from 2 to 6 Torr. These behaviors can be quantitatively explained by the excitation distribution calculated from the rate equations model and by the competition between the RRKM dissociation rate and the hard-sphere collisional deactivation of highly excited molecules. The calculated distribution of molecules in levels above the threshold is shown in Fig. II-17. The shaded areas are those molecules which have dissociated during the pulse. The unshaded portions of the bars are those excited molecules which may either dissociate or be quenched by collisions. For pressures above 0.2 Torr nearly all $\ell = 7$ molecules are quenched. At $\ell = 8$ the calculated quenching and dissociation rates are approximately equal at 1.4 Torr. Since the unshaded area at $\ell = 8$ is approximately equal to the total shaded area,

Fig. II-17(a), the yield may be expected to decrease by a factor of two as pressure increases in this range, Fig. II-12. The observed W_d decreases even more sharply than the calculated one between 0.5 and 2 Torr before leveling off. Quenching for the ℓ = 9, 10 molecules starts to occur at pressures higher than 2 Torr. The small area of those unshaded blocks corresponds to the small decrease of yield in that pressure range. The sensitivity of the excitation distribution to the assumed cross sections is shown by comparison of Figs. II-17(a) and (b), which correspond to the two calculated curves in Fig. II-12 respectively.

The fit of experimental pressure dependence by the model calculation provides support for using a hard sphere collision cross section for vibrational deactivation, in addition to the justifications given in Sec. F. Of course, in order to use such a quenching rate, the colliding partner for the highly excited molecule should be a much cooler one. This condition is fulfilled since the calculated excitation distribution, Fig. II-16, shows that up to 70% of the molecules are at v_{CH} = 0 or 1 after the 1.4 J/cm^2 pulse.

Fig. II-17. Calculated population distribution after the laser pulse for levels above the dissociation limit. The shaded area indicates the fraction of molecules which dissociate during the laser pulse. The dissociation lifetime was calculated by RRKM theory. a) and b) are calculated with the $\sigma^{a}_{\ell,\ell+1}$ of set (3) and set (4) of Table II-7, respectively.

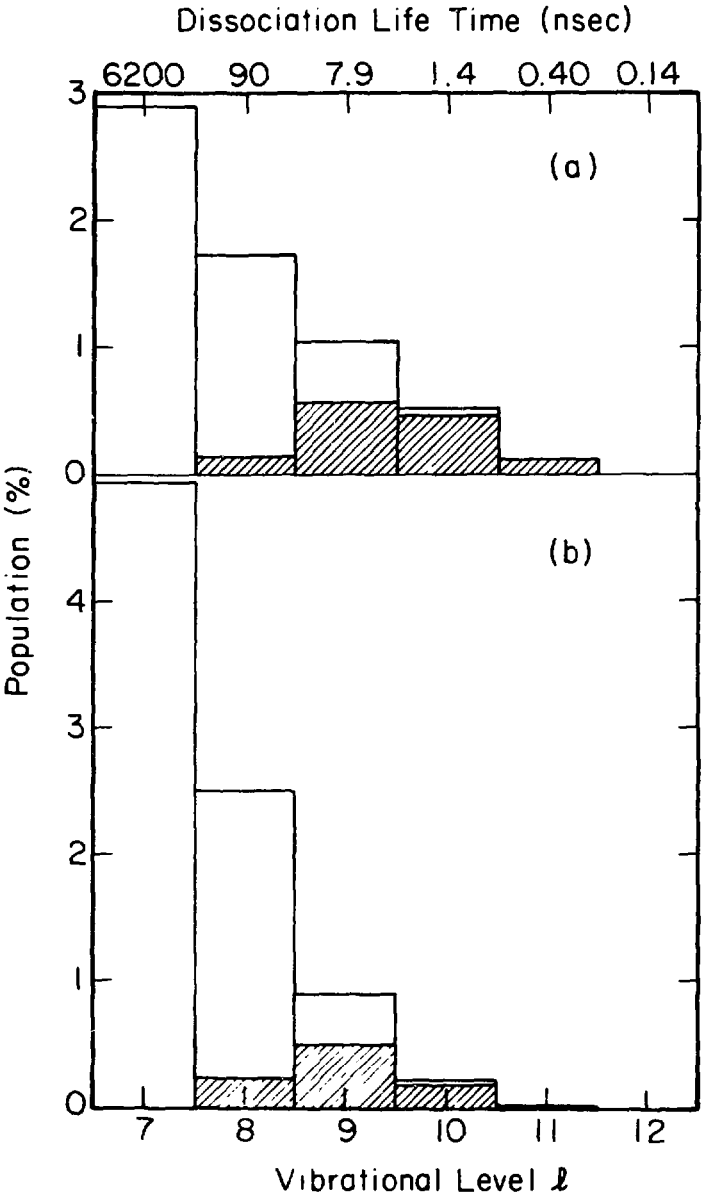
Dissociation Life Time (nsec)
6200
90
7.9
1.4
0.40
0.14
(a)
(b)
Population (%)
0
1
2
3
4
7
8
9
10
11
12
Vibrational Level ℓ

Fig. 11-17

J. Concluding Remarks

The experimental data for ethyl chloride demonstrate the importance of molecular structure and vibrational level patterns in controlling MPE and MPD. A variety in MPE and MPD phenomena comparable to the variety of vibration-rotation spectra of polyatomics should be expected. In a very recent review article, the importance of molecular spectroscopy to MPD has been recognized and illustrated.[69]

The sharp resonances in ethyl chloride MPD yield at peaks in the fundamental absorption spectrum contrast strongly with the broadened and red-shifted yield spectrum of SF_6. These resonances in ethyl chloride exist because there are several CH stretching modes in the same spectral region and because only two or three photons are required to reach the quasicontinuum. MPD resonances with structures in the first- and second-overtone spectra further demonstrate the resonant nature of the excitation mechanism. Excitation in the discrete region involves several nearly degenerate modes to compensate anharmonicity. The established model for SF_6 must be modified according to the specific molecular and spectroscopic properties to describe MPD of EtCl at 3.3 μm.

MPE and MPD may be modeled quantitatively using the rate equations analysis appropriate for the spectral properties of ethyl chloride. Most parameters in the model are fixed using independent sources of data. Normal linear ir spectroscopy gives the positions of energy levels and through their linewidths shows the onset of the quasicontinuum. Thermal dissociation kinetics data interpreted by RRKM theory

give the dissociation rates as a function of vibrational energy. Vibrational relaxation rates are taken as gas kinetic. The good fit of the experimental results on both MPE and MPD using optical cross sections close to those given by the fundamental absorption spectrum confirms the basic model for MPD. The variation of optical cross section with excitation level is small but cannot be determined in detail from the present data.

It all appears that the basic model for MPE and MPD is sound. The parameters used in the calculation were in total consistency with the knowledge of optical transitions and vibrational energy transfer, and the calculated results agree well with the experimental observations. As to the question of whether the excitation at the CH stretching modes will lead to mode-selective dissociation, there is no indication at all that the unimolecular dissociation induced by 3.3 μm MPE might be nonstatistical. The statistical RRKM dissociation rate not only generates the correct magnitude for dissociation yield, but more significantly it couples with the calculated excitation distribution to account for the pressure dependence of the yield. The very broad linewidths observed for $v_{CH} \geq 3$ overtone spectra[18] also support the use of statistical dissociation rates. These broad linewidths correspond to ultrafast rates for intramolecular relaxation.

The quality of the experiments and the calculation certainly does not allow us enough sensitivity to determine the existence of restricted intramolecular vibrational relaxation, if such restriction exists. Such nonergodic behavior may exist even though the overall reaction

rate appears to be statistical. The detection of this type of non-ergodicity through dissociation measurements relies on specific and direct coupling between the reaction coordinate and the excitation modes. From the 4-centered activated complex proposed for HCl elimination (Sec. A), it is clear that the CH stretching mode is involved in the reaction coordinate. For EtCl, C-H modes related to the CH_3 group couple more directly with reaction coordinate than do those of the CH_2 group. However, MPE in the discrete region usually excites more than one C-H mode. Even though at some well choosen frequencies the C-H modes excited all belong to one CH_n group, since EtCl has only one dissociation channel, the sensitivity for yield measurement may not be enough to allow the detection of the difference of dissociation rates resulting from pumping the two different CH_n groups.

Originally, molecular systems with several HCl elimination channels, each involved with a different CH bonds and all have comparable activation energies, were choosen to test whether any preference exists for a specific channel while exciting at a corresponding C-H fundamental band. One such molecule is 1,2-dichloropropane,[70]

$$CH_2ClCHClCH_3 \longrightarrow \begin{cases} CH_2CClCH_3 \\ \text{trans-}CHClCHCH_3 \\ \text{cis-}CHClCHCH_3 \\ CH_2ClCHCH_2 \end{cases} + HCl.$$

Although MPD was observed for this molecule under 3.3 μm radiation,[91] the project was not carried out primarily because MPE can not provide a clean excitation for any specific C-H mode even in the discrete region. Other schemes of excitation, e.g. direct excitation by a single visible photon to a C-H overtone level higher than the activation energy may be used to significantly test the possible non-ergodicity in these molecular systems.[92]

Experiments monitoring the rate of product formation may also be used to make assessment on the dissociation rates. In the rate equations model ethyl chloride molecules are produced in levels ℓ = 7, 8, 9, ... above the dissociation limit with specific total energies and corresponding lifetimes, Fig. II-17. These lifetimes decrease by large factors from one to the next, 6200, 90, 7.9, ... ns. Since the laser photon energy is much greater than the room temperature thermal spread of vibrational excitation, the actual lifetimes with respect to dissociation should be clustered about values comparable to those calculated. The sudden drop in the yield vs pressure curve followed by a plateau, Fig. II-12, is a direct consequence of this unusual lifetime distribution. A measurement, preferably by detecting the product fluorescence, of those rise times longer than the laser pulse duration as a function of wavelength (maybe even of different CH_n groups or C-H modes) would be a sensitive test of the RRKM theory parameters for the transition state. The relative populations of states above the dissociation limit would help to define more accurately

the cross sections for excitation in the continuum region. However, such a measurement may be experimentally difficult. At 1.4 J/cm^2 fluence, approximately 1.6×10^{-3} cm^3 x 2% x 3.2×10^{16} molec./cm^3-Torr x 2 Torr ≈ 2×10^{12} molec. are excited to $\ell = 8$ level for 2 Torr EtCl in the focal region. Roughly 60% of these molecules would dissociate according to RRKM rate before they are collisionally deactivated. According to some previous studies of HCl elimination reaction of chlorinated hydrocarbons, roughly two thirds of the excess energy would be in the internal degrees of freedom of the products.[52,71] By assuming that the available energy is partitioned statistically among the vibrational degrees of freedom of HCl and C_2H_4, it is estimated that the average energy in the HCl vibration is about 0.2 kcal/mole. This indicates that about 2% of the product HCl is in the $v = 1$ state. HCl has a Einstein A coefficient of 30 sec^{-1}.[72] Therefore, it is estimated that the vibrationally hot HCl would give photon flux of 2×10^{12} x 60% x 2% x 30 = 7×10^{11} photon/sec for detection. This number barely reaches the detection limit of typical ir detectors.[73]

MPE at CH stretching modes can also be used as a means to create molecular populations at high vibrational levels for kinetic studies such as the determination of the vibrational quenching rate as a function of vibrational energy. From Fig. II-17 it is conceivable that at the end of the laser pulse a significant number of molecules are excited to $\ell = 3, 4, 5 \ldots$ levels, each level separated by ~8 kcal/mole of energy. Molecules from these levels may fluoresce in near ir and visible region

from $v_{CH} = \ell$ to the vibrational ground state with a probability of approximately $1/(\Delta\omega_{mol.} \cdot \rho_{vib.})$. By monitoring the decay of this fluorescence the quenching rate of a specific vibrational level can be determined for a gaseous environment. For EtCl, roughly 10^{13} molec. can be excited to $\ell = 4$ after a focused OPO pulse. At $\ell = 4$, $\Delta\omega_{mol.}$ is ~50 cm^{-1},[18] and ρ_{vib} ~1.4 x 10^4 levels/cm^{-1}. With an Einstein A coefficient of about 10^{-2}~10^{-3} sec^{-1} for the $v_{CH} = 4 \rightarrow 0$ transition,[17] the photon flux for detection is about 10^5~10^6 photons/sec. This flux may be low for time resolution of fluorescence decay better than μsec. However, for molecules like C_2H_4, the experiment may be more feasible. MPE for C_2H_4 might be less efficient, but the fluorescence probability should be higher because of smaller $\Delta\omega_{mol.}$ and ρ_{vib}. For the $v_{CH} = 4 \rightarrow 0$ transition, there might be 10^7~10^8 photons/sec available for detection.

The pressure dependence of the dissociation yield may change with fluence. The excitation distribution is shifted to higher (lower) levels by higher (lower) pump rates at higher (lower) fluences. The lifetime distribution of dissociating molecules is consequently changed and this should result in different pressure dependent behavior. The influence of reactant pressure on the isotope selectivity, $\alpha(P)$, has been observed.[38,39,74] The variation of $\alpha(P)$ will depend on the absorption cross sections of different isotopic molecules at the excitation frequency, on the energy dependent dissociation rate and on the collisional deactivation rates. A wide range

of behaviors of $\alpha(P)$ may be anticipated. At a proper fluence the desired isotopic species, which has larger absorption cross sections, may be driven to higher levels with considerably faster dissociation rates than the undesired isotopic species. The pressure controlled collisional deactivation would then quench those molecules with longer lifetimes and thus in some pressure range isotope selectivity could increase with pressure.

The narrowness of the MPD resonances may also be utilized for laser isotope separation with small isotope shifts. However, in order to retain sharp features in MPD, either very high frequency lasers should be used or molecular systems with their QC starting at very low vibrational levels should be choosen to interact with low frequency lasers. Judging by the present development of high frequency ir lasers, it is doubtful that such an isotope separation scheme would be more economical than those developed with CO_2 lasers.

CHAPTER III. RATE EQUATIONS ANALYSIS OF VIBRATIONAL SELF-QUENCHING IN IR MULTIPHOTON DISSOCIATION OF SF_6

A. Introduction

Collisions play an important role in multiphoton excitation (MPE) and dissociation (MPD). Many collision-induced phenomena have been observed and the effect of collisions qualitatively attributed to many mechanisms: rotational relaxation during the laser pulse may bring more molecules in resonance with the laser;[31] deactivation of highly excited molecules decreases the dissociation yield;[79,80] and for small molecules vibrational up-pumping by vibration-vibration transfer can put molecules into the quasicontinuum (QC) and thus allow multiphoton absorption.[30,49] For MPD of medium size polyatomics without the presence of buffer gas, vibrational self-quenching should be the predominant collisional effect. This is because only that rotational relaxation which occurs in the early portion of the laser pulse can effectively contribute to MPE and because the rapid relaxation of high vibrational levels, primarily through near resonant V-V transfer,[81,82] affects both MPE and MPD both during and after the laser pulse.

It is difficult to make a quantitative assessment of any of the collisional mechanisms in multiphoton processes, since a quantitative description of optical transitions alone is difficult. However, several studies have quantitatively treated MPD of polyatomics in the presence of a large amount of diatomic or monoatomic buffer gas with either a rate equations calculations[53,67,83] or an information theory analysis.[84] Values ranging from 40 to 910 cm^{-1} energy were

reported for per collision deactivation of highly vibrationally excited molecules by those structureless collisional partners through vibration-translation transfer. For vibrational self-quenching, a rate equations model, which used statistical dissociation rates and gas kinetic vibrational quenching rates, has quantitatively described the pressure dependence of the dissociation yield of ethyl chloride in the 3.3 μm region.[80] In that calculation absorption cross sections were estimated from ordinary linear spectroscopy and the calculated yields agreed well with the measured absolute yield and its fluence dependence. More than 3000 cm^{-1} of vibrational energy was assumed to be removed in one collision for molecules excited above the dissociation limit (56 kcal/mole). It is certainly desirable to apply this calculation of self-quenching to other MPD systems with different conditions.

A natural candidate for further examination is SF_6 under 10 μm radiation. The pressure dependence of SF_6 MPD yield was reported by Ambartzumyan et al.[79] It was shown that between 0.05 and 1.1 Torr the yield of SF_6 under 4 J/cm^2 radiation at 947.8 cm^{-1} decreased by a factor of 8, Fig. III-1. Vibrational deactivation by collisions was thought to cause the decrease. A thorough rate equations calculation has been done by Schulz et al. for collisionless MPD of SF_6.[61] In their calculation the effect of collisions was not included since most of the experimental observables used for comparison were obtained from molecular beam data. In this report,

vibrational deactivation is added to the rate equations for the calculation of dissociation yield at different pressures and compared with the experiment.

Fig. III-1. Dissociation yield of SF_6 under 4 J/cm^2 radiation at 947.8 cm^{-1} vs SF_6 pressure. (●) are experimental measurements obtained from Ref. 79. Curves are calculated with the rate equations model with different ΔE values. Numbers on the curves indicate the magnitude of ΔE.

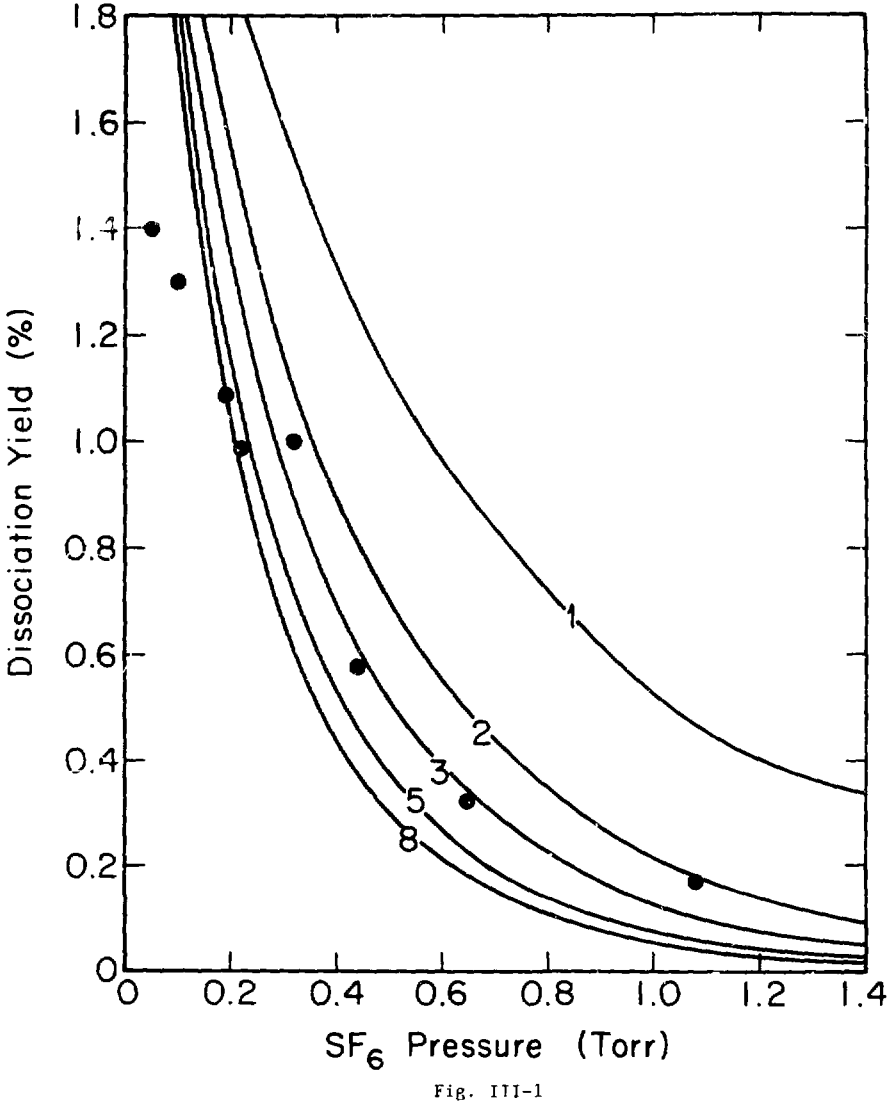
1.8
1.6
1.4
1.2
1.0
0.8
0.6
0.4
0.2
0
Dissociation Yield (%)
0
0.2
0.4
0.6
0.8
1.0
1.2
1.4
SF6 Pressure (Torr)
1
2
3
5
8

Fig. III-1

B. The Model and the Determination of Parameters

As in the original calculation in Ref. 61, rate equations were applied to molecules which had absorbed 3 or more photons. The absorption and reemission of photons for molecules in the QC and the continuum were treated as for harmonic oscillators incoherently driven by the laser field. An exponential decrease was assumed for the absorption cross section of transition to level $\ell+1$ by molecules possessing ℓ photons, $\sigma^a_{\ell,\ell+1} = \sigma\, e^{-\beta\ell}$. σ and β are the two parameters characterizing the QC absorption. In this calculation vibrational quenching is added to the rate equation

$$\frac{dN_\ell}{dt} = \left(\sigma^a_{\ell-1,\ell}\, N_{\ell-1} + \sigma^e_{\ell+1,\ell}\, N_{\ell+1}\right)\frac{I}{h\nu}$$

$$- \left(\sigma^a_{\ell,\ell+1} + \sigma^e_{\ell,\ell-1}\right)\frac{I}{h\nu}\, N_\ell - k_\ell N_\ell - kc\,(N_\ell - N_{\ell+\Delta\ell}).$$

Here $I(t)$ is the laser intensity, $\sigma^e_{\ell+1,\ell}$ is the stimulated emission cross section from level $\ell+1$ to ℓ, and k_ℓ is the unimolecular dissociation rate constant for molecules having energy $\ell h\nu$. In the collisional term, k_c is the collisional frequency, and $\Delta\ell h\nu$, a positive number, is the amount of vibrational energy removed from the excited molecule in one collision.

For the discrete region excitation ($\ell \leq 3$), a simplified 3-photon absorption model was used to calculate the population excited to $v = 3$ from the vibrational ground state as a function of laser intensity

(Ref. 61). Two parameters characterize the excitation in the discrete region: γ, a parameter related to the rotational distribution; and I_o, a reference intensity. If γ and I_o are known, the fraction of molecules entering level $\ell=3$ according to the instantaneous laser intensity can be calculated. It was assumed that once the molecules enters level $\ell=3$, they will not return to ground state. Collisional effects are neglected in the discrete region. The V-V rate for $v(\nu_3) = 1$ was measured to be 0.7-1.5 μsec-Torr,[85] a relatively slow process compared with the laser pulse duration. SF_6 requires 2.8 collisions for rotational relaxation to occur at room temperature.[86] Therefore rotational relaxation is not expected to make significant contribution to discrete region excitation for pressures $\lesssim 1$ Torr.

No calculation was performed for 947.8 cm^{-1} in Ref. 61 and the four excitation parameters (σ, β, γ, I_o) remain undetermined. However, values for these parameters were obtained for 934.9, 944.2, and 952.9 cm^{-1} by fitting the calculated dissociation yield fluence dependence to the experimental observation.[61] Additional experimental information such as fluence and pulse duration dependence of absorption at 942.9 cm^{-1} was also used to pin down these parameters. Due to the following reasons, linear extrapolation between the values at 944.2 and 952.9 cm^{-1} was used to obtain the two QC abosption parameters, σ and β, at 947.8 cm^{-1}.

1. Experiments showed collisionless MPD threshold fluence increases linearly from 935 to 953 cm^{-1}.[61,5] This threshold fluence, which

is the minimum fluence required for monitoring dissociation at the detection limit, presumbly reflects the strength of the QC absorption.

2. Collisionless MPD yield decreases almost linearly from 935 to 953 cm^{-1} at 5 J/cm^2.[61]

3. From the previous collisionless MPD calculation, the average absorption cross section in the QC which fits the data decreases linearly from 935 to 953 cm^{-1}.[61]

At 944.2 cm^{-1} $\sigma^a_{\ell,\ell+1} = 8 \times 10^{-19}\ e^{-0.042\ell}\ cm^2$ and is $4 \times 10^{-19}\ e^{-0.035\ell}\ cm^2$ at 952.9 cm^{-1}, thus at 947.8 cm^{-1} $\sigma = 6 \times 10^{-19}\ cm^2$ and $\beta = 0.039$.

γ and I_o can then be determined by calculating the dissociation yield W_d to fit the experimental collisionless yield with the new set of QC absorption parameters. Unfortunately, there was no measurement done under collisionless conditions for 947.8 cm^{-1} at 4 J/cm^2. However, at 5 J/cm^2 and 0 Torr W_d (944.2 cm^{-1})/W_d (947.8 cm^{-1}) = 1.6.[61] This ratio increases as the fluence decreases.[87] It was shown that the ratio W_d (944.2 cm^{-1})/W_d (949.5 cm^{-1}) increased by 32% from 6 to 4 J/cm^2.[87] Thus it is reasonable to assume $1.6 \leq W_d$ (944.2 cm^{-1})/W_d (947.8 cm^{-1}) $\leq 1.6 \times 1.3$ at 4 J/cm^2. W_d (944.2 cm^{-1}) at 4 J/cm^2 was measured to be 20%,[61] so W_d (947.8 cm^{-1}) should be about 10%. γ was alwasy set at 0.5 for SF_6 at all the CO_2 laser lines between 935 and 953 cm^{-1}.[61] With I_o set at 60 MW/cm^2 W_d was calculated to be 9.64% at 4 J/cm^2. As a comparison, I_o (944.2 cm^{-1}) = 20 MW/cm^2 and I_o

($952.9\ cm^{-1}$) = $400\ MW/cm^2$.[61] I_o ($947.8\ cm^{-1}$) should be between 20 and $400\ MW/cm^2$. The variation of I with all other excitation parameters fixed will change the calculated dissociation yield at zero pressure for a given fluence. For a larger I_o, the fraction of molecules excited to the QC is smaller, giving a smaller dissociation yield.

RRKM theory was used to calculate the dissociate rate. The activated complex and the dissociation energy were taken to be the same as in Ref. 61.. A hard sphere cross section of 110 $Å^2$,[88] which corresponds to a 93 nsec-Torr collisional rate, at room temperature, was used to calculate k_c at different pressures. The laser pulse rises in 90 nsec to maximum intensity, has a sharp peak with 90 nsec FWHM which contains 60% of the energy, and has a total length of 0.52 μsec.[89,39] The numerical integration was carried out with 0.01 nsec increments on the computer till the end of the laser pulse. It was found that the results are within 1% of those calculated with 1 psec increment. The computer integration calculated the fraction of molecules dissociated within the laser pulse and the excitation distribution $N_\chi(t_e)$ at the end of the pulse, t_e. After the optical field is gone, there is only competition between deactivation and dissociation for the molecules excited above the dissociation limit. The contribution to dissociation yield form the post-pulse era is calculated as

$$W_d(t>t_e) = \sum_{\ell \geq 34} N_\ell(t_e) f_\ell .$$

Here f_ℓ is the probability of dissociation for $N_\ell(t_e)$ and is calculated as

$$f_\ell = f_\ell^o + (1-f_\ell^o) f_{\ell-\Delta\ell}$$

and

$$f_\ell^o = \frac{k_c(P)}{k_c(P) + k_{RRKM}(\ell h\nu)} ,$$

where P denotes the pressure and $\Delta\ell h\nu$ is the magnitude of the energy transfer per collision.

C. Results and Discussion

As a support for the values determined for the 4 excitation parameters at 947.8 cm^{-1}, calculations by the rate equations model show that the average photons absorbed <n> of all the molecules irradiated by 5.4 J/cm^2 pulse under collisionless condition is 15.3 $h\nu$, only slightly lower than but within the error limit of the experimental value of 17.5 $h\nu$ with the same fluence but at 0.45 Torr.[90] <n> is expected to be higher at higher pressure. Both in the experiment and in the calculation, <n> is obtained as total number of photons absorbed divided by the total number of molecules. Collisional quenching will shift the excitation distribution towards lower energy levels where the absorption cross section are higher. Therefore collision would enhance the total absorption and make <n> larger at higher pressure. However, since only collisions occurring during the laser pulse would have such an effect, the magnitude of the enhanced absorption is not expected to be large.

The calculated W_d as a function of pressure are plotted in Fig. III-1 for various $\Delta\ell$ values. The best agreement with the experimental points seems to be the $\Delta\ell = 3$ curve for pressure range between 0.2 and 1.1 Torr. The $\Delta\ell = 3$ curve is about a factor of 2 higher than the experiments for pressures lower than 0.1 Torr and might be lower than experimental yield for $P \geq 1$ Torr. The discrepancy at higher pressure might result from rotational relaxation during the laser pulse that would increase the yield. The discrepancy in the lower pressure

region is most likely due to uncertanties in the excitation parameters for calculation, and/or in the experimental measurements of laser fluence and dissociation yield. Though it seems unlikely that extrapolation of W_d from the experimental points to zero pressure would reach 9.6%, however molecular beam experiments showed W_d (947.8 cm^{-1}) at 0 Torr should be about 10% at 4 J/cm^2 and any set of excitation parameters choosen for calculation should fulfill this condition.

It was found that the uncertainty of laser fluence has a great effect on the comparison between the calculation and the experiments. By assuming a 5% error on the reported fluence, i.e. the experimental yields was obtained at 3.8 J/cm^2 rather than 4 J/cm^2, the $\Delta\ell = 2$ curve agrees well with the measurements over almost the entire pressure range, Fig. III-2. With the experimental fluence set at 3.6 J/cm^2, a 10% error, even the $\Delta\ell = 1$ curve is found in good agreement with the experimental points. However, no satisfactory fit with the experiments can be obtained for the $\Delta\ell \geq 4$ curves no matter what fluence was assumed. Although a collimated laser beam was used for excitation,[79] uncertainty in the measurement of beam diameter as well as the non-cylindrical intensity distribution of the laser transverse profile make a 10% uncertainty for average fluence very possible. The same argument on laser fluence may also be made for the molecular beam experiments. Should the dissociation yield at 4 J/cm^2 is less than 10%, a larger number than 60 MW/cm^2 for I_o would be required to produce

Fig. III-2. Pressure dependence of MPD yield with varied fluence values. (●) are experimental measurements. (·····) is calculated with $\Delta\ell = 1$ and fluence = 3.6 J/cm^2. W_d (0 Torr, 3.6 J/cm^2) = 6.2%. (———) is calculated with $\Delta\ell = 2$ and fluence = 3.8 J/cm^2. W_d (0 Torr, 3.8 J/cm^2) = 7.7%. (-----) is calculated with $\Delta\ell = 3$ and fluence = 3.9 J/cm^2. W_d (9 Torr, 3.9 J/cm^2) = 8.4%.

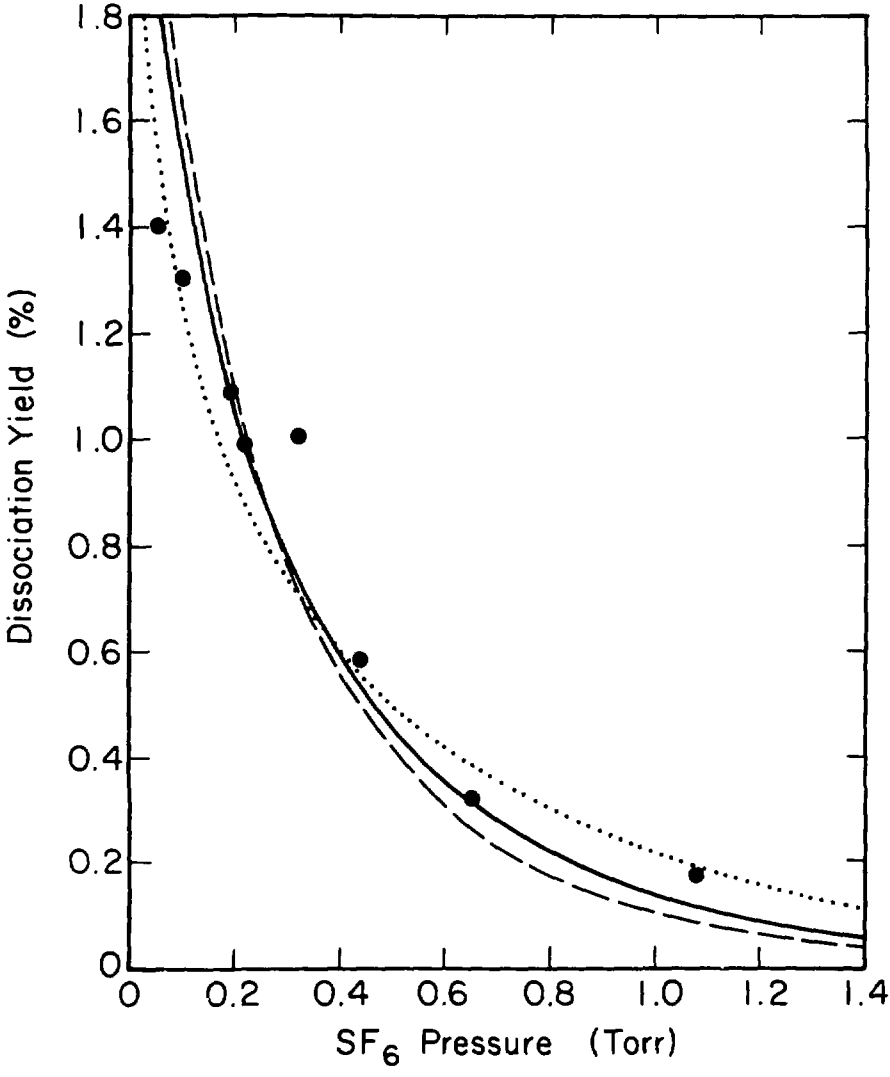
1.8
1.6
1.4
1.2
1.0
0.8
0.6
0.4
0.2
0
Dissociation Yield (%)
0
0.2
0.4
0.6
0.8
1.0
1.2
1.4
SF6 Pressure (Torr)

Fig. III-2

the smaller W_d. Again better agreement with the experimental yields can be obtained for the $\Delta\ell \leq 3$ curves than in Fig. III-1.

Even though ν_3 is the highest frequency mode of SF_6, removal of 3000 cm^{-1} energy per collision is conceivable. There is ample evidence from thermal unimolecular studies that molecules excited up to the dissociation limit may lose more than 10 kcal/mole per collision.[59] In particular, data from chemical activation studies complied in Ref. 59 showed that energy $\geq$6 kcal/mole (2100 cm^{-1}) was removed for some highly excited polyatomics in collision with a cold SF_6 molecule, Table III-1. These chemically activated molecules may have vibrational energy as high as the bond energies. For the case of vibrational self-quenching of SF_6 excited to comparable energy content, the magnitude of energy removal may be even larger since the V-V transfer is a more nearly resonant process. The calculation with 4 J/cm^2 fluence and at 0 Torr pressure showed that at the end of the laser pulse about 2/3 of the molecules are still in the vibrational ground state, and the average excitation for the molecules in the QC is 22 $h\nu$. Thus $\Delta\ell h\nu$ used in the calculation may be viewed as the average energy transferred per collision between a molecule excited to $\geq$60 kcal/mole and a cold molecule in the discrete region.

As has been demonstrated previously, the pressure dependence of W_d strongly depends upon the excitation distribution which is a strong function of laser fluence, and the dissociation rate as a function of energy, Chapter II, Section I.[80] The calculation with

Table III-1. Vibrational quenching by SF_6 of highly excited molecules generated by chemical activation.[a]

Molecule	Chemical Activation System	Energy Removed per Collision[b] (kcal/mole)	Reference
Butyl-2	H + cis-butene	≥ 9	93
$C_2H_4Cl_2$	$CH_2Cl + CH_2Cl$	7.0	94
C_2H_5F	$CH_3 + CH_2F$	7	95
$C_2H_4F_2$	$CH_3F + CH_3F$	7	95
CH_3CF_3	$CF_3 + CH_3$	6.0, 7.0[c]	96

[a]Data complied in Ref. 59.

[b]A stepladder model was used for collisional deactivation.

[c]The SF_6 temperature is 196°K. All the other numbers are obtained for an SF_6 temperature of 300°K.

3.8 J/cm^2 and 0 Torr shows the QC population peaks at $\ell = 29$. A major fraction of dissociation after the pulse comes from the levels right above the dissociation limit, Fig. III-3. These levels are easily accessible for collisional deactivation even at very low pressure. The in-pulse dissociatin is from levels with much shorter dissociation lifetimes; it only contributes a small fraction to W_d at lower fluences. Collisional deactivation has much less prominent effect on the in-pulse dissociation than on the post-pulse dissociation; $W_d(t<t_e)$ dropped only 30% form 0 to 0.2 Torr with $\Delta\ell = 2$ while $W_d(t>t_e)$ decreased by a factor of 6 in that pressure range. So as the fluence increases, the QC population peak shifts toward higher levels, the contribution to W_d from the in-pulse dissociation becomes more important, and the post-pulse dissociation contains a larger contribution from levels which require higher pressures to quench effectively. As a result, the effect of pressure on dissociation yield at higher fluences is much less dramatic than at lower ones. This can be clearly seen from the calculations plotted in Fig. III-4. At 10 J/cm^2 W_d decreases by a factor of 2 from 0 to 1.2 Torr, but a 4 J/cm^2 W_d dropped 70 times in the same pressure range.

Fluence dependence of dissociation yield has long been considered an important characterization for any MPD system. It was shown by the calculation that the fluence dependence of W_d changes at different pressures, Fig. III-4. The slopes of the W_d-fluence curves on a log-log plot for the same W_d range are very much the same, independent

of the pressures. However, for the same range of fluence these slopes vary strongly with pressure.

In Ref. 79, an empirical formula $W_d = W_o \exp(-P/P_o)$ was suggested to fit the experimental points in Fig. III-1. The calculation of W_d over a wider range of pressure shows that such a formula can serve as a good approximation for a small range of pressure. The slope of the W_d-P curve on semi-log plot varies less than 50% from 0.2 to 2 Torr, Fig. III-5. However, the curve takes a sharp turn at pressures below 0.1 Torr, reflecting the effect of collisional deactivation of the comparably large population excited just above the dissociation limit at these low pressures.

Fig. III-3. Calculated population distribution after the laser pulse for levels above the dissociation limit with fluence = 3.8 J/cm^2 and $\Delta\ell = 2$. The dashed line (----) defines the population at 0 Torr and the solid line (———) at 0.19 Torr. The shaded area indicates the fraction of molecules that dissociate during the laser pulse. The dissociation lifetime was calculated by RRKM theory.

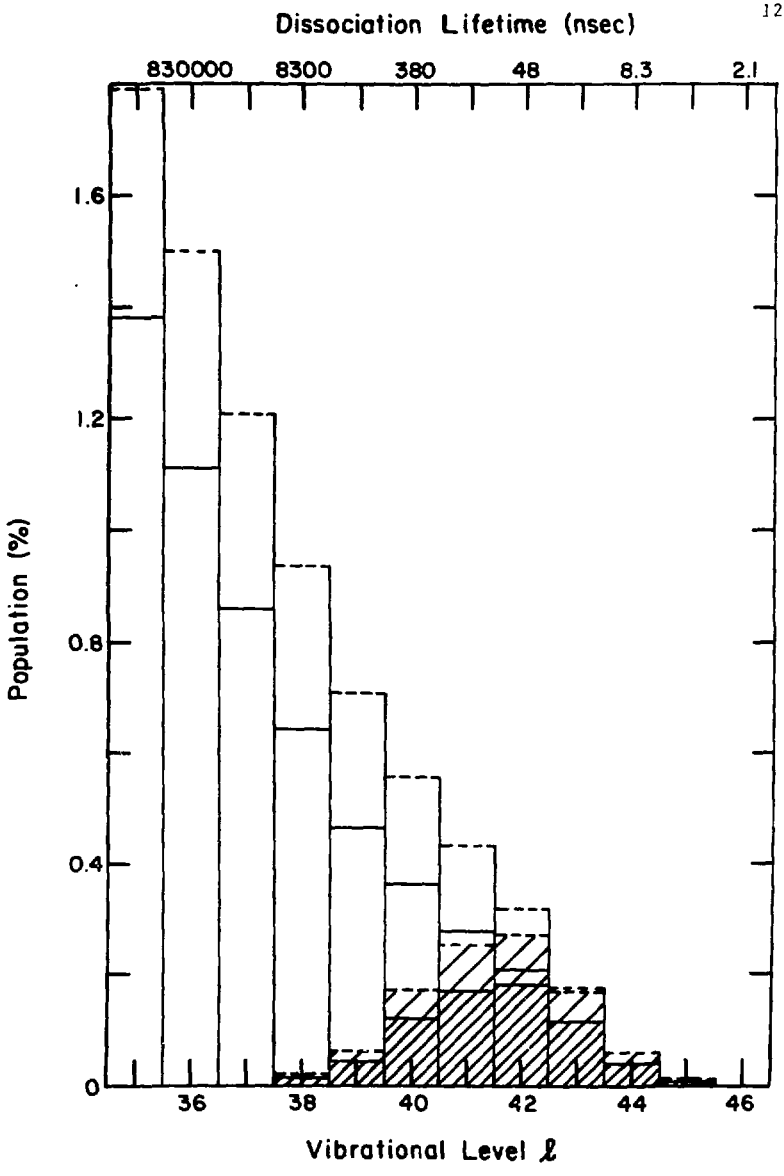
Dissociation Lifetime (nsec)
830000
8300
380
48
8.3
2.1
1.6
1.2
0.8
0.4
0
Population (%)
36
38
40
42
44
46
Vibrational Level ℓ

Fig. III-3

Fig. III-4. Fluence dependence of MPD yield at various pressures calculated from the rate equations model with $\Delta\ell$ = 2. Numbers on the curves indicate the SF_6 pressure. The average slope between 4 and 8 J/cm^2 is 2.2 for 0 Torr, 3.8 for 0.08 Torr, 4.6 for 0.4 Torr, and 6.4 for 1.2 Torr.

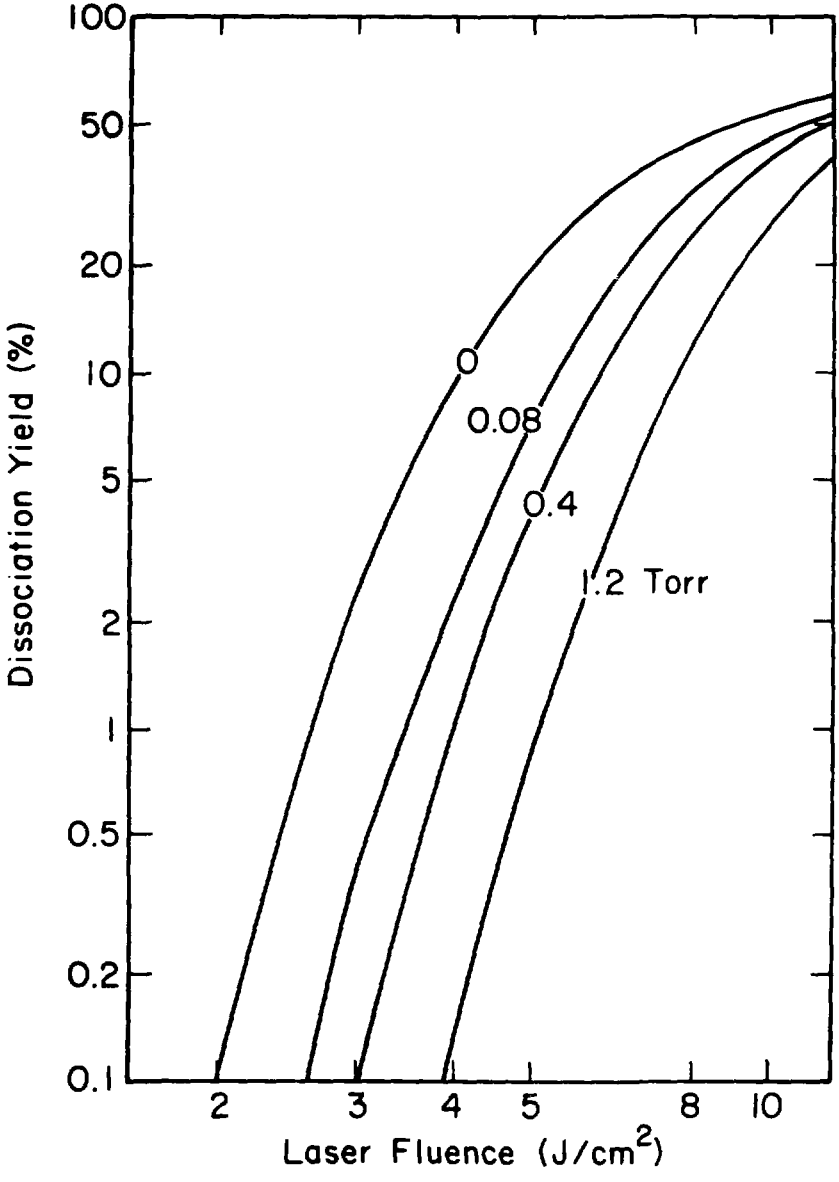
100
50
20
10
5
2
1
0.5
0.2
0.1
Dissociation Yield (%)
0
0.08
0.4
1.2 Torr
2
3
4
5
8
10
Laser Fluence (J/cm²)

Fig. III-4

Fig. III-5. Pressure dependence of MPD yield calculated from the rate equations model with $\Delta\ell = 2$ and fluence = 3.8 J/cm^2.

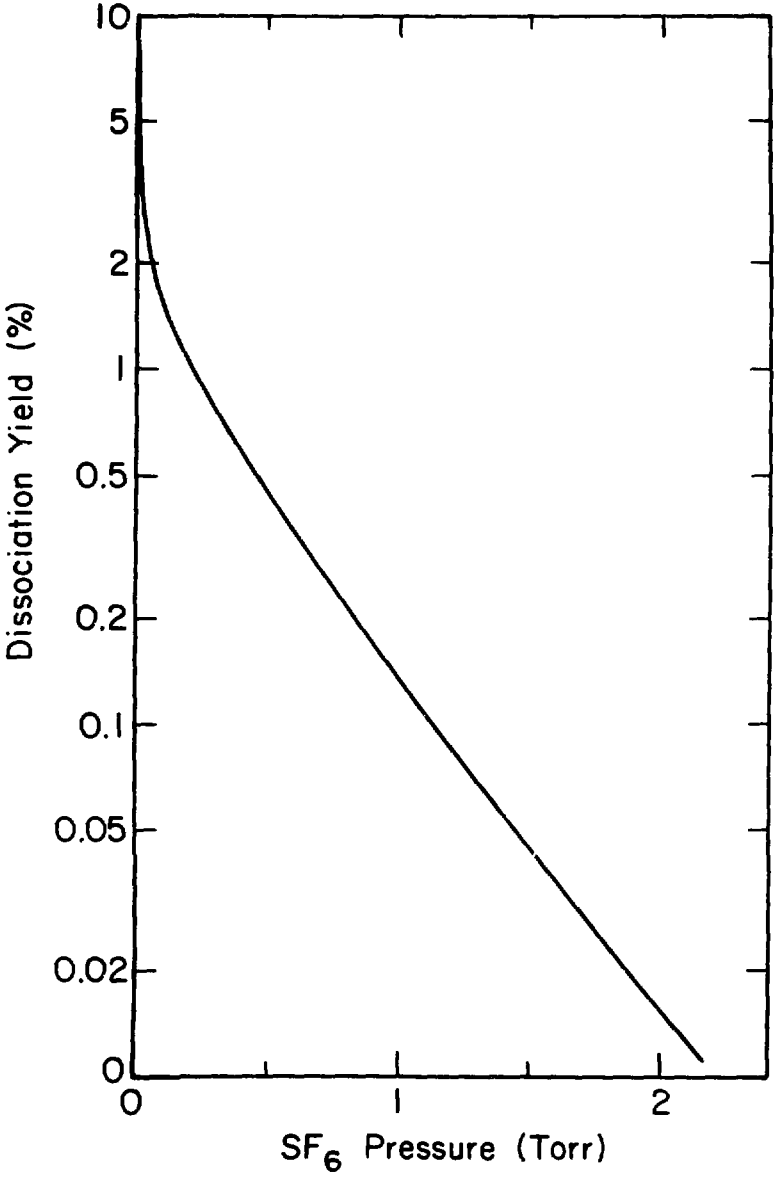
10
5
2
1
0.5
0.2
0.1
0.05
0.02
0
Dissociation Yield (%)
0
1
2
SF6 Pressure (Torr)

Fig. III-5

D. Conclusion

With parameters determined from independent sources, a rate equations model can be used to quantitatively calculate the pressure dependence of dissociation yield caused by vibrational self-quenching. Although the uncertainty of experimental parameters does not allow an accurate determination of the quenching rate, from the comparison between calculation and experimental measurement it does show that between 1000-3000 cm^{-1} energy is removed for SF_6^* excited to $\gtrsim$60 kcal/mole by collision with a cold SF_6 molecule at gas kinetic rate. The calculation also demonstrates that the pressure dependence of the dissociation yield is a strong function of laser fluence as well as that the fluence dependence of dissociation yield varies strongly with the pressure.

CHAPTER IV. DETERMINATION OF THE ARRHENIUS PARAMETERS FOR UNIMOLECULAR REACTIONS BY SENSITIZED LASER PYROLYSIS

A. Introduction

After a decade of intensive research on multiphoton dissociation of polyatomic molecules by intense infrared optical fields, a good understanding of both the excitation and the dissociation has been established, at least semi-quantitatively. As the fundamental physics of the multiphoton processes were revealed and many theoretical models tested, kinetic and spectroscopic applications utilizing these processes were also in development. One such kinetic application is to study the mechanism of unimolecular decomposition of organic molecules.[97]

It was demonstrated under collisionless conditions that molecules under multiphoton excitation (MPE) dissociate firstly through the lowest activation energy channel.[98] MPE of alkyl halides in the presence of high pressure buffer gas showed dissociation always into the lowest reaction channel. This behavior is consistent with the statistical nature of the excitation and the dissociation: as the molecule absorbs many photons in the quasicontinuum, intramolecular vibrational relaxation randomizes energy among all the modes and RRKM theory can be used effectively to calculate the dissociation rate.[77] However, such microscopic statistical dissociation does not necessarily mean that the multiphoton excitation and dissociation is a thermal process. The energy distribution might be different from a Boltzmann

distribution for the entire ensemble of molecules after irradiation.[23] The excitation distribution depends strongly on the laser fluence and the molecular properties. Without precise knowledge of the excitation distribution, the kinetic data from MPD can often be ambiguous.[78] The method of sensitized reaction can be applied to partially resolve such difficulty. A molecule, such as SiF_4, which does not significantly dissociate at low and medium laser fluences is used as a photon-absorbing medium through MPE. Collisions during and shortly after the laser pulse will transfer energy from the absorbing gas to the reactant gas which is not in resonance with the laser. A thermal equilibrium is established for the reactant after sufficient collisions for energy transfer. In this manner, MPE is used as a means of thermal heating. It has the advantage that contact of the hot gas with surfaces and therefore surface reactions can be avoided. The usefulness of this technique has been demonstrated in obtaining qualitative information about unimolecular reaction pathways of some organic molecules.[35,36,115]

In the sensitized IR laser pyrolysis, each laser pulse creates a transient high temperature pulse (or pulses) during which reactions occur, in the gas medium. If temperature as a function of time can be determined, then the pyrolysis can be done quantitatively and quantities such as activation energy E_a and preexponential factor A of a reaction may be extracted.

The following method was attempted in this chapter to achieve such a quantitative goal. In addition to the absorbing gas and the reactant in the gas medium, a second reactant with well known E_a and A for its

reaction was added as an "internal standard." The product yield of the internal standard coupled with a phenomenological model calculation is used to deduce the parameters needed to describe the gas medium temperature history in the model. Additional information, such as the decay of the temperature, obtained through monitoring the ir fluorescence from the irradiation volume, was also used in the calculation. Then by adjusting their values to reproduce the measured product yield through calculation with the now defined temperature history, E_a and A of any specific reaction channel of the reactant can be secured.

1,1,2-trichloroethane was chosen as the reactant here. It was of interest for studies of photochemistry induced by single-photon excitation of high vibrational overtones. The reaction channels as

$$CHCl_2CH_2Cl \longrightarrow \left\{ \begin{array}{l} \text{1,1-dichloroethene,} \\ \text{trans-dichloroethene,} \\ \text{cis-dichloroethene,} \\ \text{vinyl chloride} \end{array} \right. + \left(\begin{array}{l} \text{corresponding} \\ \text{dissociation} \\ \text{products} \end{array} \right)$$

were observed.[92] The HCl elimination reactions were reported to have very low values of E_a, 38 and 34 kcal/mole, and A, $10^{9.7}$ and $10^{9.9}$, in two flow pyrolyses,[100,101] respectively. A more recent chemical activation study suggested a 3-centered activated complex in addition to the 4-centered one for HCl elimination and placed the E_a's of dichloroethenes between 57 and 60 kcal/mole.[71] No observation of

vinyl chloride was reported. Here, each of the reactions producing the three $C_2H_2Cl_2$'s and vinyl chloride are studied by SiF_4- sensitized CO_2 laser pryolysis and their E_a's and A's reported. For comparison, the HCl elimination reaction of 1,1,1-trichloroethane was also studied. The internal standard choosen in this study is ethyl chloride. Its HCl elimination reaction is expected to have comparable E_a values as the reactions of trichloroethanes. Through eight previous studies, $E_a = 57.4 \pm 1.0$ kcal/mole and $\log A = 13.8 \pm 0.2$ at high pressure limit were determined for $C_2H_5Cl \rightarrow HCl + C_2H_4$.[41,42]

B. Experimental

1. Pyrolysis

All the chemicals originally reagent grade or technical grade were purified by fractional distillation. The purity of their vapors was checked by a Varian 3700 gas chromatograph with gas sample injection and flame ionization detector to be >99.9% for ethyl chloride (EtCl), >99.6% for 1,1,2-trichloroethane (112TCE), >99.5% for 1,1,1-trichloroethane (111TCE), and >99.9% for SiF_4. No impurities as the pyrolysis products of the molecules were detected. The unpurified 111TCE (Eastman Kodak, technical grade) originally contains 3.5% p-dioxane and 0.25% sec-butanol as inhibitors for polymerization. After distillation there was still 0.4% impurities as p-dioxane (<0.1%) and C_2HCl_3. The pyrolysis mixture contained between 0.1~0.5% impurities of 111TCE depending on the individual preparation procedure. The gases were handled in a vacuum line with greaseless stopcocks. Before each preparation for the pyrolysis sample, the vacuum line was pumped down to $\lesssim 10^{-6}$ Torr. Unless otherwise specified, a pyrex cell 3.8 cm long 3.8 cm in diameter with two polished NaCl windows (4 mm in thickness) attached perpendicular to the cell axis with Torrseal epoxy, and a gas mixture consisting of 4.9 ± 0.1 Torr SiF_4, 0.37 ± 0.02 Torr ethyl chloride, and 0.37 ± 0.02 Torr reactant (either 112TCE or 111TCE) were used for each pyrolysis. The gas pressure was measured by a calibrated variable-reluctance manometer (Validyne) with

a 50 Torr range and the mixture was prepared with the aid of a sidearm on the pyrolysis cell and liquid nitrogen cooling.

A grating-tuned Tachisto model 215 CO_2 transversely excited atmosphere laser was used to provide light pulses. The operational details and the design of the laser can be found in Ref. 49. With the internal iris set at 8.0 mm in diameter and without external iris, the transverse cross section of the multimode beam has a near-Gaussian profile (Fig. IV-1(a)) and a FWHM of 4.0 ± 0.4 mm. The laser pulse for pyrolysis at 1027.4 cm^{-1} (P(40) line) is typically 0.2 J/pulse. Pulse-to-pulse energy variation was ±10%. Long term energy stability is usually about 10%. The total pulse duration is 1.3 μsec long and has a 70 nsec spike peaked at 35 nsec. The beam from the laser was used for pyrolysis without focusing or collimation. A 4 mm thick polished NaCl flat was placed right in front of the laser at 45° to reflect about 5% of the beam to a Scientech powermeter for monitoring the long term fluctuation of the laser energy during the experiment. The laser beam then entered into the pyrolysis cell and a calibrated Scientech powermeter placed after the cell for measuring the laser pulse energy. The percentage absorption of the beam by the gas mixture was determined by the ratio of the pulse energies after the cell with the gas mixture in the cell and with the mixture frozen in the side-arm at liquid N_2 temperature. Polished CaF_2 flat, NaCl flat or Ge flat were placed between the NaCl beam splitter and the cell in order to obtain the desirable pulse energy. Between 20 and 30% of the 0.2

Fig. IV-1. a) CO_2 laser beam profile measured with a 0.2 mm pin-hole. Open circles (○) indicate the incident laser intensity which has been corrected for the entrance window loss. Closed circles (●) indicate the laser intensity after gas absorption. b) The profile of gas absorption is the difference of the incident and the exit laser beams. (■), obtained from Fig. a), and (x) are for 0.18 J/pulse incident energy. (▽) are for 0.12 J/pulse.

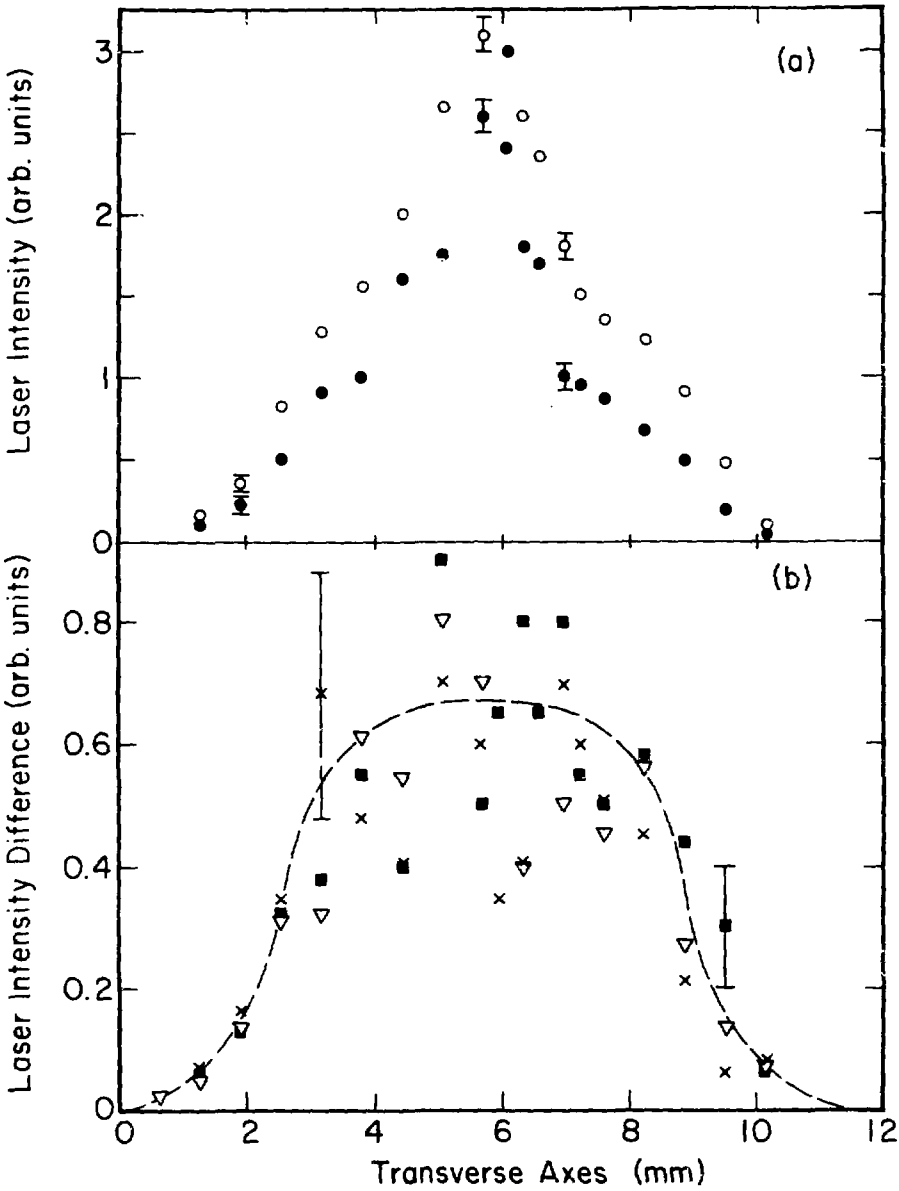
(a)
(b)
Laser Intensity (arb. units)
Laser Intensity Difference (arb. units)
Transverse Axes (mm)
0
1
2
3
0.2
0.4
0.6
0.8
4
6
8
10
12

Fig. IV-1

to 0.08 J/pulse laser energy entering the cell was absorbed by the mixture. The real energy absorbed by the mixture was obtained by multiplying the absorption percentage and the pulse energy after the attenuator corrected for cell window reflection. The laser was operated at 0.87 Hz repetition rate for pyrolysis with energy >0.15 J/pulse and at 0.33 Hz for lower energies. The slow repetition rate was meant to allow complete diffusion of the products and the reactants between the irradiation column and the unirradiated part between two consecutive laser pules. It was estimated from a calculated theoretical diffusion constant[102] that it requires roughly 0.4 sec for the product to diffuse through a distance of 3.2 mm, the radius of the irradiation zone (Section B-3), in the 5.6 Torr mixture at room temperature. The higher temperature induced by the laser excitation in the reaction zone would hasten the diffusion. For lower fluences, a slower repetition rate was used to guarantee a complete mass diffusion. The powermeter was calibrated for different operational repetition rate of laser pulses with a Scientech model 362 power-energy meter which gave the energy reading of a single pulse from the powermeter.

After the pyrolysis, the mixture was immediately transferred to a 4 cm^3 volume GC sample loop which was attached to the cell and pumped clean on the vacuum line before the preparation of the mixture. A column made of 100/120 mesh size Porapak Q in 12 feet long and 1/8 inch in diameter stainless steel tubing was used for separating the

reactants and the products. The retention times at 120°C column temperature and 30 cm^3/min. carrier gas flow rate are 3 min. for C_2H_4, 7 for C_2HCl, 9 for vinyl chloride, 15 for EtCl, 28 for CCl_2CH_2, 38 for trans-CHClCHCl, 52 for cis-CHClCHCl, 110 for 111TCE, 140 for C_2HCl_3, and 260 for 112TCE. The GC responses for all the molecules mentioned above except C_2HCl and C_2HCl_3 were calibrated absolutely. HCl and Cl_2 do not respond to flame ionization detection. The large quantity of SiF_4 in the mixture gave a very small signal at 2 min.

The GC peak area measurement and the detector response calibration give a combined uncertainty of ±8% for the product yield. The yield as CCl_2CH_2 was less accurate partly because it was difficult to accurately measure the area of its small GC peak sitting on the tail of the strong EtCl peak. The pyrolysis laser energy was reported as the average energy of the incident beam into the gas mixture after the first cell window. All the experimental parameters linearly related to the laser energy have an uncertainty of ±5~10% because of the laser energy fluctuation.

2. IR Fluorescence

Ir fluorescence from the irradiation zone was monitored and temporally resolved for the mixture of 5 Torr SiF_4, 0.38 Torr EtCl and 0.38 Torr 111TCE. The pyrex fluorescence cell is 4 cm in length and 5.1 cm in diameter with ends sealed by two 4 mm thick NaCl

windows attached perpendicular to the cylinder axis by Torrseal epoxy. The laser passes through the center of these windows. Along the direction perpendicular to the laser propagation, two holes 1.7 cm in diameter were opened up at the center section of the cell and were sealed with NaCl windows for transmitting the fluorescence. A liquid He cooled 5 mm x 10 mm Hg:Ge photoconductive ir detector was placed above a fluorescence window. The distance between the irradiation volume and the detector was about 8 inches. A 2-inch diameter CaF_2 lens with 4-inch focal length was placed in the middle between the detector and the laser pathway to focus the fluorescence to the detector. The response time for the detector itself is about 0.4 μsec. A Keithley model 104 wideband amplifier was used to amplify the detector signal 100 times before it was recorded and averaged over 32 pulses using a Biomation Transient Recorder and a Northern NS-575A Digital Signal Analyzer. The trigger pulse used for triggering the CO_2 laser was also used to trigger the transient recorder. The time-resolved signal of the fluorescence passing through the 3-6 μm circular variable interference filter, which was cooled internally in the detector at liquid N_2 temperature, was eventually plotted by a Hewlett-Packard 7004B X-Y recorder. When the filter was set to a narrow band pass (FWHM 60 cm^{-1}) centered at 5.0 μm, strong fluoresence was observed. Fluorescence around 3.3 μm was also searched for, but no signal after 32 pulses integration was found.

3. Determination of the Irradiation Volume and the Product Yield

The area of the GC peaks of each reactant and product was measured with a planimeter and multiplied by the GC detector response of each molecule. For the case that there is only one dissociation channel for the reactant, the total fraction of reactant dissociated in the cell, F, after n pulses can then be calculated. Since F is generally non-negligibly large, the product yield per pulse, ϕ, for the reactant in the irradiation volume V_r is not simply $(F/n)\cdot(V/V_r)$, where V is the cell volume. Instead, ϕ is calculated as follows. After n pulses, the fraction of reactant which remains undissociated in the cell is

$$1 - F = (1 - \phi \frac{V_r}{V})^n. \qquad \text{(IV-1)}$$

Therefore, ϕ is calculated as

$$\phi = \frac{V}{V_r} [1 - (1 - F)^{1/n}]. \qquad \text{(IV-2)}$$

When there is more than one reaction for a reactant, Equation (IV-2) can still be used with F and ϕ defined as $F = \sum_i F_i$ and $\phi = \sum_i \phi_i$. F_i is the fraction of reactant in the cell turned into product i after n pulses and ϕ_i is the per-pulse yield for product i in the irradiation volume. ϕ_i is then calculated as

$$\phi_i = \frac{F_i}{F} \phi. \qquad \text{(IV-3)}$$

In the pyrolysis experiments, a wide range of laser pulse energies was used. In general, between 50 to 200 pulses were used for each pyrolysis to make F between 5 to 30%.

On the right hand side of Equation (IV-2), all the quantities except V_r can be measured directly and unambiguously. The volume of the 3.8 cm pyrolysis cell is 50 cm^3. However, there is no distinct boundary in the transverse profile of the laser pulse that can be used to calculate V_r. The transverse profile was measured by attaching a 0.2 mm diameter pinhole 2 mm in front of the sensor of a Molectron Model J-3 pyroelectric detector mounted on a 3-D translator. The detector signal was read directly from a Tektronix 7704 oscilloscope with a 50 Ohm input impedance amplifier module.

The dissociation yield might be incorrectly evaluated by using the FWHM to calculate V_r. The amount of molecules in the laser profile is about 3 times more than the one in the area defined by the FWHM, Fig. IV-1(a). The situation is complicated by the fact that the reaction rate increases exponentially with the temperature; the temperature distribution right after the laser pulse may be inhomogeneous. Furthermore, it was noted in the pyrolysis experiments that the percentage absorption by the gas mixture decreased as the incident laser pulse energy increased. At 0.09 J/pulse incident energy, which corresponds to 0.7 J/cm^2 average fluence as calculated with the FWHM, 33% of the pulse energy was absorbed, yet at 0.21 J/pulse (1.7 J/cm^2) only 24% was absorbed. Such a decrease results both from that as the

excitation level of the molecule getting higher through multiphoton excitation the absorption cross section decreases and that saturation occurs in the discrete region excitation at higher fluences. Even though the measured percentage absorption in the pyrolysis is a convolution of absorption at continuously varying fluences along the transverse laser profile, the trend of absorption percentage dependence on fluence indicates that at the lower intensity parts of the laser profile the stronger absorption would make the contribution to reaction from these areas more important. Thus V_r should be defined by the profile that shows the spatial dependence of energy absorbed by the mixture after the laser pulse. Such a profile can be obtained from the difference between the two laser profiles before and after entering the mixture. A typical measurement of the exit laser profile after the mixture and the incident profile corrected for one window loss are shown in Fig. IV-1(a). It is apparent that substantial narrowing of the laser beam occurs after the mixture absorption due to stronger absorption at the edge of the incident beam. The FWHM of the exit beam was measured to be only 3.0 ± 0.3 mm. The difference of the two profiles from three sets of measurements are plotted in Fig. IV-1(b). Even though the scattering and the uncertainty of the points are large, a much broader profile is apparent. It was also observed that the FWHM of the irradiation volume does not change much as the laser pulse energy changes from 0.18 J to 0.12 J as indicated in Fig. IV-1(b). The FWHM of this profile was determined to be 6.4 ± 0.3 mm, and the value of 1.3 cm^3 was used for V_r.

C. The Model Calculation

This model gives the product yield of a reactant in the irradiation volume with an assumed temperature history. The temperature T in the column under irradiation is assumed to be uniform at any given time. It rises to a maximum value, T_m, at time zero after optical excitation and collisional thermalization, then as the heat starts flowing out of the column, it is assumed to decrease exponentially just like a thin layer of material at T_m transferring heat to the environment at an ambient temperature T_r.

$$T = (T_m - T_r)e^{-Dt} + T_r \qquad \text{(IV-4)}$$

where D is the decay rate constant for the column temperature and t denotes time. The reactant starts to dissociate from time zero according to a first order reaction rate with a rate constant which may be expressed in Arrhenius form. After integration of the first order reaction from time zero to infinity, the product yield of a unimolecular reaction after one laser pulse can be formulated as

$$\ln(1 - \phi) = -\int_0^\infty A\exp\left(\frac{-E_a}{k(T_m - T_r)\exp(-Dt) + kT_r}\right)dt. \qquad \text{(IV-5)}$$

The analytical solution of the integral can only be obtained in a non-converging polynomial form. Therefore a computer program was written to calculate the numerical solution (Appendix II). The numerical integration uses the trapezoidal rule with the integration

interval determined by an allowable error, which is usually set at 5% of $\ln(1 - \phi)$. A typical calculation that integrates from time zero to 10D sec takes a few minutes on a Commodore PET-2001 microprocessor.

Equation (IV-5) is legitimate only for the case that there is only one reaction channel for the reactant. In the case that there are several reactions for a reactant, Equation (IV-5) should be modified as

$$\ln(1 - \sum_i \phi_i) = -\int_0^\infty \sum_i A_i \exp\left(\frac{-E_{a,i}}{k(T_m - T_r)\exp(-Dt) + kT_r}\right) dt. \qquad \text{(IV-6)}$$

Apparently the calculation for ϕ_i couples with one another and this would make the deduction of $E_{a,i}$ and A_i rather difficult. For reactions with comparable activation energies, an approximate approach can be taken. It is considered that at any given time after time zero the number of reactant molecules available for reaction i is reduced by all the other reactions $j \neq i$ of the same reactant. Thus the product yield calculated from Equation (IV-5) is higher than the experimental value ϕ_i. At time zero there is no interference from other reactions and at the end of the reaction the reactant available is reduced by about $(1 - \sum_{j \neq i} \phi_j)$ times. So approximately during the course of the reaction the average effect of all other reactions on the yield of product is to reduce it by about $(1 - \frac{1}{2} \sum_{j \neq i} \phi_j)$ times. Therefore, the adjusted form $\ln(1 - \phi_i/(1 - \frac{1}{2} \sum_{j \neq i} \phi_j))$ from experiment is used in the left side of

Equation (IV-5) for calculating the i product yield of a reactant with several unimolecular reactions. Both the approximation for ϕ_i with Equation (IV-5) and the calculation with Equation (IV-6) are tried depending on the conditions for each individual reaction as discussed later. Of course, for photolyses in which the total yields are less than the experimental uncertainty, 8%, Equation (IV-5) can be used directly without any correction.

D. Results and Discussion

1. Pyrolysis

The per-pulse product yield of ethyl chloride in the irradiation column vs the laser pulse energy is shown in Fig. IV-2. The strong dependence of the yield on the laser energy, i.e. the yield increased more than 20 times as the pulse energy was doubled, indicates the dramatic effect of heating by the laser. However the data points in Fig. IV-2 scatter from each other. Several sources contribute to this scatter. The product yield has an uncertainty of ±8%. The main uncertainty of these data points seems to be with the determination of the laser energy due to the pulse-to-pulse fluctuation and the long-term drift of the laser. To avoid such uncertainty of laser energy in the later comparison of measured product yield with the model calculation, the product yield of 111TCE and 112TCE is plotted against that of ethyl chloride, which is used as an internal standard in the pyrolysis for monitoring the temperature. The major product observed for 111TCE is CCl_2CH_2, Table IV-1 and Fig. IV-3. Two other products, C_2HCl and vinyl chloride, were also observed with yields roughly two orders of magnitude smaller. C_2HCl is believed to be from the secondary decomposition of CCl_2CH_2. All four chlorinated ethylenes mentioned in the Introduction were observed in the pyrolysis of 112TCE, Table IV-2 and Fig. IV-4. In pyrolyses where the ethyl chloride yield was larger than 10% a small amount of C_2HCl was also observed as product. This

Fig. IV-2. Ethyl chloride dissociation yield vs incident laser pulse energy. (○) indicate pyrolyses with the long cell, (◐) the short cell, and (●) the short cell and higher pressure. Typical uncertainty of the data is shown for three points.

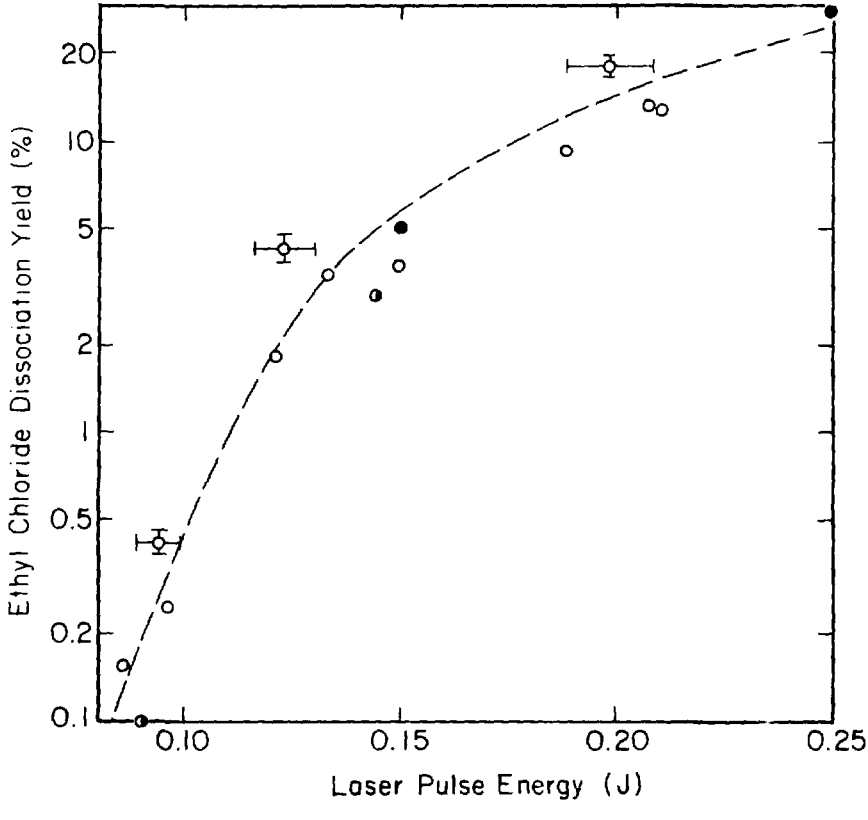
Ethyl Chloride Dissociation Yield (%)
20
10
5
2
1
0.5
0.2
0.1
0.10
0.15
0.20
0.25
Laser Pulse Energy (J)

Fig. IV-2

Table IV-1. Experimental results for sensitized laser pyrolysis of the CCl_3CH_3 mixtures.

Sample[a]	Incident Laser Energy[b] (J/pulse)	Absorbed Energy[c] (J/pulse)	Number of Pulses	Pulse Repetition Rate (Hz)	C_2H_5Cl Dissociation Yield (%)[d]	Product Yield of CCl_3CH_3 (%)		
						CCl_2CH_2	C_2H_3Cl[e]	C_2HCl[f]
L-I	0.188	0.046	50	0.87	9.20	29.1	0.41	--
L-I	0.133	0.034	100	0.34	3.53	16.2	0.090	--
L-I	0.121	0.028	100	0.34	1.82	10.2	0.042	--
L-I	0.086	0.029	200	0.34	0.15	1.18	0.007	--
S-IIA	(0.25)[b]	0.062	150	0.87	29.0	48.0	2.50	0.9
S-IIB	0.150	0.045	150	0.87	5.2	22.0	0.45	--

a. L-I, 4.9 Torr SiF_4 - 0.37 Torr C_2H_5Cl - 0.37 Torr CCl_3CH_3 in the 3.8 cm long cell. S-II, 21.5 Torr SiF_4 - 1.64 Torr C_2H_5Cl - 1.64 Torr CCl_3CH_3 in the 0.9 cm short cell.
b. All the L-I samples were irradiated by P(40) line. S-IIA was irradiated by P(36) line and S-IIB by P(34) line. The uncertainty for the pulse energy is ±5-10%. P(36) pulses for S-IIA originally contain ~0.22 J/pulse. However, for comparison with other pyrolyses, 0.062/0.25 was used as the incident energy, since it was observed that in the pyrolyses with P(40) line the percentage absorption is $\leq$25% for pulse energy >0.18 J.
c. Uncertainty ~ ±10%.
d. The per pulse yield in the irradiation volume is reported here. The uncertainty is ±8% except for C_2HCl.
e. From radical reactions involving both C_2H_5Cl and CCl_3CH_3.
f. From secondary decomposition of CCl_2CH_2.

Fig. IV-3. The CCl_2CH_2 yield from CCl_3CH_3 dissociation vs the corresponding ethyl chloride dissociation yield. (○) indicate experimental results from the long cell. (●) is from the short cell at higher pressure. The solid lines (——) are from the model calculation for CCl_3CH_3 dissociation with E_a = 47 and 49 kcal/mole and logA = 12.7 and 13.0, respectively. The calculation using E_a and A previously determined for the molecular elimination is shown as the dashed line (-----).

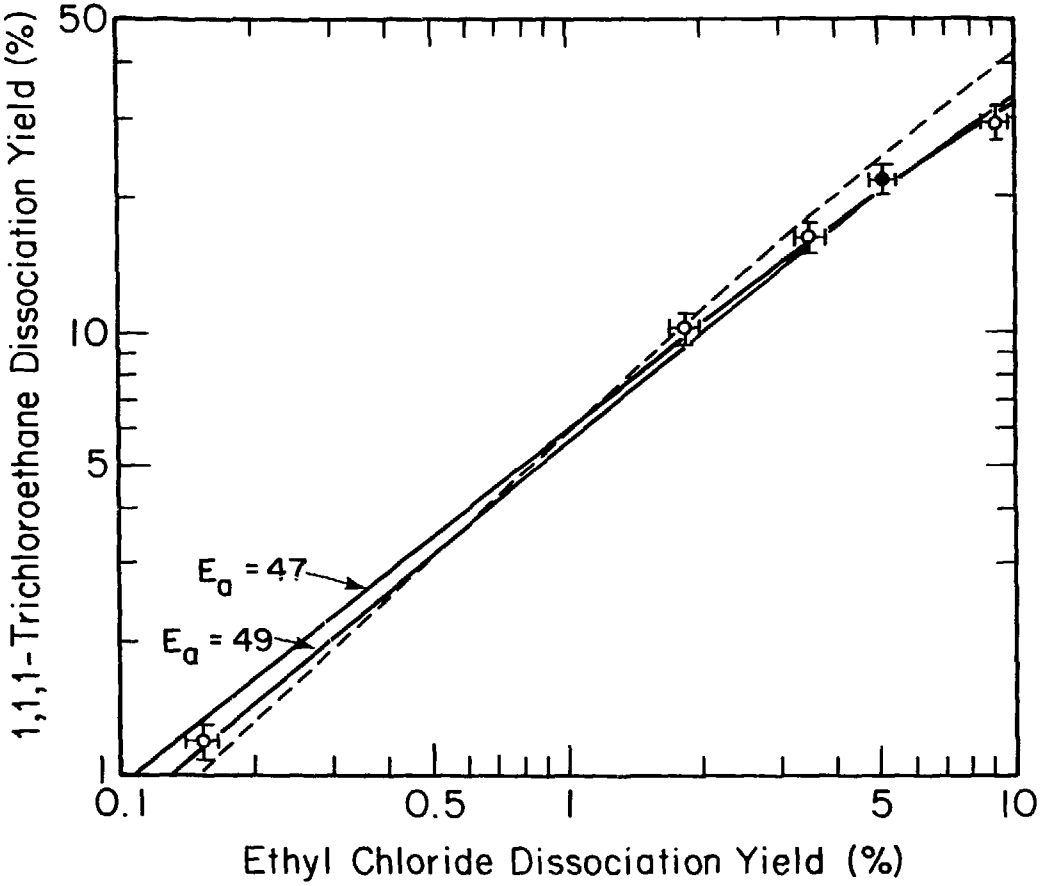
1,1,1-Trichloroethane Dissociation Yield (%)
50
10
5
1
0.1
0.5
1
5
10
Ethyl Chloride Dissociation Yield (%)
E_a = 47
E_a = 49

Fig. IV-3

Table IV-2. Experimental results for sensitized laser pyrolysis of the $CHCl_2CH_2Cl$ mixtures.

Sample[a]	Incident Laser Energy[b] (J/pulse)	Absorbed Energy[c] (J/pulse)	Number of Pulses	Pulse Repetition Rate (Hz)	C_2H_5Cl Dissociation Yield (%)[d]	Product Yield of $CHCl_2CH_2Cl$ (%)[d,e]				
						cis-$C_2H_2Cl_2$	trans-$C_2H_2Cl_2$	CCl_2CH_2	C_2H_3Cl[f]	C_2HCl[g]
L-I	0.198	0.052	200	0.87	18.4	15.6	13.3	0.44	1.58	0.4
L-I	0.207	0.048	100	0.87	13.6	10.3	8.13	0.33	0.82	0.3
L-I	0.210	0.051	200	0.87	13.0	9.05	7.32	0.24	0.69	0.2
S-II	0.165	--	300	0.87	5.18	3.92	2.82	0.063	0.096	0.02
L-I	0.123	0.034	200	0.34	4.39	3.34	2.46	0.19	0.25	0.08
L-I	0.149	0.033	160	0.34	3.74	3.34	2.44	0.17	0.14	0.05
S-I	0.144	0.007	40	0.67	3.00	2.46	1.77	0.08	0.12	--
L-I	0.094	0.026	200	0.34	0.42	0.27	0.20	0.11	0.0080	--
L-I	0.096	0.023	200	0.34	0.24	0.22	0.16	0.050	0.0047	--
L-III	--	--	100	0.34	--	0.21	0.14	0.070	0.0022	--
S-I	0.090	--	720	0.44	0.10	0.089	0.062	0.008	0.0026	--

a. L denotes the 3.8 cm long cell and S the 0.9 cm short cell. Sample I is 4.9 Torr SiF_4 - 0.37 Torr C_2H_5Cl - 0.37 Torr $CHCl_2CH_2Cl$. Sample II is 5.2 Torr SiF_4 - 0.26 Torr C_2H_5Cl - 0.38 Torr $CHCl_2CH_2Cl$ - 0.14 Torr toluene. Sample III is 4.9 Torr SiF_4 - 0.70 Torr $CHCl_2CH_2Cl$.

b. P(40) line pulse energy with uncertainty ±5-10%.

c. Uncertainty ~ ±10%.

d. The per pulse yield has uncertainty of ±8% except for C_2HCl.

e. C_2HCl_3 was also observed in some pyrolyses. However, the amount was too small to allow meaningful measurement.

f. From radical reactions involving both C_2H_5Cl and $CHCl_2CH_2Cl$.

g. From secondary decomposition of dichloroethenes.

Fig. IV-4. The product yield from 1,1,2-trichloroethane dissociation vs the corresponding ethyl chloride dissociation yield. Points are experimental results. The curves are the best fits from the model calculation with the E_a and A shown in Table IV-8. (s) denotes the short cell pyrolyses at the same pressure. (p) denotes the pyrolyses without ethyl chloride. (t) is the pyrolysis with toluene in the mixture.

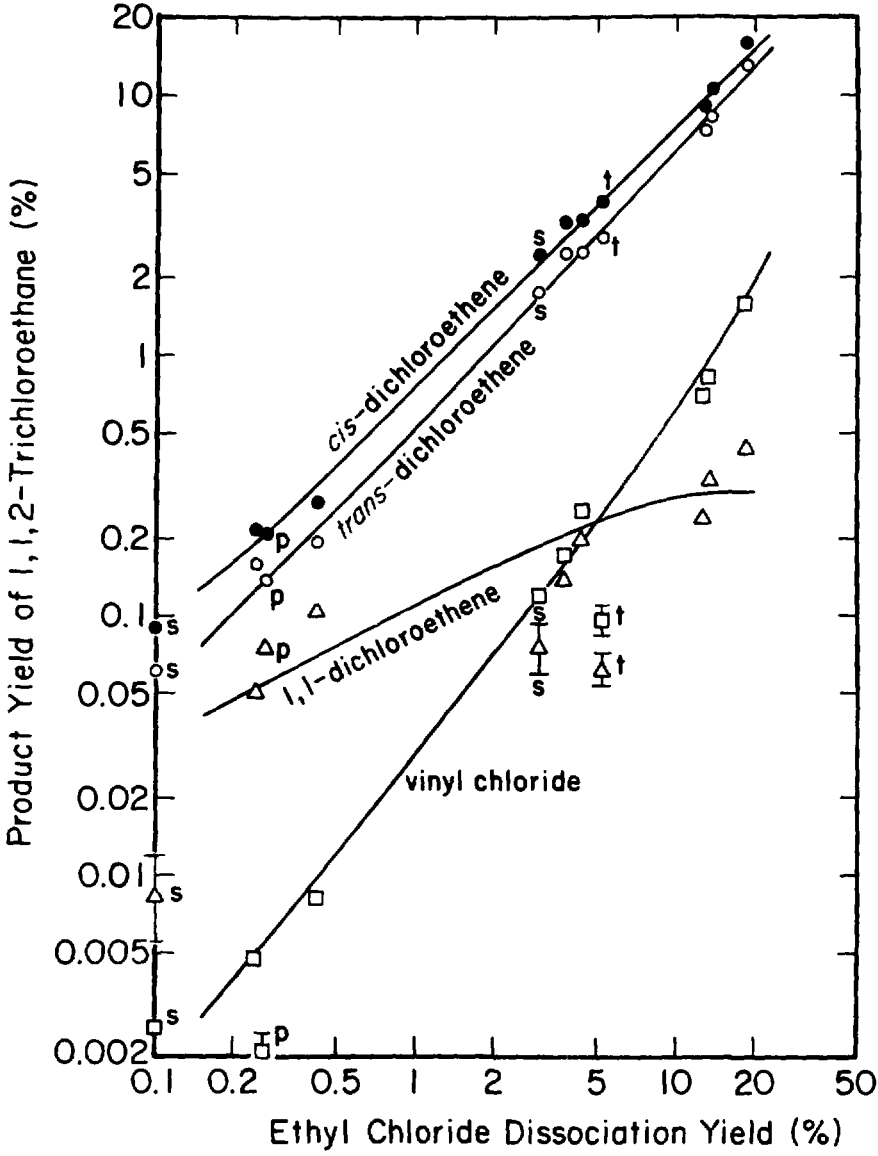
Product Yield of 1,1,2-Trichloroethane (%)
20
10
5
2
1
0.5
0.2
0.1
0.05
0.02
0.01
0.005
0.002
0.1
0.2
0.5
1
2
5
10
20
50
Ethyl Chloride Dissociation Yield (%)
cis-dichloroethene
trans-dichloroethene
1,1-dichloroethene
vinyl chloride
s
p
t

Fig. IV-4

compound should be from the secondary HCl elimination reaction of trans-dichloroethene (see discussion below) and its quantity was added to the trans-dichloroethene yield. The C_2HCl correction amounts to less than 5% of the trans-dichloroethene yield in the three high yield pyrolyses of Fig. IV-4.

Before taking the results in Fig. IV-3 and IV-4 to compare with the model calculation, the following questions regarding the pyrolysis process should be clarified. Are all the product yields from sensitized reactions; is there any contribution from direct multiphoton dissociation (MPD)? Are those observed yields affected by secondary reactions, such as trans-cis isomerization, and even by bimolecular reactions? Is the thermalization in the irradiation column complete before the reaction starts? Can the gas medium during the reaction be described by a single temperature?

Significant dissociation of SiF_4 by MPD is not anticipated even at the highest fluence, 1.7 J/cm^2, used for pyrolysis. SiF_4 has a fairly high bond energy, 143 kcal/mole.[103] $\langle n \rangle$, the average number of photons absorbed per SiF_4 molecule in the irradiation column was measured to be about 8 at 1.7 J/cm^2. For SF_6, which has a dissociation energy 50 kcal/mole lower, the MPD yield is $\lesssim$0.01% where $\langle n \rangle$ is about 8.[11] Also in the product analysis no hydrocarbons containing fluorine were detected, indicating no dissociation of SiF_4 in the pyrolysis. As for the possibility of MPD of all other reactants and products, the examination of their infrared fundamentals shows that except for

ethylene and vinyl chloride there is no absorption at 1027.4 cm^{-1} for all the other molecules. The threshold for MPD of vinyl chloride at the strong 940 cm^{-1} band was estimated to be 20-40 J/cm^2.[104] Therefore irradiation at the weaker 1030 cm^{-1} band with 1.7 J/cm^2 would hardly cause any dissociation. For ethylene MPD close to the 950 cm^{-1} band center the threshold was estimated to be about 20 J/cm^2.[105] At 1.7 J/cm^2 irradiation at the shoulder of the R branch would also not cause dissociation of ethylene.

The secondary reactions of the pyrolysis products generally have E_a about 10 kcal/mole higher than these of the dissociation reactions of the reactant, except for the trans-cis isomerization of 1,2-dichloroethene for which E_a was estimated around 55 kcal/mole.[106] The pyrolysis of 0.76 Torr cis-dichloroethene in 4.8 Torr SiF_4 with 0.2 J/pulse showed a 5% conversion per pulse from cis to trans form, Table IV-3. The heat of formation of the cis form is 1 kcal/mole higher than that of the trans form,[41] so E_a for the cis→trans reaction should be 1 kcal/mole lower than the trans→cis reaction. It is reasonable to assume then that the trans→cis rate constant is comparable to the cis→trans rate constant. The cell volume is about 40 times that of the irradiation column. After each laser pulse, more than 97% of the product would diffuse out of the irradiation column. Therefore the net effect of the isomerization on the product yield is negligible. In the same pyrolysis of cis-dichloroethene very small amount of C_2HCl was observed. Also a pyrolysis of 0.72 Torr CCl_2CH_2

Table IV-3. Experimental results of some test pyrolyses.

Sample[a]	Number of Pulses[b]	Product	Yield (%)[c]
0.76 Torr cis-$C_2H_2Cl_2$	50	trans-$C_2H_2Cl_2$	5.0
		C_2HCl	$\leq$0.14
		CCl_2CH_2	$\leq$0.002
0.72 Torr CCl_2CH_2	100	C_2HCl	0.10
0.36 Torr HCl +	150	CCl_3CH_3	<0.001
0.34 Torr CCl_2CH_2		$CHCl_2CH_2Cl$	<0.001

a. In presence with 4.9 ± 0.1 Torr SiF_4 in the 3.8 cm long cell.
b. P(40) line with pulse energy ~0.19-0.20 J at a repetition rate of 0.87 Hz.
c. The per pulse yield in the irradiation column has an uncertainty of ±8%. The detection limit is ~0.001%.

in 4.9 Torr SiF_4 with 0.2 J/pulse showed that that the yield of C_2HCl is only 1%. The small quantity of C_2HCl observed in the pyrolysis of 112TCE with high pulse energies must be from the dissociation of trans-dichloroethene. A test on the possibility of bimolecular recombination reaction by the products was also tried. However, no reaction was detected at the detection limit of 0.001% per pulse yield for the gas mixture of 0.36 Torr HCl- 0.34 Torr CCl_2CH_2- 5 Torr SiF_4 after 150 pulses of 0.2 J/pulse.

Two assumptions were made in modelling the pyrolysis process. (1). It was assumed that collisions between SiF_4 and the reactants would transfer energy fast enough so that a thermal equilibrium can be established before the energy starts to transfer out of the irradiation column. Therefore a maximum temperature is quickly reached after the laser pulse but before a significant amount of reaction occurs. (2). Both the E_a and A used for calculating the yield of the internal standard, ethyl chloride, are taken from their high pressure limit. Therefore in the pyrolysis experiments, the working pressure for the reactant should be much larger than the half-quenching pressure $P_{1/2}$, if a meaningful comparison with the calculation is to be made.

These two assumptions can be examined by comparing the yield from the pyrolysis experiments described in the Experimental section with the yield from pyrolysis at higher pressures. If the thermalization of the absorbed energy were incomplete before the energy were lost from the irradiation column or if the reaction rate in the original

pyrolysis was not close to the high pressure value, then the increased number of collisions between SiF_4 and the reactants at a higher pressure of the mixture would have increased the product yield. Such a high pressure pyrolysis must be performed at the same molar ratio of the mixture and the total energy absorbed per molecule must be the same as in the original pyrolysis. A mixture of 22 Torr SiF_4- 1.7 Torr 111TCE-1.7 Torr ethyl chloride in a shorter cell 0.9 cm in length was irradiated with laser pulses at the 1033.5 cm^{-1} (P(34) line), Table IV-1. The pressure of each component in the mixture was about 4 times the original pressure. The pressure and the cell length were matched so that the total number of molecules in the irradiation column was the same as in the original pyrolysis. Because of the higher absorption at higher pressures for the same amount of molecules, P(34) line, where the absorption by SiF_4 is lower than at the P(40) line at the same SiF_4 pressure, was choosen to make the total percentage absorption similar to the original pyrolysis. The product yields of the high pressure pyrolysis were found to be within the error limits of those of the lower pressure pyrolysis, Fig. IV-2. It is then concluded that the two assumptions can be used in modelling the pyrolysis. Another implication from the short cell pyrolysis is that the product of 111TCE dissociation comes from homogeneous gas phase reaction and the wall induced dissociation is negligible. The irradiation column was about 2 cm away from the pyrex wall of the cell. When the heat diffuses to the pyrex wall, the heat content of the molecules there

should be very roughly (irradiaton column diameter)/(cell diameter) times that in the irradiation column. Therefore unless the E_a of the glass wall induced reaction is exceedingly low, no contribution from the glass surface reaction to the product yield is expected. However, there is also concern for the NaCl window surface directly in contact with the irradiation column. In the short cell the ratio of the NaCl surface area vs the irradiation volume is about 4 times that in the long cell. The number of collisions of the hot gas on the window is 4 times higher in the short cell. The product yield in the short cell did not increase correspondingly, thus indicating no NaCl surface induced dissociation.

2. IR Fluorescence

The observed fluorescence at 5 μm must be from the $\Delta v = 2$ transition of the 1022 cm^{-1} mode of SiF_4. The fluorescence is a good indicator of the temperature in the irradiation column. Figure IV-5 shows the dependence of the quantity $\sum_{v\geq 2} v(v-1)N_v(T)$ on temperature; N_v is the population at vibrational level v. Despite the dependence of oscillator strengths on the symmetry of the vibrational state, the 5 μm fluorescence intensity should be approximately proportional to this quantity. From Fig. IV-5 it seems that the fluorescence intensity increases almost linearly from T larger than 800°K for an interval of 400° within ±10% error. A typical time-resolved fluorescence trace is shown in Fig. IV-6. The fluorescence rises in the combined time

Fig. IV-5. SiF_4 ν_3 mode population multiplied by the quantum number dependence for $\Delta v = 2$ transition as a function of temperature.

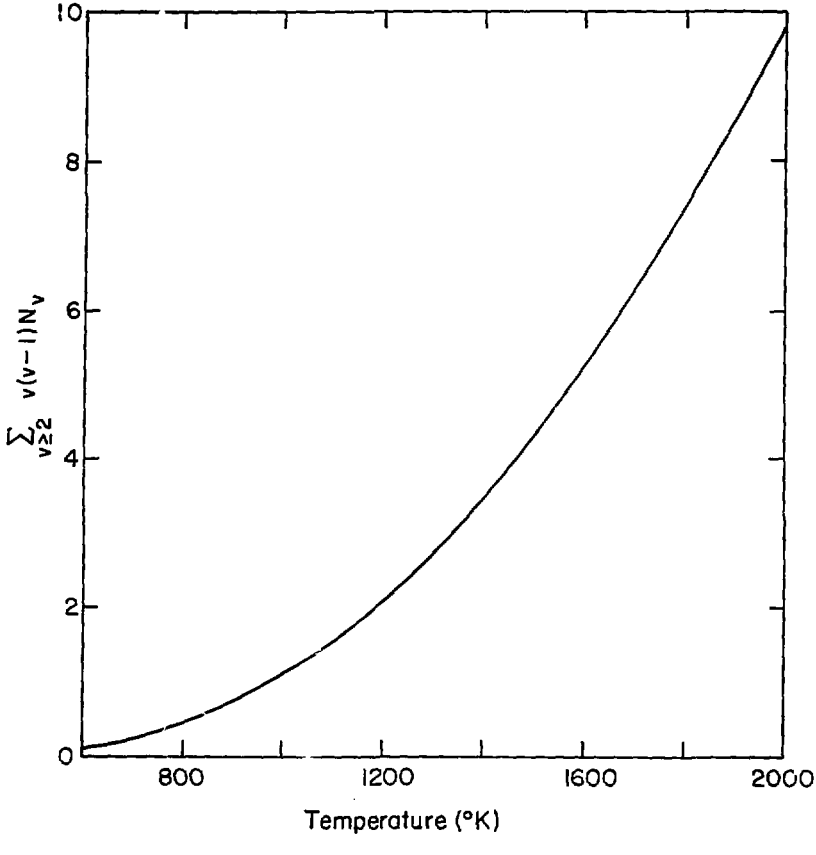

Fig. IV-5

Fig. IV-6. Fluorescence trace at 5.0 μm from the gas mixture excited by 0.175 J/pulse laser. The first spike is enlarged in the insert (a). The dashed line (-----) indicates the exponential decay with $D = 3.5 \times 10^4$ sec^{-1}.

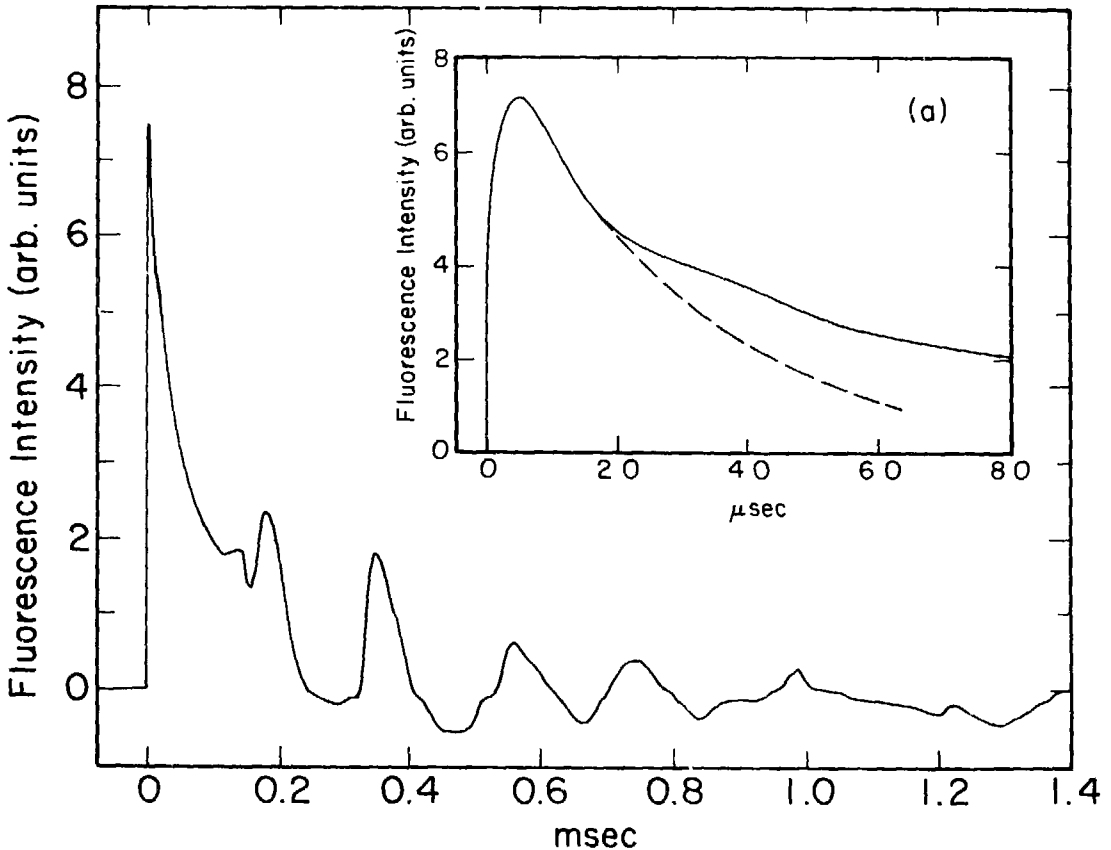
Fluorescence Intensity (arb. units)
8
6
4
2
0
0
0.2
0.4
0.6
0.8
1.0
1.2
1.4
msec
(a)
Fluorescence Intensity (arb. units)
8
6
4
2
0
0
20
40
60
80
μsec

Fig. IV-6

of the 1.3 μsec laser pulse duration and the 0.4 μsec detector response time. The thermalization in the mixture in the irradiation column should be completed before the maximum fluorescence intensity is reached. The V-V energy transfer between a highly excited SiF_4 molecule and a cold reactant or SiF_4 molecule should occur on a near gas kinetic time scale (see Chapter III and Refs. 59 and 82). The vibrational frequencies of the fundamentals of SiF_4 and the reactants are listed in Table IV-4. For each reactant there are several vibrational modes with frequencies very close (difference smaller than kT_r) to those of the SiF_4 modes to make near-resonant V-V transfer possible. For the V-T (vibration-translation) process, it was concluded after a series of studies with many polyatomics that the rate of such processes is usually determined by the V-T transfer rate for the lowest vibrational mode.[107] The frequency of the lowest mode of SiF_4 is 260 cm^{-1}. From the Lambert-Slater plot[107] it was estimated that V-T relaxation occurs in 65 collisions through this low frequency mode. The reactants have frequencies even lower than 260 cm^{-1}. V-T relaxation through the reactants would then be even faster since the fast V-V rate may provide rapid vibrational equilibration between SiF_4 and reactants. During the laser pulse alone more than 65 collisions per molecule occur at the pyrolysis pressure at room temperature. Since the translational temperature would increase during the process of vibrational relaxation, many more collisions within and shortly after the laser pulse for each molecule in the irradiation column should be expected. Thus the

Table IV-4. Vibrational frequencies of the molecules in the pyrolysis mixtures.

Frequency (cm^{-1})			
SiF_4[a]	C_2H_5Cl[b]	CCl_3CH_3[c]	$CHCl_2CH_2Cl$[d]
1022(3)[e]	3014	3005(2)	3013
800	2986	2938	2995
420(3)	2967	1444(2)	2956
260(2)	2946	1378	1477
	2887	1081(2)	1322
	1470	1067	1256
	1448	712(2)	1215
	1448	521	1160
	1385	343	1015
	1289	343(2)	911
	1251	239(2)	822
	1081	-- [f]	711
	1036		666
	974		393
	786		326
	677		256
	336		191
	251		101

a. From Ref. 116.
b. From Ref. 45.
c. From Ref. 117.
d. From Ref. 71.
e. Number in the parenthesis indicates degeneracy.
f. The CH_3 tortional mode is not IR and Raman active.

complete thermalization of the absorbed energy is anticipated at the maximum fluorescence. This point is also supported by the results from the high pressure pyrolysis described in the previous subsection.

A series of sharp spikes with decreasing amplitude appear in the fluorescence trace, Fig. IV-6. These spikes are believed to be due to modulation of temperature in the irradiation column by shockwaves propagating between the center of the column and the cold wall of the fluorescence cell. During the propagation the shockwave dissipates energy to the originally cold gas outside the irradiation column and to the cell wall, therefore the retuning shockwave from the wall to the column carries less energy each time and the fluorescence intensity decreases from one spike to the next. The time interval between two consecutive spikes corresponds to the round-trip travelling time of the shockwave between the column and the wall. This time interval increases from about 175 μsec between the first two spikes to about 220 μsec between the 5th and 6th spikes. The shockwave speed varies as the square root of its amplitude.[108] The 1.5 times increase of the shockwave travelling time indicates a 2.2 times decrease of the temperature in the column. This is reflected by the fluorescence intensity which decreases by an order of magnitude from the maximum to the 5th spike (c.f. Fig. IV-5). The radius of the fluorescence cell is 2.5 cm. The 175 μsec time interval gives approximate speed of 2.8 x 10^4 cm/sec for the initial propagation of the shockwave in the 6 Torr mixture. The radius of the irradiation column is only 0.32 cm. This

means that it only takes on the order of 10 μsec for the shock wave to carry the energy out of the column. A shoulder was observed 30 μsec after the fluorescence maximum on the slope of the first spike, Fig. IV-6(a). This could result from a shock wave moving longitudinally due to a 20-30% energy difference between molecules at the two ends of the cell. The amplitude of the second fluorescence spike is only about 1/3 of that of the maximum. The temperature at the second spike must be many hundreds degree Kelvin lower than the maximum temperature. This means that the pyrolysis occurs predominantly in the time interval of the first spike. The decay of the fluorescence shown in Fig. IV-6(a) is certainly not a single exponential. However by neglecting the small shoulder, the decay in the first 20 μsec can be treated as a single exponential and a rate constant can be extracted. This rate constant should be sufficient in defining the temperature variation during the course of the reactions. The ~30% drop in fluorescence intensity during this 20 μsec indicates a several hundred degree decrease in temperature. Almost all the reactions should occur within this period. The rate constant was later used as D for the temperature decay in the model calculation. It was also found that this decay rate depends on the incident pulse energy, Fig. IV-7. As the laser energy changes, the energy absorbed and thus the maximum temperature in the irradiation column changes. The higher the temperature is, the faster the shock wave moves. This was clearly indicated by the trend of the time interval between the first two fluorescence spikes at different pulse energy; the time

Fig. IV-7. Decay rate constant of the first ir fluorescence spike as a function of incident laser pulse energy.

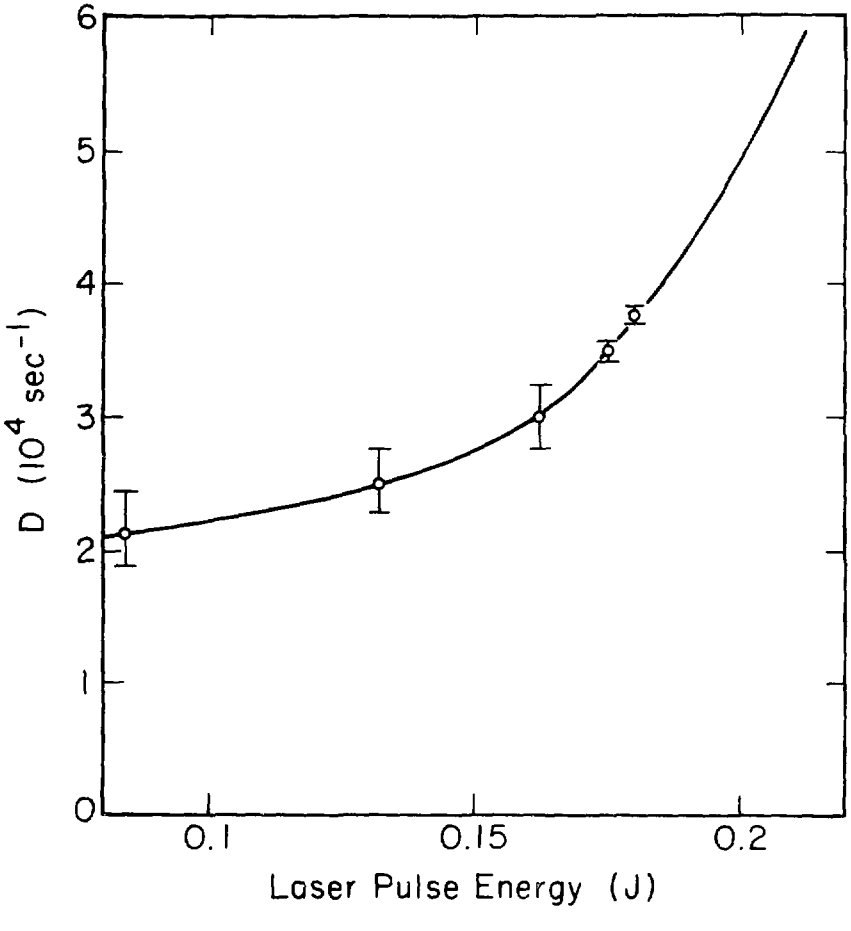

Fig. IV-7

interval increased from 175 μsec at 0.175 J/pulse to 205 μsec at 0.132 J/pulse. However, since the variation of the energy absorbed is less than a factor of two between the highest and the lowest pulse energies in Fig. IV-7, the variation of the decay rate should only be about a factor of $\sqrt{2}$.

The reasons that no fluorescence at 3.4 μm was observed may be as follows. (1). The CH stretching 1→0 fluorescence from the irradiation column was filtered out by the cold gas outside the column. (2). The 2→1 fluorescence was too weak to be detected, since even at 1600°K $v_{CH} = 2$ population would be smaller than 0.2%.

3. Model Calculation and the Extraction of E_a and A

In the model described in Section C parameters T_m, D, E_a and A are required to calculate ϕ. With D obtained from ir fluorescence and ϕ measured for EtCl dissociation, E_a and A of which are known, T_m can be determined. T_m as a function of ϕ(EtCl) is shown in Fig. IV-8. The curve is used later to calculate ϕ(reactant) with assumed E_a and A. Consequently E_a and A for a specific reaction of the reactant are obtained by fitting the calculated yield curve to the experimental points.

Also shown in Fig. IV-8 is the maximum temperature calculated by assuming that the measured absorbed energy is statistically distributed among all of the degrees of freedom of the molecules present in the irradiation column.[49] T_m calculated from the model spans a range of 400°K for the ethyl chloride yield range from 0.1% to 20%. This

Fig. IV-8. Maximum temperature in the reaction zone after laser excitation vs the corresponding ethyl chloride yield. The points are calculated by statistical distribution of the measured absorbed energy with a ±10% uncertainty. The solid line is calculated from the phenomenological model calculation.

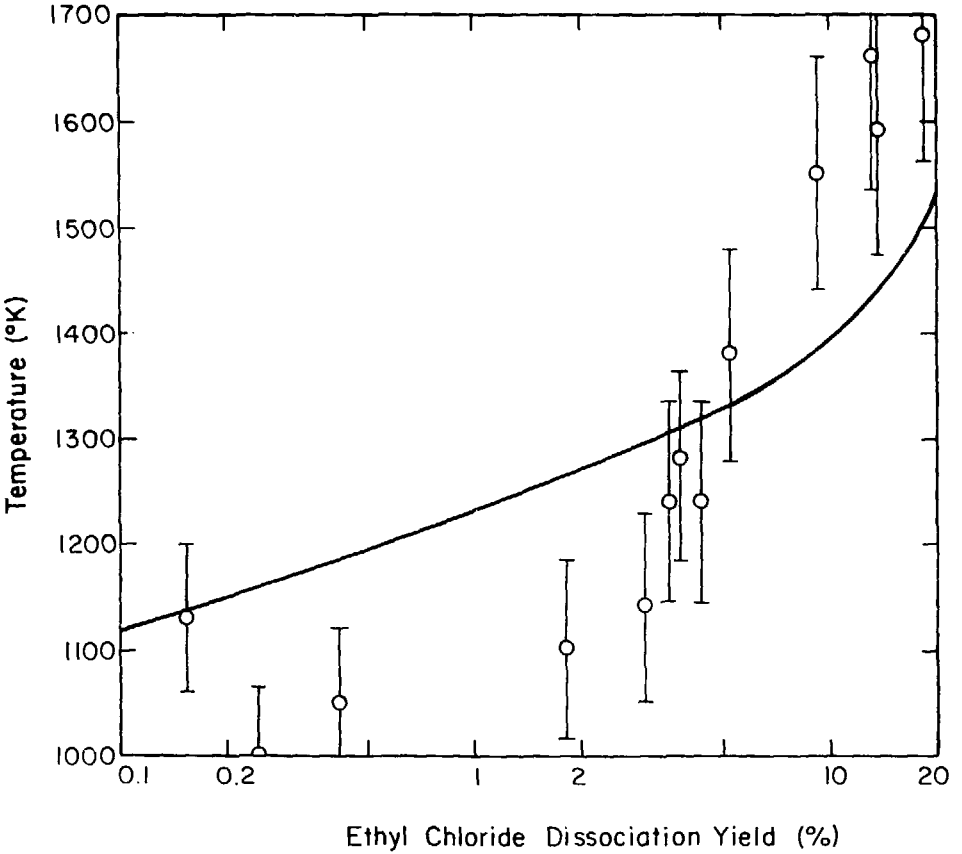
1700
1600
1500
1400
1300
1200
1100
1000
Temperature (°K)
0.1
0.2
1
2
10
20
Ethyl Chloride Dissociation Yield (%)

Fig. IV-8

temperature span seems to be somewhat smaller than the one estimated from the absorbed energy, which is about 600° ± 200° wide. Such a mismatch may well be induced by the simplified picture of a unified temperature decay in the reaction zone in the model calculation. However any defect that might result from this simplified treatment of the temperature history is compensated by the usage of the "internal standard". Even though T_m and D may not represent the true temperature history in the reaction zone, the two parameters can certainly characterize the pyrolysis process in the phenomenological model that produces correct yield for ethyl chloride and may be transferred to characterize the dissociation of other reactants simultaneously present with ethyl chloride in the irradiation column. The sensitivity of the result to these parameters is tested by the following calculations which used sets of T_m and D values different from Figs. IV-7 and IV-8. These D and T_m values were matched to give correct ϕ for ethyl chloride. It was found that these calculations gave similar E_a and A values to those obtained for 111TCE dissociation from calculations with the curves in Figs. IV-7 and IV-8. The test calculations performed were:

1. By decreasing the irradiation volume by 75% (the 1/e width of the laser profile was used as the diameter of the irradiation column), all the ϕ's were increased by 75% while ϕ(reactant)/ϕ(EtCl) is still the same. Fig. IV-7 was still used for D yet a new T_m curve was calculated to fit the new ϕ(EtCl). T_m was about 50° higher than the curve in Fig. IV-8.

2. The D values obtained from ir fluorescence were varied by 30% and a new T_m curve, about 10°K away from the Fig. IV-8 curve, was calculated to fit the ethyl chloride yield.

In both calculations the E_a and logA values of 111TCE dissociation that best fitted the ϕ(111TCE)-ϕ(EtCl) curve fell in the range of 49 ± 1 kcal/mole and 13 ± 0.2 respectively, Fig. IV-9 and Table IV-5.

Because of the exponential dependence of the reaction rate constant on temperature, the longitudinal and transverse inhomogeneity of temperature in the irradiation column, resulted from the laser intensity distribution and the large percentage absorption by the mixture, may affect the value of the product yield. The product yield can not be designated to a definitive temperature, since the temperature of the reaction zone varies with time. With the usage of the internal standard, it is the ratio of ϕ(reactant)/ϕ(internal standard) rather than ϕ(reactant) that determines the evaluation of the kinetic parameters. The temperature inhomogeneity may cause the absolute value of ϕ to deviate from the true value, but its effect on the ratio of the yields is small. The effect of the longitudinal temperature inhomogeneity is discussed here. It is clear from Equation (IV-2) that the product yield is inversely proportional to the reaction zone $V_{reac.}$,

$$\phi = C/V_{reac.} \qquad \text{(IV-7)}$$

Fig. IV-9. Test calculations for CCl_3CH_3 dissociation. A 75% smaller irradiation volume was used to evaluate the experimental yields, (⧫). The yields here are 75% higher than in Fig. IV-3. Solid lines are the fitting curves from the model calculation. The numbers at the curve indicate the E_a value. E_a and logA are 52 and 13.55, 50 and 13.07, 48 and 12.92, and 46 and 12.60, respectively. The best values that fit the points are E_a = 49 and logA = 13.0.

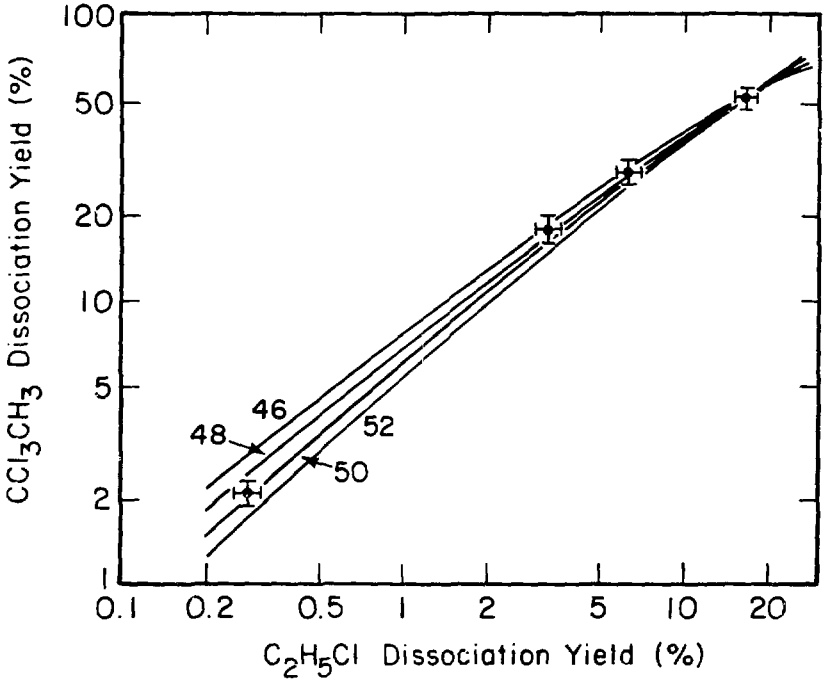
100
50
20
10
5
2
1
0.1
0.2
0.5
1
2
5
10
20
46
48
52
50
CCl_3CH_3 Dissociation Yield (%)
C_2H_5Cl Dissociation Yield (%)

Fig. IV-9

Table IV-5. Test calculations for CCl_3CH_3 dissociation using different sets of T_m and D.

Set	ϕ(EtCl)(%)	D($10^4 sec^{-1}$)	T_m(°K)	E_a(kcal/mole)	logA	ϕ(111TCE)(%)
I[a]	0.15	2.10	1136	49	13.018	1.11
	10.0	3.63	1393	49	13.018	33.3
II[b]	0.15	2.[illegible]9	1148	49	13.025	1.12
	10.0	3.53	1391	49	13.025	33.8

a. This is the set of calculations for the E_a = 49 kcal/mole curve shown in Fig. IV-3. The D values are from the curve in Fig. IV-7.

b. The D values are taken at the edge of the error limit of the points in Fig. IV-7. There is essentially no change for the fitted E_a and A from the values in Set I.

C is a shorthanded form for all the other observables in Equation (IV-2) related to that particular pyrolysis experiment. If there is longitudinal temperature inhomogeneity in the cell, then $V_{reac.}$ in principle is not simply the volume of the irradiation column V_r as in Equation (IV-2). In order to obtain the true product yield for the temperature T_i at the entrance window, the volume of the irradiation column should be normalized according to the reaction rate which varies along the cell longitudinal axis with the temperature. The normalized $\bar{V}_r$ is

$$\bar{V}_r = \pi r^2 \int_0^L e^{-\frac{E_a}{RT(x)}} dx / e^{-E_a/RT_i} \qquad \text{(IV-8)}$$

$$T(x) = T_i(1 - ax/L) \qquad \text{(IV-9)}$$

a is the percentage of the laser energy absorbed by the mixture, L is the cell length, and r is the irradiation column radius. For simplicity a linear decrease of temperature along the longitudinal axis is assumed, Equation (IV-9). The integral in Equation (IV-8) can not be solved analytically. However it can be truncated in m + 1 divisions and evaluated as

$$\bar{V}_r = \frac{V_r}{(m+1)} \sum_{\ell=0}^{m} e^{-\frac{E_a}{RT_i(1-\frac{\ell a}{m})}} / e^{-\frac{E_a}{RT_i}} \qquad \text{(IV-10)}$$

The ratio of ϕ(reactant) and ϕ(int. std.) is

$$\frac{\phi(\text{reactant})}{\phi(\text{int. std.})} = \frac{C_{\text{reactant}}}{C_{\text{int. std.}}} \cdot \frac{\bar{V}_r(E_{a,\ \text{int. std.}})}{\bar{V}_r(E_{a,\ \text{reactant}})} \qquad \text{(IV-11)}$$

For the case of a = 25%, $E_{a,\ \text{int. std.}}$ = 60 kcal/mole, $E_{a,\ \text{reactant}}$ = 30 kcal/mole, the yield ratio is shown in Table IV-6 for three differen T_i. Even though the ratio $V_r/\bar{V}_r$ may be as large as 3-4 at these temperatures for a = 25% and E_a ~ 60 kcal/mole, indicating that $\phi(T_i)$ would heavily underestimated with $V_{\text{reac.}} = V_r$. However, the effect of $V_{\text{reac.}}$ on the yield ratio is small. Even with a 30 kcal/mole difference between $E_{a,\ \text{reactant}}$ and $E_{a,\ \text{int. std.}}$, the yield ratio without considering the temperature inhomogeneity is only ~30% higher than the one for the true yields. Furthermore, the variation of the yield ratio between 1000°K-1500°K is only 6%. This means that E_a and A obtained for the reactant from the yields evaluated according to Equation (IV-2) are only 6% and ~30% different from those that would be obtained without longitudinal temperature inhomogeneity existing in the cell. For an E_a difference of less than 30 kcal/mole, the percentage error would be even smaller. The ϕ has a precision of ±8%. The values obtained for E_a and A in Figs. IV-3 and IV-4 already have uncertainties ~ ±4% and ±200% respectively. Therefore, the error on the determined kinetic parameters caused by the longitudinal inhomogeneous temperature distribution is really minimized by the usage of the internal standard. The same argument can also be applied to the radial temperature inhomogeneity.

Table IV-6. The effect of longitudinal temperature inhomogeneity on the ratio of the reactant dissociation yield and the internal standard dissociation yield.

T_i (°K)	ϕ(reactant)/ϕ(internal standard)[a]	
	$V_{reac.} = V_r$ [b]	$V_{reac.} = \bar{V}_r$ [c]
1500	1	0.67
1250	1	0.69
1000	1	0.72

a. The ratio, in units of $C_{reactant}/C_{int.std.}$, was calculated for the case of 25% absorption of the laser energy. E_a, reactant was assumed to be 30 kcal/mole and $E_{a,int.std.}$ = 60 kcal/mole.

b. Without considering the temperature inhomogeneity, the irradiation volume was taken as the reaction volume.

c. The irradiation volume was normalized according to the longitudinal temperature variation and Eqn. (IV-24) with m = 9.

Thus it can be concluded that the model calculation coupled with the usage of an internal standard can be used effectively to determine E_a and A for an unknown reaction, even for the situation that the E_a of the internal standard is 30 kcal/mole away from that of the unknown reaction.

4. 1,1,1-Trichloroethane Dissociation

Results from the model calculation for the 111TCE dissociation producing CCl_2CH_2 are shown in Fig. IV-3. The best fit with the experiments can be obtained with E_a = 49 kcal/mole and logA = 13.0. The sensitivity of the calculated curve on the values of E_a and A is also displayed in Fig. IV-3. The uncertainty of the experimental points gave a corresponding uncertainty of ±2 kcal/mole for E_a and ±0.3 for logA. It should be noted that in Fig. IV-3 the slope of the ϕ(111TCE) vs ϕ(EtCl) curve is primarily determined by the value of E_a while the variation of A shifts the magnitude of the yield curve.

The values of E_a and A obtained in this study agree with the ones reported by Barton and Onyon,[109] Table IV-7. It was reported in their static pyrolysis that homogeneous dissociation reaction of 111TCE contained two mechanisms; a radical reaction mechanism involving Cl and $CCl_3\dot{C}H_2$ radicals which can be completely surpressed by $\geq$1.5% propylene, and a direct HCl elimination reaction. Under uninhibited conditions (pure 111TCE) the radical reaction dominates. In our

Table IV-7. Kinetic data for the CCl_3CH_3 dissociation producing CCl_2CH_2.

	This Work	Ref. 109
Method	Sensitized Laser Pyrolysis	Static Pyrolysis
Temperature Range (°K)	1000 - 1600	635 - 707
E_a(kcal/mole)[a]	49 ± 2	50.0
logA[a]	13.0 ± 0.3	13.34

a. All the values were obtained from the uninhibited overall reaction rate. In Ref. 109 the maximally inhibited rate gave E_a = 54.2 kcal/mole and logA = 14.0 for the molecular elimination reaction. The radical chain reaction rate gave E_a = 47.9 kcal/mole and logA = 12.53. A shock tube pyrolysis also determined E_a = 54 kcal/mole and logA = 14.0 for the molecular elimination, Ref. 41.

sensitized laser pyrolysis, the radical reaction should not be inhibited by p-dioxane which was at most 0.1% of the amount of 111TCE in the gas mixture. SiF_4 does not affect the radical reaction rate. The very high bond energy of SiF_4 excludes its participation in the radical chain reactions. However, the possible involvement of EtCl in the radical chain reactions of 111TCE should be considered. The most probable radical reaction for EtCl in this system is[110]

$$Cl + C_2H_5Cl \xrightarrow{k_{12}} HCl + \dot{C}HClCH_3 \,. \qquad \text{(IV-12)}$$

$\dot{C}HClCH_3$ does not dissociate into stable molecules without a proton transfer process occurring first. It will be terminated most probably by reacting with a Cl atom

$$Cl + \dot{C}HClCH_3 \xrightarrow{k_{13}} \begin{cases} \xrightarrow{k_{13a}} CHCl_2CH_3 & \text{(IV-13a)} \\ \xrightarrow{k_{13b}} HCl + C_2H_3Cl & \text{(IV-14a)} \end{cases}$$

generating 1,1-dichloroethane and/or vinyl chloride. Since no 1,1-dichloroethane was detected in the pyrolysis at the detection limit of 0.1% yield and the yield of vinyl chloride was two orders of magnitude smaller than the yield of CCl_2CH_2, the effect of EtCl in the radical reactions of 111TCE was negligible. Therefore in the sensitized laser pyrolysis the dissociation of 111TCE is considered as uninhibited and the E_a and A obtained should be compared with the ones from the overall reaction rate in Ref. 109.

5. 1,1,2-Trichloroethane Dissociation

The yield curves from the model calculation that best fit the measured 112TCE product yields are shown in Fig. IV-4 and the values determined for E_a and A are listed in Table IV-8. In the calculation, the yields of cis- and trans-dichloroethene were corrected by the factor $(1 - \frac{1}{2} \sum_{j \neq i} \phi_j)$ (see Model Calculation). Since the yield curves of these two major products are very close and parallel, which indicates that E_a and A for the two reactions are very similar, such a correction should be satisfactory. For the calculation of the yield of the other two products, 1,1-dichloroethene and vinyl chloride, predetermined values of E_a and A for cis- and trans-dichloroethene are used to solve Equation (IV-6). Due to the uncertainty of the experimental points, all the values of E_a and A determined have similar uncertainties except for the product 1,1-dichloroethene, for which the uncertainty is larger due to the larger scattering of the experimental points.

In this study of 112TCE dissociation the microscopic reaction channel, i.e. the elimination of specific H and Cl atoms, can not be identified for each product. The E_a and A obtained can only be viewed as the Arrhenius parameters for the "generation" reaction of the products. E_a for the production of trans- and cis-dichloroethene agree well with the values reported by Kim and Setser in a chemical activation study,[71] Table IV-8. In that study both a 4-centered and a 3-centered activated complex were proposed for the HCl elimination mechanism to produce the dichloroethenes. However, no radical reaction mechanism was discussed.

Table IV-8. Kinetic data for the dissociation of $CHCl_2CH_2Cl$.

	Method	Temperature Range (°K)	E_a (kcal/mole), logA			
			cis-$C_2H_2Cl_2$[a]	trans-$C_2H_2Cl_2$[a]	CCl_2CH_2[b]	C_2H_3Cl[c]
This Work	Sensitized Laser Pyrolysis	1000-1600	60 ± 2, 14.0 ± 0.4	57 ± 2, 13.6 ± 0.4	30 ± 5, 7.7 ± 1	73 ± 2, 15.2 ± 0.4
Ref. 71	Chemical Activation	-- [d]	59 - 60,[e] --	59 - 60,[e] --	57, --	-- --
Ref. 100	Flow Pyrolysis	620-770	-- --	-- --	38, 9.7[f]	-- --
Ref. 101	Flow Pyrolysis	640-800	-- --	-- --	34, 9.9[f]	-- --

a. Values are for the predominant molecular elimination reaction.
b. Determined from the overall rate including contributions from molecular elimination, radical reactions and possibly heterogeneous reactions.
c. Determined from the yield from radical reactions involving both 112TCE and EtCl.
d. The initial energy content of 112TCE was ~90 kcal/mole.
e. 59 kcal/mole is for the 4-centered elimination and 60 kcal/mole for the 3-centered elimination.
f. Determined from the total reaction rate of all products. CCl_2CH_2 was the major product.

E_a for the 4-centered HCl elimination producing CCl_2CH_2 was given as 57 kcal/mole, more than 20 kcal/mole higher than the value determined in this study. The later value, however, agrees more with E_a for the overall dissociation of 112TCE reported in two earlier flow pyrolysis at lower temperatures,[100,101] Table IV-8. In these two studies, CCl_2CH_2 was the major product. In view of the yield curves in Fig. IV-4, it is conceivable that the yield curves of cis- and trans-dichloroethene and that of 1,1-dichloroethene would cross at a temperature lower than 1000°K and 1,1-dichloroethene would become the product with highest yield in the temperature ranges of these two flow pyrolyses. It is not surprising that at these temperatures no vinyl chloride was reported as product. In the chemical activation study, in which the initial energy content of the activated molecule was as high as 90 kcal/mole, vinyl chloride was detected but no kinetic data was reported.

The dissociation mechanisms of 112TCE can be classified into three groups; homogeneous molecular elimination, homogeneous radical chain reactions, and heterogeneous reactions which may involve both radicals and molecules. The homogeneous molecular elimination produces dichloroethenes

$$CHCl_2CH_2Cl \longrightarrow \begin{cases} CCl_2CH_2 + HCl & \text{(IV-14a)} \\ \text{trans-}CHClCHCl + HCl & \text{(IV-14b)} \\ \text{cis-}CHClCHCl + HCl & \text{(IV-14c)} \end{cases}$$

through a 4-centered or a 3-centered activated complex.[71]

Radical chain reactions were reported for the dehydrohalogenation of the primary bormides and most of the polyhalogenated hydrocarbons.[111] In the flow pyrolysis of 112TCE at 720°K, about 90% of the uninhibited overall reaction rate was surpressed by adding toluene to 112TCE.[101] The reaction rate reached a constant level when the toluene concentration was $\gtrsim$5%. Toluene functioned as an inhibitor for the radical chain reaction.[111] At 720°K, $\phi(CCl_2CH_2)/\phi$(trans- and cis-CHClCHCl) = 0.7.[101] After carefully examining the radical reaction rate of the radical reactions involving chlorinated-hydrocarbon radicals,[112] a homogeneous radical chain mechanism for 112TCE dissociation analogous to the mecharism proposed for 1,2-dichloroethane[111] is sketched here.

Initiation $\quad CHCl_2CH_2Cl \xrightarrow{k_i} Cl + \dot{C}HClCH_2Cl \qquad$ (IV-15)

Propagation $\quad Cl + CHCl_2CH_2Cl \xrightarrow{k_a} \dot{C}Cl_2CH_2Cl + HCl \qquad$ (IV-16a)

$\quad Cl + CHCl_2CH_2Cl \xrightarrow{k_a} CHCl_2\dot{C}HCl + HCl \qquad$ (IV-16b)

$$\dot{C}HClCH_2Cl \underset{k_{-17}}{\overset{k_{17}}{\rightleftharpoons}} Cl + C_2H_3Cl \qquad \text{(IV-17)}$$

$$\dot{C}Cl_2CH_2Cl \rightleftharpoons Cl + CCl_2CH_2 \qquad \text{(IV-18)}$$

$$CHCl_2\dot{C}HCl \rightleftharpoons Cl + CHClCHCl \qquad \text{(IV-19)}$$

Termination

$$Cl + \dot{C}HClCH_2Cl \xrightarrow{k_t} CHClCHCl + HCl \qquad \text{(IV-20)}$$
$$\rightarrow CHCl_2CH_2Cl$$

$$Cl + \dot{C}Cl_2CH_2Cl \rightarrow C_2HCl_3 + HCl \qquad \text{(IV-21)}$$
$$\rightarrow CCl_3CH_2Cl$$

$$Cl + CHCl_2\dot{C}HCl \rightarrow C_2HCl_3 + HCl \qquad \text{(IV-22)}$$
$$\rightarrow CHCl_2CHCl_2$$

CHClCHCl may be either in trans- or cis- configuration. The chain is initiated by the rupture of the C(1)-Cl(1) bond, the weakest bond in 112TCE. In general, C-Cl bond is 5-20 kcal/mole weaker than C-C or C-H bonds and the addition of Cl to the carbon atom would lower that bond dissociation energy further by 5-10 kcal/mole.[113] In the propagation the dissociation of the chlorinated radicals should always occur to the Cl atom attached to the carbon next to the radical site. The dissociation of $\dot{C}$-Cl would not occur without a radical rearrangement first. The Cl abstraction was not considered for Cl + 112TCE reaction because generally the Cl abstraction has a much higher E_a than the H abstraction and even at 1600°K its rate may be at most 5% of the H abstraction rate.[112] The recombination reaction of Cl + Cl and the reactions of organic radicals are not included in the termination process because the former is a 3-body reaction and the latter generally have a low A value, logA = 10~11.[112] This mechanism is

consistent with the detection of C_2HCl_3 in the sample after pyrolysis. However the yield of C_2HCl_3 was less than 10% of that of CCl_2CH_2, suggesting that the radicals produced in Equation (IV-16) dissociated mostly through Equations (IV-18) and (IV-19). There might be heterogeneous contribution to the radical reactions, especially in the termination reactions as suggested by some previous studies.[109,110]

Heterogeneous reaction certainly is a distinct possibility for the dissociation of halogenated hydrocarbons.[110] In the flow pyrolysis of 112TCE, E_a = 27.3 kcal/mole and logA = 6.5 were determined from the maximally-inhibited overall reaction rate.[101] CCl_2CH_2 was the main product. The A factor is unreasonably low for a molecular elimination process. The value of E_a is very close to the values previously determined for some glass wall induced molecular elimination reactions.[110] To demonstrate the effect of heterogeneous reaction on the dissociation of 112TCE, two pyrolysis experiments were conducted with the short cell 0.9 cm in length and 4.8 cm in diameter. The pressure was the same as in the long cell experiments and the P(40) line of the laser was used for excitation. The NaCl surface area in contact with the gaseous reaction zone increased by 4 times relative to the volume and the glass surface area in the short cell compared to the long cell. However, none of the 4 products showed higher yield in the short cell pyrolysis, Fig. IV-4. The yield of EtCl was used as an indicator for the temperature here since it has been shown in Section C-1 and Fig. IV-2 that the heterogeneous contribution to the EtCl dissociation was

negligible. Therefore the possibility of heterogenous dissociation of 112TCE on the NaCl window surfaces can be discounted. In contrast, in the short cell pyrolyses the yield of CCl_2CH_2 decreased substantially vs the yields of the other three products. One possible explanation for this decrease is glass wall induced dissociation of 112TCE. In the pyrolysis after the laser excitation, energy absorbed by the irradiation column, $E_{abs.}$, will be dissipated to the surrounding cold gas as the shock wave propagates outward radially. As the heat diffuses to the glass wall, the energy content of the molecules at the wall is higher in the long cell than in the short cell. The short cell diameter is about 25% larger than the long cell. The lower energy content of molecules at the short cell wall may lead to a smaller contribution from wall reactions. The decrease could be fairly substantial if the E_a of the wall induced dissociation is on the order of 27 kcal/mole. Therefore the product yields from the short cell can be viewed as surface-reaction inhibited. The scattering of the data points of CCl_2CH_2 in Fig. IV-4 may be partly due to the contribution from the wall reaction. If the laser beam did not go through the exact same spot of the cell in each pyrolysis, the geometrical variation would cause the temperature at the wall to change and therefore different wall reaction yield from pyrolysis to pyrolysis. A second possible explanation for the decrease of the CCl_2CH_2 yield is through the termination of the radical chain on the NaCl surface. If the termination reactions, Eqns. (IV-20), (IV-21) and (IV-22), occur on the NaCl surface, then the 4

times higher NaCl surface/volume ratio would decrease the radical reaction contribution to the yield. However, since no such yield decreases were observed for the vinyl chloride yield and for the 111TCE dissociation yield, both were predominantly from radical mechanisms, in the short cell pyrolyses, this possibility seemed less likely. There was no discernable decrease for the yields of trans- and cis-dichloroethene. Even though there might be heterogeneous contributions to their yields, the magnitude was within the error limit of the measurements.

With all the reactions considered, the mechanism of the generation of each individual product can now be examined. For the generation of trans- and cis-dichloroethene, the molecular elimination, Eqn. (IV-14b) and Eqn. (IV-14c), should be the predominant mechanism. The heterogeneous contribution has been shown to be negligible. The yield from homogeneous radical reactions depends largely on the rate of reaction (IV-16b). The two reactions, Eqn. (IV-16a) and Eqn. (IV-16b), have been studied and their rate constant determined, $k_a = 10^{12.95} \exp(-3100/RT)$ and $k_b = 10^{13.15} \exp(-3700/RT)$.[114] In the pyrolysis temperature range, $k_b \approx k_a$. Therefore, the yield of either trans- or cis-dichloroethene from radical reaction is comparable to or even smaller than the yield of CCl_2CH_2, which is negligible to the total yield of trans- and cis-dichloroethene for $T \gtrsim 1000°K$. The observed trans- and cis-dichloroethene yield in these sensitized pyrolyses must be primarily from the molecular elimination mechanism

and the E_a and A in Table IV-8 are determined for Eqn. (IV-14b) and Eqn. (IV-14c).

For the generation of CCl_2CH_2, the value 57 kcal/mole determined for the HCl elimination reaction (IV-14a) by the chemical activation study is in contrast with the trend of E_a observed for the HCl elimination reactions of chlorinated ethanes.[71] It was observed that α- and β-chlorination would lower and raise the activation energy by several kcal/mole for the HCl elimination reaction respectively.[42,110] α- and β-positions are defined as Cl-Cl(α)-C(β). This trend agrees with the behavior of the C-Cl bond energy. The α-chlorination would lower the C-Cl bond energy by 5-10 kcal/mole.[113] From this trend, E_a of Eqn. (IV-14a) is expected to be several kcal/mole higher than 59 kcal/mole. The seemingly low 57 kcal/mole may be resulted from that the contribution from the radical chain mechanism to the yield was not considered in the chemical activation study. The yield from molecular elimination tangled with the yield from the radical reactions under uninhibited conditions may give a lower value for E_a as was shown for 111TCE dissociation discussed in the previous subsection. In addition to the possibly high E_a, Eqn. (IV-14a) should have a small A factor. The reaction path degeneracy of the H(1)-Cl(2) elimination is 4 times smaller than that of the H(2)-Cl(1) elimination.[42,71] As a result of higher E_a and smaller A, the yield of CCl_2CH_2 from Eqn. (IV-9a) would be considerably smaller than the trans- and cis-dichloroethene yields to the extent that it is comparable to, if not smaller than, the yield

from radical chain mechanism and heterogeneous reactions. In the sensitized pyrolysis, the surface reaction-inhibited yield from the short cell experiments showed a higher E_a than the one determined from the overall reaction. The slope of the two data points in Fig. IV-4 indicates an $E_a \geq 40$ kcal/mole. In order to obtain the true E_a of Eqn. (IV-14a) the pyrolysis must be performed under maximally-inhibited and surface reaction free conditions.

The contribution from radical reactions to CCl_2CH_2 was demonstrated by a laser pyrolysis with toluene added in the mixture as a radical chain inhibitor. With toluene amounts to 18% of the EtCl-112TCE quantity, the yields of CCl_2CH_2 and C_2H_3Cl decreased by more than a factor of three than the uninhibited pyrolysis yields, Table IV-2 and Fig. IV-4. Though the inhibited pyrolysis was done in the short cell, in which the contribution from the wall induced dissociation is less, the effect of toluene on CCl_2CH_2 yield is still apparent when it is compared with other short cell pyrolyses. In contrast, the inhibited pyrolysis has cis- and trans-dichloroethene yields the same as the uninhibited ones. This also demonstrates that cis- and trans-dichloroethene are predominantly from molecular elimination reactions. Although from the C_2H_3Cl yield it was shown that ~80% of the radical reactions were suppressed by adding 18% toluene, in order to completely eliminate the radical reactions more toluene or a better inhibitor should be used.

The yield of vinyl chloride must be solely from the homogeneous radical chain mechanism. The Cl_2 elimination is excluded because of the very high E_a. The heterogeneous contribution has been shown to be negligible. In the proposed radical mechanism, only reactions (IV-15), (IV-17) and (IV-20) are related to vinyl chloride. However, EtCl in the mixture may also involve the production of vinyl chloride through reactions (IV-12) and (IV-13). Indeed this was demonstrated by a pyrolysis with only 112TCE and SiF_4 in the mixture. All the experimental conditions were the same as described in the Experimental Section except the mixture was composed of 4.9 Torr SiF_4 and 0.7 Torr 112TCE. The EtCl-absent pyrolysis with a low laser fluence showed a 50% decrease of the vinyl chloride yield than that of the EtCl-present pyrolysis at the same fluence, Fig. IV-4. With steady state assumption for the radicals $\dot{C}HClCH_3$ and $\dot{C}HClCH_2Cl$, the rate constant for vinyl chloride production is

$$k_{VC} = \frac{k_{17}(k_i[112TCE] + k_{-17}[Cl][C_2H_3Cl])}{(k_{17} + k_t[Cl])[112TCE]} - \frac{k_{-17}[Cl][C_2H_3Cl]}{[112TCE]} + \frac{k_{12}k_{13b}[Cl][EtCl]}{k_{13}[112TCE]} \qquad \text{(IV-23)}$$

$$\frac{d[VC]}{dt} \equiv k_{VC}[112TCE] \qquad \text{(IV-24)}$$

For the pyrolysis temperature range $k_t[Cl] << k_{12}$ for typical rate constants of H abstraction by Cl and $\dot{C}C$-Cl dissociation.[112] Therefore Eqn. (IV-23) can be written as

$$k_{VC} = k_1 + \frac{k_{12}k_{13b}[Cl][EtCl]}{k_{13}[112TCE]} \qquad \text{(IV-25)}$$

It is clear that pyrolysis of 112TCE in the absence of EtCl would give E_a and A for the C-Cl fission reaction (IV-15). Though in the pyrolysis with EtCl the contribution to the vinyl chloride yield from EtCl may be as high as 50%, the E_a and A obtained still reflect those of the C-Cl fission reaction. In general, for a carbon-halogen bond fission reaction $E_a \approx$ bond dissociation energy and $\log A \approx 15 \pm 1$.[113]

E. Concluding Remarks

The combination of SiF_4 as a sensitizer and a CO_2 pulsed laser as an energy source provides a convenient way to generate transient high temperature pulses in a reaction medium. A wide temperature range can be obtained simply by adjusting the laser energy absorption. With the implementation of an internal standard and the use of a phenomenological model calculation, it was demonstrated that the sensitized laser pyrolysis can be done quantitatively and the values of E_a and A can be determined for an unknown reaction. The results of the dissociation of 1,1,1- and 1,1,2-trichloroethane are summarized in Tables IV-7 and IV-8, respectively. In addition to the HCl molecular elimination reactions, radical chain reactions and even glass wall-induced reactions may contribute to the dissociation of the polychloroethanes. However, these complications for the reaction may be reduced by adding a radical chain inhibitor to the reaction mixture or by proper design of the pyrolysis cell. Furthermore, improvements in other technical aspects may be achieved to improve the quality of the pyrolysis and the model calculation, thereby more accurate values of the kinetic parameters can be obtained:

1. A laser pulse with constant transverse intensity and a well-defined boundary (a cylindrical beam, ideally) is preferred to heat up the gas medium. This would make an accurate measurement of the yield possible. The temperature history of the reaction zone with a homogeneous temperature distribution can also be modelled more realistically.

2. The simple phenomenological model may be revised to more realistically describe the pyrolysis process. Instead of simply assuming an exponential decay for the reaction zone temperature, differential equations for thermal diffusion of a segment of the reaction zone may be introduced.
3. The exact relationship between the fluorescence intensity and the temperature of the fluorescing medium should be established so that the time-resolved fluorescence can be used more precisely for probing the temperature evolution of the medium. Furthermore, instead of SiF_4 a nonreactive gas with similar energy transfer properties as the reactant may be put into the mixture as a fluorescing probe gas for the temperature evolution.
4. The temperature range of the pyrolysis should be extended further. This would certainly create a larger yield range for model calculation fitting, so better accuracy of the determination of the kinetic parameters can be achieved. Also since most of the reactions including the ones choosen as internal standards studied by other methods were with temperatures below 1000°K, laser pyrolysis with a lower temperature range would make the comparison of kinetic parameters with the ones from other methods more significant.
5. For pyrolysis in which glass surface reactions may contaminate the homogeneous reaction rate measurement, either a small diameter laser beam or a large diameter cell are preferred. A large

ratio of total amount of gas in the cell vs the amount of gas in the irradiation volume should make the temperature of the gas at the glass wall so low that the surface reaction is negligible. In contrast, for pyrolysis in which the temperature homogeneity is more of concern than surface reactions, a laser beam with diameter equal to the cell diameter is preferred. In this case the energy loss in the irradiation column will not be caused by shock wave propagation, instead it will be limited by the thermal conduction between the gas and the cell wall, which is a much slower process. Therefore the initial high temperature after the laser excitation would last much longer and the faster gas phase collisional energy transfer would cause a temperaturewise more uniform medium in the cell.

6. SiF_4 pressure, cell length and CO_2 laser line should be properly matched not to cause too large an absorption of the laser beam. Otherwise the medium might have a severe longitudinal inhomogeneity in temperature. However, with the usage of the internal standard, the problem caused by this inhomogeneity was minimized.

APPENDIX I. COMPUTER PROGRAM FOR THE RATE EQUATIONS CALCULATION OF MULTIPHOTON DISSOCIATION

The following changes were made in the original program of Schulz et al.:[61]

1. The rate equation calculation starts from the vibrational ground state population.
2. Formulae are added in to calculate Q_{01} according to Equations (II-10) and (II-11).
3. In addition to I(t), k_ℓ, $\sigma^a_{\ell,\ell+1}$, and vibrational frequencies (for the calculation of $\rho_{vib.}$), inputs for ω_{VB}, $\Delta\omega_\ell$, n, and ω_R at 100 MW/cm^2 are needed.
4. P_{12} in Equation (II-6) was used after the computer calculation to evaluate W_d. The computer calculation from the beginning of the laser pulse till τ_c gives the fraction of molecules dissociated before τ_c as "Yield on". The value of τ_c is calculated as $(7.7\ \mu s^{-1}\ Torr^{-1} \cdot P)^{-1}$ as an input to the program. P is the EtCl pressure. W_d is then calculated as W_d = (Yield on) $\cdot$ P_{12}.

Results of a calculation for 1.7 Torr EtCl irradiated by a 1.1 J/cm^2 narrowband OPO pulse at 2976.6 cm^{-1} are shown after the program.

PROGRAM REAMPA

```
      PROGRAM REAMPA (INPUT,OUTPUT,TAPE5=INPUT,TAPE6=OUTPUT)
C
C RATE EQUATIONS ANALYSIS OF MULTIPHOTON ABSORPTION.
C THIS PROGRAM CALCULATES MPA BY INTEGRATION OF A SET OF RATE EQUATIONS.
C THE RATE EQUATIONS INCLUDE VIBRATIONAL LEVELS FROM V = 0 UPWARD.
C THE INTEGRATION OVER TIME IS DONE AT INTERVALS OF DT = 0.001 NSEC.
C THERE ARE 3 SUBROUTINES.
C A WORD ABOUT UNITS?
C TIME IN NANOSECONDS.  ENERGY IN KCAL/MOLE.  RATE CONSTANTS IN GHZ.
C C POWER DENSITY IN MEGAWATTS/CM2.   CROSS SECTIONS IN 1.0E-19 CM2.
C FREQUENCIES IN CM-1.  FLUENCE IN J/CM2.
C
      COMMON DT
      DIMENSION TITLE(20),RTK(60),ABS(60),SE(60),PEP(60),PDPRV(61)
      DIMENSION DISSCN(60),POW(400)
      DIMENSION P(60),PPRV(61),RTK2(60),ABS2(60),SE2(60),DISS2(60)
      DATA CONST,NDIMN/.0144,60/
C CONST IS A CONVERSION CONSTANT NEEDED FOR THE VARIABLE C.
C
CARD 20A4.  TITLE
CARD 2I10,2F10.4.  NP,NTBP,DT,TMAX.
CARD 4I10.  LEVEL,LDISS,LEVE2,LDIS2.
CARD 8F10.4.  RTK.  LEVEL-LDISS*1 NUMBERS EXPECTED.
CARD 8F10.4.  RTK2. LEVE2-LDIS2*1 NUMBERS EXPECTED.
CARD 6F10.4.  ABS(1),ABS(2),ABS(3),ABSF,ABS2(1),ABSF2.
CARD I10,3F10.4,I10,2F10.4.  NFREQ,EZERO,BETA,DE,NFREQ2,EZERO2,BETA2.
CARD 8F10.4. POW.  NP NUMBERS EXPECTED.
CARD F10.4.  ENRG
C
700   FORMAT (3F10.7,I10)
900   FORMAT (20A4)
801   FORMAT (2I10,2F10.4)
802   FORMAT (I10,3F10.4,I10,2F10.4)
803   FORMAT (8F10.4)
804   FORMAT (4I10)
900   FORMAT (1H120A4)
901   FORMAT (* TIME INCREMENT =*,F5.3,* NSEC.*)
902   FORMAT (1H ,10F10.3)
903   FORMAT (*0THE LASER POWER IN MW/CM2.*/*POWER IS GIVEN AT INTERVALS
     1 OF*,F8.4,* NSEC.  TOTAL ENERGY =*,F6.2,* J/CM2*,35X,*ENERGY*)
904   FORMAT (*0PARAMETERS IN THE FIRST DISSOCIATION?*)
905   FORMAT (* MAXIMUM LEVEL =*,I3,* DISSOCIATIVE LEVEL =*I3,*(INCLUDIN
     1G LEVEL 0.)*)
906   FORMAT (*0PARAMETERS IN THE SECOND DISSOCIATION?*)
950   FORMAT (*NRT=*,I10)
960   FORMAT (*BWL=*,F10.7,*RFSTD=*,F10.7,*RBW=*,F10.7)
1     READ (5,800) TITLE
C
C NP NUMBER OF POWERS TO BE INPUT.  IT IS EITHER THE LENGTH OF THE
C LASER PULSE OR THE ELAPSE OF TIME FOR INTEGRATION IN NSEC.
C NTBP NUMBER OF TIME INTERVALS TO THE OUTPUT OF THE POP. DISTRIBUTIONS.
C DT TIME INCREMENT FOR THE INTEGRATION.
C TMAX DURATION OF THE LASER PULSE.  TMAX/DT=NO. OF TIME INTERVALS.
C ALL VARIABLES BEGINNING WITH L ARE INTEGERS WHICH CORRESPOND TO AN
C ENERGY OF DE*LXXXX. THE SAME VARIABLE PRECEDED BY AN I, AS IN ILXXXX,
```

```
C IS JUST ILXXXX=LXXXX+1.  THIS IS TO GET RID OF THE PROBLEM THAT THE
C POPULATION AT 0 ENERGY RESIDES IN THE VARIABLE POP(1).
C ILEVEL IS THE NUMBER OF LEVELS INCLUDED IN THE FIRST DISSOCIATION.
C ILEVE2 IS THE NUMBER OF LEVELS INCLUDED IN THE SECONDARY DISSOCIATION.
C LDISS,LDIS2 CORRESPOND TO THE DISSOCIATION ENERGIES(1 AND 2), RESP.
C LUP IS THE LEVEL IN THE SECOND ABSORPTION BEYOND WHICH THER IS NO
C DECAY INTO HIGHER LEVELS OF THE SECOND MOLECULE FROM THE FIRST.
C RFSTO IS THE RABI FREQ OF THE PUMP MODE FUNDAMENTAL TRANSITION
C AT 100 MW/CM2.
C RBW IS THE ROTATIONAL BRANCH WIDTH
C BWL IS THE LASER BAND WIDTH.
C NRT IS THE NUMBER OF ROTATIONAL TRANSITIONS IN THE ROTATIONAL BRANCH.
C PB IS THE POWER BROADENING FOR THE FUNDAMENTAL TRANSITION.
C EF IS THE LASER FLUENCE UP TO TIME T FOR THE SATURATION OF THE
C FUNDAMENTAL TRANSITION.
C AA DEFINES THE FREQUENCY RANGE FOR SATURATION.
C
      READ (5,800) NF,NTEP,DT,TMAX
      READ (5,804) LEVEL,LDISS,LEVE2,LDIS2
      ILDISS = LDISS+1
      ILEVEL = LEVEL+1
      LUP = ILEVEL-LDISS
      ILUP = LUP+1
      ILDIS2 = LDIS2+1
      ILEVE2 = LEVE2+1
      DO 5 I=1,LDISS
5     RTK(I) = 0.
      DO 6 I= 1,LDIS2
6     RTK2(I) = 0.
C
C 2 FOLLOWING A VARIABLE INDICATES THAT IT REFERS TO THE SECOND DISS..
C RTK,RTK2 RRKM RATE CONSTANTS FOR THE DISSOCIATION.
C ABS(1),ABS2(1) FIRST ABSORPTION CROSS SECTION.
C ABSF,ABSF2  LAST ABSORPTION CROSS SECTION.
C ABS(2) AND ABS(3) ARE THE V = 1-2 AND 2-3 ABSORPTION CROSS SECTIONS
C RESPECTIVELY.  ABS(3) DECREASES EXPONENTIALLY TO ABSF.  FOR CONSTANT
C ABSORPTION CROSS SECTIONS IN THE GO SET ABS(3) = ABSF.
C DE ENERGY OF THE LASER PHOTON.
C NFREQ,NFREQ2 VIBRATIONAL DEGREES OF FREEDOM IN THE MOLECULE.
C EZERO,EZERO2 ZERO POINT ENRGY OF THE MOLECULE.
C BETA,BETA2  FREQUENCY DISPERSION PARAMETER. SEE ROBINSON AND MOLBERG.
C POW IS THE ARRAY OF POWER DENSITIES OF THE LASER AS A FUNCTION OF TIME
C
      READ (5,803) (RTK(I),I=ILDISS,ILEVEL)
      IF (LEVE2.NE.0) READ (5,803) (RTK2(I),I=ILDIS2,ILEVE2)
      READ (5,803) ABS(1),ABS(2),ABS(3),ABSF,ABS2(1),ABS(2
      READ (5,802) NFREQ,EZERO,BETA,DE,NFREQ2,EZERO2,BETA2
      READ (5,803) (POW(I),I=1,NP)
      READ (5,800) RFSTO,RBW,BWL,NRT
C
C THIS PROGRAM ASSUMES THAT FOR VERY SHORT LIFETIME STATES, MOLECULES AT
C TIME T DISSOCIATE AT TIME T+DT.
      DO 7 I=ILDISS,ILEVEL
7     IF (RTK(I)*DT.GT.1.) RTK(I)=1./DT
      DO 8 I=ILDIS2,ILEVE2
```

```
8       IF (RTK2(I)*DT.GT.1.) RTK2(I)=1./DT
C
C INITIALIZE AND SET THE ARRAYS NECESSARY.
C
        POW(NP+1) = 0.
10      WRITE (6,900) TITLE
        WRITE (6,904)
        WRITE (6,905) LEVEL,LDISS
        CALL PREP(ABS,ABSF,SE,LEVEL,NFREQ,EZERO,BETA,DE,POP,DISSCN,POPPRV,
       INDIMN)
        IF (LEVE2.EQ.0) GO TO 15
        WRITE (6,906)
        WRITE (6,905) LEVE2,LDISS2
        CALL PREP(ABS2,ABSF2,SE2,LEVE2,NFREQ2,EZERO2,BETA2,DE,P,DISS2,PPRV
       1,NDIMN)
15      E = 0.
        DO 20 I=1,NP
20      E = E+POW(I)
        E = E*TMAX/(NP*1000.)
C INITIAL POPULATION DISTRIBUTION.
        POP(1) = NRT*BWL/RBW
        POPPRV(1) = NRT*BWL/RBW
        PPRV = NRT*BWL/RBW
        POWMAX = 0.
C
C PRINT OUT THE ENERGY AND POWER DENSITIES OF THE LASER.
C ENRG TOTAL ENERGY DENSITY IN J/CM2 FOR NORMALIZING POWER DENSITY.
C E IS THE TOTAL ENERGY DENSITY OF THE LASER.
C
        READ (5,803) ENRG
        IF (ENRG .LE. 0.) STOP
        DO 30 I=1,NP
30      POW(I) = POW(I)*ENRG/E
        WRITE (6,903) (TMAX/NP),ENRG
        WRITE (6,902) (POW(I),I=1,NP)
        NRT = TMAX/DT
        WRITE (6,901) DT
        WRITE (6,950) NRT
        WRITE (6,960) BWL,RBSTD,RBW
C
C NOW DO THE INTEGRATION.  INCREMENT OVER TIME, AND FOR EACH TIME CALCU-
C LATE THE POPULATION DISTRIBUTION WHICH RESIDES IN THE ARRAYS POP AND P.
C THE INTEGRATION FOR THE DISCRETE LEVEL EXCITATION IS CARRIED OUT
C TILL THE MAX LASER INTENSITY, THE END OF THE 8TH NSEC IN THIS CASE.
C IF THE LASER INTENSITY MAX IS AT THE M NSEC, THE NUMBER IN STATEMENT
C 75 SHOULD BE CHANGED TO M*1000.  IF THE LASER FLUENCE IS SO LARGE
C THAT THE TOTAL POPULATION >1, THEN THE INTEGRATION VIA STATEMENT 75
C CAN ONLY BE CARRIED OUT TILL A TIME BEFORE THE INTENSITY MAX TO
C MAKE THE TOTAL POPULATION <1.
C TIME DEPENDENT POWER BROADENING EFFECT IS CONSIDERED.
C ABS,ABS2 ARE THE FULL ARRAY OF ABSORPTION CROSS SECTIONS.
C SE,SE2 ARE THE ARRAYS OF STIMULATED EMISSION CROSS SECTIONS FROM PREP.
C C A COEFFICIENT IN THE RATE EQUATIONS INVOLVING THE POWER DENSITY.
C  POPPRV IS THE PREVIOUS POPULATION DISTRIBUTION FOR THE PRIMARY DISSOC.
C PPRV IS THE PREVIOUS POPULATION DISTRIBUTION FOR THE SECOND DISSOC.
```

```
C DISSCN,DISS2 CONTAIN THE TOTAL DISSOCIATION YIELDS FROM EACH LEVEL.
C
      DO 100 I=1,NNT,NTBP
      CALL DISTR (ILEVEL,NDIMN,POPPRV,I,ABS,SE)
      IF (LEVE2.NE.0) CALL DISTR  (ILEVE2,NDIMN,PPRV,I,ABS2,SE2)
      DO 90 J=1,NTPP
      JJ = J+ I - 1
      JJ = JJ/1000
      POWER = PDWI(I+(I+J-2)*NP/NNT)
      L=POWER*DT*CONST/DE
75    IF (JJ .GT. 8000) GO TO 78
      PB = SQRT (POWER/100 ) * RESTO
      EP = 0.
      IF (JJ .EQ. 0) GO TO 401
      DO 400 IW = 1, JJ
400   EP = POW(IW)/100**3 + EP
401   EP = POW(JJ+1)*(JI-JJ*1000)/10**6 + EP
      VALUE = ABS(1)*BWL*2*EP* 14.4 /(DE*(0.005+PB)) -1
      IF (VALUE) 500, 500, 501
500   AA = 0.
      GO TO 76
501   AA = SQRT(ABS(1)*BWL*2*EP* 14.4 /(DE*(0.005+PB)) - 1)
76    F = NRT * (PB * (AA + 1) + BWL) / RBW
      POP(1) = POPPRV(1)+C*(SE(1)*POPPRV(2)-ABS(1)*POPPRV(1))+F-FPRV
      FPRV = F
      GO TO 79
78    POP(1) = POPPRV(1)+C*(SE(1)*POPPRV(2)-ABS(1)*POPPRV(1))
79    DO 80 K = 2, ILEVEL
      POP(K) = POPPRV(K)*(1.-DT*RTK(K))+C*(ABS(K-1)*POPPRV(K-1)+SE(K)*P
     1PPRV(K+1)-(ABS(K)+SE(K-1))*POPPRV(K))
      DISSCN(K) = DT*RTK(K)*POP(K)+DISSCN(K)
80    POPPRV(K-1) = POP(K-1)
      POPPRV(1) = POP(1)
      POPPRV(ILEVEL) = POP(ILEVEL)
      IF (LEVE2.EQ.0) GO TO 90
C
C CALCULATE THE ABSORPTION FOR THE SECOND STEP.
C
      P(4) = PPRV(4)+C*(SE2(4)*PPRV(5)-ABS2(4)*PPRV(4))+POPPRV(4+LDISS)
     1*RTK(4+LDISS)*DT
      DO 85 L=5,LOP
      P(L) = PPRV(L) +C*(ABS2(L-1)*PPRV(L-1) +SE2(L)*PPRV(
     1L+1)-(ABS2(L)+SE2(L-1))*PPRV(L))+POPPRV(L+LDISS)*DT*RTK(L+LDISS)
85    PPRV(L-1)= P(L-1)
      DO 86 L=LOP,ILEVE2
      P(L) = PPRV(L)*(1.-DT*RTK2(L))+C*(ABS2(L-1)*PPRV(L-1)+SE2(L)*PPRV(
     1L+1)-(ABS2(L)+SE2(L-1))*PPRV(L))
      DISS2(L) = DT*RTK2(L)*P(L)+DISS2(L)
86    PPRV(L-1) = P(L-1)
      PPRV(ILEVE2)    P(ILEVE2)
90    CONTINUE
100   CONTINUE
C
C CONCLUDE THE PROGRAM BY PRINTING OUT THE DESIRED INFORMATION.
C
```

```
                CALL DISTR (ILEVEL,NDIMN,POP,I,ABS,SE)
                IF (LEVE2.NE.0) CALL DISTR  (ILEVE2,NDIMN,P,I,ABS2,SE2)
                CALL CONCL (DISS,RTK,DISSCN,POP,NDIMN,ILEVEL)
                IF (LEVE2.NE.0) CALL CONCL(DISS2,RTK2,DISS2,P,NDIMN,ILEVE2)
225             GO TO 10
                END


  SUBROUTINE PREP

 1              SUBROUTINE PREP(ABS,ABSF,SE,LEVEL,AFREQ,EZERO,BETA,DE,A,B,C,N)
          C
          C PREP PREPARES FOR THE REST OF THE PROGRAM BY INITIALIZING ARRAYS AND
          C CALCULATING THE CROSS SECTIONS FOR ABSORPTION AND STIMULATED EMISSION.
 5        C ABS AND SE ARE RELATED BY THE RATIO OF THE DENSITY OF STATES AS
          C CALCULATED BY THE WHITTER-RABINOVITCH APPROXIMATION INCLUDING ROTATION
          C ROS IS THE RATIO OF THE DENSITY OF STATES.
          C RES VALUES HERE ARE FOR ETHYL CHLORIDE.
          C
10              DIMENSION ABS(60),SE(60),ROS(60),G(60),A(60),B(60),C(61)
          902   FORMAT (1H 10F10.5)
          904   FORMAT (*ERATIO OF THE DENSITY OF STATES BETWEEN ADJACENT LEVELS*)
          905   FORMAT (*ABSORPTION CROSS SECTION IN 1.0E-19 CM2.*)
                DO 5 I=1,N
15              A(I)=0.
                B(I)=0.
          5     C(I)=0.
                C(N+1) = 0.
                G(1) = .5
20              G(2) = .5
                G(3) = .5
                DO 8 I = 3,LEVEL
                ABS(I+1)= ABS(3)*(ABSF/ABS(3))**((I-2.)/(LEVEL-3.))
                EPR = 1*DE/EZERO
25              W = EXP(-2.4191*EPR**0.25)
                WPR = -0.60478*W*EPR**(-0.75)
                G(I+1) = (EPR+1.-BETA*WPR)**(NFREQ-1)  *(1.-BETA*WPR)
          8     ROS(I) = G(I)/G(I+1)
                ROS(1)=1.
30              ROS(2) = .1
                ROS(3) = .0534
                ROS(4) = .0257
                DO 10 I=1,LEVEL
          10    SE(I) = ABS(I)*ROS(I)
35              ABS(LEVEL+1) = 0.
                SE(LEVEL+1) = 0.
                WRITE (6,904)
                WRITE (6,902) (ROS(I),I=1,LEVEL)
                WRITE (6,905)
40              WRITE (6,902) (ABS(I),I=1,LEVEL)
                RETURN
                END
```

SUBROUTINE DISTR

```
1             SUBROUTINE DISTR (ILEVEL,N,PCP,I,ABS,SE)
        C
        C DISTR OUTPUT THE POPULATION DISTRIBUTION WHICH RESIDES IN PCP.
        C SUM CONTAINS THE TOTAL POPULATION IN THE MOLECULE(UNDISSOCIATED.)
5       C AVG CONTAINS THE AVERAGE NUMBER OF PHOTONS ABSORBED.
        C
              COMMON DT
              DIMENSION PCP(N),ABS(N),SE(N)
        901   FORMAT (*0POPULATION DISTRIBUTION AFTER*,F8.2,* NSEC. SUM =*,F ...
10           1* AVERAGE EXCITATION =*F6.2* CROSS SECTION =*F6.2)
        902   FORMAT (1H ,10F10.7)
              AVG = 0.
              SUM=0.
              CS = ABS(1)*PCP(1)
15            DO 63 K=2,ILEVEL
        63    CS = (ABS(K)-SE(K-1))*PCP(K)+CS
              DO 70 K=1,ILEVEL
              AVG = AVG+(K-1.)*PCP(K)
        70    SUM=SUM+PCP(K)
20            IF (SUM.LE.1.E-8) SUM=1.
              WRITE (6,901) DT*(I-1),SUM,AVG/SUM,CS/SUM
              WRITE (6,902) (PCP(K),K=1,ILEVEL)
              RETURN
              END
```

SUBROUTINE CONCL

```
1             SUBROUTINE CONCL(LDISS,RTK,DISSCN,PCP,N,ILEVEL)
        C
        C CONCL CONCLUDES THE PROGRAM BY PRINTING THE DISSOCIATION YIELDS AT THE
        C END OF THE PULSE.
5       C
              DIMENSION RTK(N),DISSCN(N),PCP(N)
        906   FORMAT (*1DISSOCIATION YIELD*/5HLEVEL,8X,13HRATE CONSTANT,7X,[illegible]
             1LD (N,10X,9HYIELD OFF,10X,11HTOTAL YIELD)
        907   FORMAT (1H0,I4,8X,F10.5,10X,F8.5,11X,F8.5,11X,F8.5)
10            TOON = 0.
              TOOFF = 0.
              WRITE (6,906)
              ILDISS = LDISS+1
              DO 120 I=ILDISS,ILEVEL
15            WRITE (6,907) I-LDISS,RTK(I),DISSCN(I),PCP(I),PCP(I)*DISSCN(I)
              TOON = TOON + DISSCN(I)
        120   TOOFF = TOOFF+PCP(I)
              I=0
              A=0.
20            WRITE (6,907) I,A,TOON,TOOFF,TOON+TOOFF
              RETURN
              END
```

```
ETCL MPC CALCULATION BY RATE EQUATIONS, ML DAI, SEPT 1976

PARAMETERS IN THE FIRST DISSOCIATION?
MAXIMUM LEVEL = 15 DISSOCIATIVE LEVEL =  7(INCLUDING LEVEL 0.)

RATIO OF THE DENSITY OF STATES BETWEEN ADJACENT LEVELS
   1.00000    .10000    .05340    .08570    .12458    .16061    .19454    .22736    .25784    .28[illegible]
   .31317    .33823    .36170    .38370    .40434

ABSORPTION CROSS SECTION IN 1.0E-19 CM2.
  30.00000   5.00000   2.50000   2.50000   2.50000   2.50000   2.50000   2.50000   2.50000   2.5[illegible]
   2.50000   2.50000   2.50000   2.50000   2.50000

THE LASER POWER IN MW/CM2.
 WER IS GIVEN AT INTERVALS OF  1.0000 NSEC.  TOTAL ENERGY =  1.10 J/CM2
     5.270    15.611    30.116    46.233    66.585    87.878   103.901   105.407   100.396    [illegible]
    85.079    73.785    62.491    51.196    40.657    31.622    23.340    15.811     9.039     [illegible]
     0.        0.        0.        0.        0.        0.        0.        0.        0.        0.
     0.        0.        0.        0.        0.        0.        0.        0.        0.        0.
     0.        0.        0.        0.        0.        0.        0.        0.        0.        0.
     0.        0.        0.        0.        0.        0.        0.        0.        0.        0.
     0.        0.        0.        0.        0.        0.        0.        0.        0.        0.
     0.        0.        0.        0.        0.        0.        0.        0.        0.        0.
TIME INCREMENT = .001 NSEC.
IT=      4
ML=  .15000000FSTO= .31800000PB=16.00000000

POPULATION DISTRIBUTION AFTER    0.   NSEC. SUM =  .037500 AVERAGE EXCITATION =  0.   CROSS SECTION = [illegible]
  .037500  0.        0.        0.        0.        0.        0.        0.        0.        [illegible]
  0.        0.        0.        0.        0.

POPULATION DISTRIBUTION AFTER    8.00 NSEC. SUM =  .503986 AVERAGE EXCITATION =  2.15 CROSS SECTION = [illegible]
  .090654  .081533  .135622  .101271  .055155  .023962  .008243  .002639  .000721  [illegible]
  .000254  .000024  .000001  .000000  .000000  .000000

POPULATION DISTRIBUTION AFTER   16.00 NSEC. SUM =  .495425 AVERAGE EXCITATION =  4.23 CROSS SECTION = [illegible]
  .017637  .018716  .057534  .065743  .055936  .066833  .062756  .037017  .014468  [illegible]
  .001463  .000534  .000010  .000000  .000000  .000000

POPULATION DISTRIBUTION AFTER   24.00 NSEC. SUM =  .484969 AVERAGE EXCITATION =  4.34 CROSS SECTION = [illegible]
  .015297  .014452  .050164  .083370  .097633  .089144  .066853  .042468  .021064  [illegible]
  .000225  .000000  .000000  .000000  .000000  .000000

POPULATION DISTRIBUTION AFTER   32.00 NSEC. SUM =  .482732 AVERAGE EXCITATION =  4.30 CROSS SECTION = [illegible]
  .015297  .014452  .050164  .083370  .097633  .089144  .066853  .042361  .019267  [illegible]
  .000001  .000000  .000000  .000000  .000000  0.

POPULATION DISTRIBUTION AFTER   40.00 NSEC. SUM =  .478181 AVERAGE EXCITATION =  4.28 CROSS SECTION = [illegible]
  .015297  .014452  .050164  .083370  .097633  .089144  .066853  .042343  .017[illegible]  [illegible]
  .000000  .000000  .000000  .000000  .000000  0.        0.

POPULATION DISTRIBUTION AFTER   48.00 NSEC. SUM =  .476315 AVERAGE EXCITATION =  4.26 CROSS SECTION = [illegible]
  .015297  .014452  .050164  .083370  .097633  .089144  .066853  .042243  .016[illegible]  [illegible]
  .000000  .000000  .000000  .000000  .000000  0.        0.

POPULATION DISTRIBUTION AFTER   56.00 NSEC. SUM =  .474776 AVERAGE EXCITATION =  4.25 CROSS SECTION = [illegible]
  .015297  .014452  .050164  .083370  .097633  .089144  .066853  .042365  .014747  [illegible]
  .000000  .000000  .000000  .000000  .000000  0.        0.

POPULATION DISTRIBUTION AFTER   64.00 NSEC. SUM =  .473425 AVERAGE EXCITATION =  4.24 CROSS SECTION = [illegible]
  .015297  .014452  .050164  .083370  .097633  .089144  .066853  .042161  .013[illegible]  [illegible]
  .000000  .000000  .000000  .000000  .000000  0.        0.
```

```
POPULATION DISTRIBUTION AFTER   72.00 NSEC. SUM =  .472208 AVERAGE EXCITATION =  4.23 CROSS SECTION =  2.25
 .0152507  .0144852  .0505164  .0833708  .0976331  .0891844   .0668453  .0421338  .0123400  .0030083
 .0000000  .0000000  .0000000 0.         0.        0.

POPULATION DISTRIBUTION AFTER   80.00 NSEC. SUM =  .471058 AVERAGE EXCITATION =  4.22 CROSS SECTION =  2.25
 .0152507  .0144852  .0505164  .0833708  .0976331  .0891844  .0668453  .0420815  .0112474  .0030039
 .0000000  .0000000  .0000000 0.         0.        0.
```

DISSOCIATION LEVEL	YIELD RATE CONSTANT	YIELD ON	YIELD OFF	TOTAL YIELD
1	.00016	.00045	.04208	.04253
2	.01114	.01253	.01129	.02382
3	.12700	.01296	.00330	.01297
4	.65293	.00573	.00000	.00573
5	2.56600	.00115	.00000	.00115
6	6.97400	.00005	.00000	.00005
7	16.08000	.00000	0.	.00000
8	32.35000	.00000	0.	.00000
9	56.66000	.00000	0.	.00000
0	0.	.03292	.05337	.08629

APPENDIX II. COMPUTER PROGRAM FOR THE MODEL CALCULATION OF SENSITIZED LASER PYROLYSIS

A. The Reactant Has Only One Dissociation Channel

```
100 REM SENSITIZED LASER PYROLYSIS MODELLING
101 REM THIS PROGRAM IS TO BE USED ON COMMODORE PET MICROPROCESSOR
102 REM PRINTER DEVICE # ND=4 AND SCREEN DISPLAY ND=3
110 REM TRAPEZOIDAL RULE IS USED TO NUMERICALLY SOLVE EQN (IV-5)
120 REM THE INTEGRATION INTERVAL H IS DETERMINED BY AN ALLOWABLE ERROR ER
130 REM A AND EA ARE THE ARRHENIUS PARAMETERS FOR THE UNIMOLECULAR REACTION
140 REM TM IS THE MAXIMUM TEMPERATURE AFTER THE LASER PULSE
150 REM D IS THE RATE CONSTANT FOR TEMPERATURE DECREASE
160 REM TE IS THE LENGTH OF TIME AFTER THE LASER PULSE FOR REACTIONS TO OCCUR
170 REM TM 3 MEANS THE CUBE OF TM
180 DEF FNF(T)=EXP(-BA/(BB*EXP(-D(J)*T)+TR))
190 DF=0:BA=0:BB=0:T=0:TR=295:I=0:H=0
200 INPUT"A";A
210 INPUT"EA (KCAL/MOLE)";EA
211 INPUT"N (# OF CALCULATIONS)";N
212 FORL=1TON
213 PRINT"L=";L
220 INPUT"TM(L) (KELVIN)";TM(L)
230 INPUT"D(L) (SEC-1)";D(L)
240 INPUT"TE(L) (SEC)";TE(L)
250 INPUT"ER(L) (-LN(1-YIELD))";ER(L)
251 NEXT
260 INPUT"OUTPUT ON PRINTER OR SCREEN";O$
270 IF LEFT$(O$,1)="P" THEN ND=4:GOTO 290
280 ND=3
290 IF ND=4 THEN INPUT"TITLE";T$
300 BA=EA*503.217
301 FORJ=1TON
310 BB=TM(J)-295
320 BD=-BA*BB*D(J)
330 SF=BD*EXP(-BA/TM(J))*(2*BB*D(J)/TM(J)^3+BD/TM(J)^4-D(J)/TM(J)^2)
340 M=INT(SQR((TE(J)^3)*SF*A/(12*ER(J)))+1)
350 H=TE(J)/M
360 DF=(FNF(0)+FNF(TE(J)))/2
370 F=M-1
380 FORI=1TOF:DF=DF+FNF(I*H):NEXT
390 IT=DF*H
400 LN=-A*IT
401 WD=(1-EXP(LN))*100
410 OPEN2,ND,0
420 IF ND=4 THEN PRINT#2,T$
430 PRINT#2,"A=";A
440 PRINT#2,"EA=";EA;"(KCAL/MOLE)"
450 PRINT#2,"TM=";TM(J);"(KELVIN)"
460 PRINT#2,"D=";D(J);"(SEC-1)"
470 PRINT#2,"TE=";TE(J);"(SEC)"
480 PRINT#2,"ER=";ER(J);"(-LN(1-YIELD))"
490 PRINT#2,"INTEGRATION INTERVAL=";H;"(SEC)"
491 PRINT#2,"YIELD=";WD;"(%)"
500 PRINT#2,"LN=";LN;"(LN(1-YIELD))"
510 PRINT#2,CHR$(10);CHR$(10);CHR$(10)
520 CLOSE 2
521 NEXT
READY.
```

```
111TCE DISSOCIATION
A= 1.042E+13
EA= 49 (KCAL/MOLE)
TM= 1126 (KELVIN)
D= 21000 (SEC-1)
TE= 3E-04 (SEC)
ER= 2E-04 (-LN(1-YIELD))
INTEGRATION INTERVAL= 1.36487716E-07 (SEC)
YIELD= 1.1138205 (%)
LN=-.0112006994 (LN(1-YIELD))
```

B. The Reactant Has Several Dissociation Channels

```
100 REM 112TCE DISSOCIATION PRODUCES 4 PRODUCTS
110 REM THIS PROGRAM CALCULATES THE YIELD OF CCL2CH2 OR C2H3CL
120 REM A AND EA PREVIOUSLY DETERMINED FOR C- AND T-C2H2CL2 PRODUCTION
130 REM THEY ARE USED IN 181 AND 182
140 REM FOR OTHER COMMENTS SEE REMARKS IN THE PROGRAM FOR SINGLE REACTION
180 DEF FNF(T)=EXP(-BA/(BB*EXP(-D(J)*T)+TR))
181 DEF FNO(T)=4.38E13*EXP(-20609/(BB*EXP(-D(J)*T)+TR))
182 DEF FNC(T)=1.08E14*EXP(-30199/(BB*EXP(-D(J)*T)+TR))
190 DF=0:BA=0:BB=0:T=0:TR=295:I=0:H=0:OC=0
200 INPUT"A";A
210 INPUT"EA (KCAL/MOLE)";EA
211 INPUT"N (# OF CALCULATIONS)";N
212 FORL=1TON
217 PRINT"L=";L
220 INPUT"TM(L) (KELVIN)";TM(L)
230 INPUT"D(L) (SEC-1)";D(L)
240 INPUT"TE(L) (SEC)";TE(L)
250 INPUT"ER(L) (-LN(1-YIELD))";ER(L)
251 NEXT
260 INPUT"OUTPUT ON PRINTER OR SCREEN";O$
270 IF LEFT$(O$,1)="P" THEN ND=4:GOTO 290
280 ND=2
290 IF ND=4 THEN INPUT"TITLE";T$
300 BA=EA*500.317
301 FORJ=1TON
310 BB=TM(J)-295
320 BD=-BA*BB*D(J)
330 SF=BD*EXP(-BA/TM(J))*(2*BB*D(J)/TM(J) 2+BD/TM(J) 4-D(J)/TM(J) 2)
340 M=INT(SQR((TE(J) 2)*SF*A/(12*ER(J)))+1)
350 H=TE(J)/M
360 DF=(FNF(0)+FNF(TE(J)))/2
361 OC=H*(FNO(0)+FNO(TE(J)))/2+H*(FNC(0)+FNC(TE(J)))/2
370 I=M-1
380 FORI=1TO
381 DF=DF+FNF(I*H)*(1-OC)
382 OC=OC+(FNO(I*H)+FNC(I*H))*H*(1-OC)
383 NEXT
390 IT=DF*H
400 LN=-A*IT
401 WD=(1-EXP(LN))*100
410 OPEN2,ND,0
420 IF ND=4 THEN PRINT#2,T$
430 PRINT#2,"A=";A
440 PRINT#2,"EA=";EA;"(KCAL/MOLE)"
450 PRINT#2,"TM=";TM(J);"(KELVIN)"
460 PRINT#2,"D=";D(J);"(SEC-1)"
470 PRINT#2,"TE=";TE(J);"(SEC)"
480 PRINT#2,"ER=";ER(J);"(-LN(1-YIELD))"
490 PRINT#2,"INTEGRATION INTERVAL=";H;"(SEC)"
491 PRINT#2,"YIELD=";WD;"(%)"
500 PRINT#2,"LN=";LN;"(LN(1-YIELD))"
510 PRINT#2,CHR$(10);CHR$(10);CHR$(10)
520 CLOSE 2
521 NEXT
READY.
```

References

1. N. R. Isenor and M. C. Richardson, Appl. Phys. Lett. 18, 225 (1971).

2. R. V. Ambartzumian, V. S. Letokhov, E. A. Ryabov, and N. V. Chekalin, JETP Lett. 20, 273 (1974); R. V. Ambartzumian, Yu. A. Gorokhov, V. S. Letokhov, and G. N. Makarov, JETP Lett. 21, 171 (1974); J. L. Lyman, R. J. Jensen, J. Rink, C. P. Robinson, and S. D. Rockwood, Appl. Phys. Lett. 27, 87 (1975).

3. N. Bloembergen, Optics Commun. 15, 416 (1975).

4. M. Sargent III, M. O. Scully, and W. E. Lamb, Jr., Laser Physics (Addison-Wesley, Reading, Mass., 1974), Chapter II.

5. M. C. Gower and K. W. Billman, Optics Commun. 20, 123 (1977), Appl. Phys. Lett. 30, 514 (1977).

6. P. Kolodner, C. Winterfeld and E. Yablonovitch, Optics Commun. 20, 119 (1977).

7. J. G. Black, E. Yablonovitch, N. Bloembergen, and S. Mukamel, Phys. Rev. Lett. 38, 1131 (1977).

8. R. V. Ambartzumian, Yu. A. Gorokhov, V. S. Letokhov, G. N. Makarov, and A. A. Puretzkii, JETP Lett. 22, 177 (1975).

9. C. D. Cantrell and H. W. Galbraith, Optics Commun. 18, 513 (1976).

10. J. R. Ackerhalt and H. W. Galbraith, Eleventh Int. Quantum Elect. Conf., Boston, June 1980.

11. R. V. Ambarzumian and V. S. Letokhov in Chemical and Biochemical Applications of Lasers, Vol. III, edited by C. B. Moore

(Academic Press, New York, 1977). Also see F. D. Proch in Advances in Laser Chemistry, edited by A. Zewail (Springer-Verlag, New York, 1978) p.443; W. Fuss, K. L. Kompa, and F. M. G. Tablas, Faraday Discuss. Chem. Soc. 67, 180 (1979).

12. A. V. Nowak and J. L. Lyman, J. Quantum Spectrosc. Radiat. Transfer, 15, 945 (1975).

13. D. S. Bomse, R. L. Woodin, J. L. Beauchamp, in Advances in Laser Chemistry, edited by A. Zewail (Springer-Verlag, New York, 1978) p.362.

14. R. V. Ambartzumian, N. P. Furzikov, Yu. A. Gorokhov, V. S. Letokhov, G. N. Makarov, and A. A. Puretzky, Optics Commun. 18, 517 (1976); Optics Lett. 1, 22 (1977).

15. See for example C. D. Cantrell and K. Fox, Optics Lett. 2, 151 (1978).

16. H. S. Kowk and E. Yablonovitch, Phys. Rev. Lett. 41, 745 (1975).

17. R. G. Bray and M. J. Berry, J. Chem. Phys. 71, 4909 (1979).

18. C. K. Cheng, H. L. Dai, C. B. Moore, and J. S. Wong, Second Chem. Congress of the North Am. Continent, August 1980.

19. G. L. Wolk, R. E. Weston, and G. W. Flynn, J. Chem. Phys. 73, 1649 (1980).

20. P. A. Schulz, Aa. S. Sudbo, D. J. Krajnovich, H. S. Kwok, Y. R. Shen, and Y. T. Lee, Ann. Rev. Phys. Chem. 30, 379 (1979).

21. J. C. Stephenson, S. E. Bialkowski, and D. S. King, J. Chem. Phys. 72, 1161 (1980).

22. E. Yablonovitch, Optics Commun. 1, 87 (1977).

23. E. R. Grant, P. A. Schulz, Aa. S. Sudbo, Y. R. Shen, and Y. T. Lee, Phys. Rev. Lett, 40, 115 (1978).

24. M. J. Schultz and E. Yablonovitch, J. Chem. Phys. 68, 3007 (1978).

25. J. G. Black, P. Kolodoner, M. J. Shultz, E. Yablonovitch, and N. Bloembergen, Phys. Rev. A19, 704 (1979).

26. M. Quack, J. Chem. Phys. 69, 1282 (1978).

27. H. S. Kowk, E. Yablonovitch, and N. Bloembergen, Physics Review A (submitted).

28. J. S. Wong, J. Mol. Spectrosc. 82, 449 (1980).

29. M. J. Coggiola, P. A. Schulz, Y. T. Lee, and Y. R. Shen, Phys. Rev. Lett. 38, 17 (1977).

30. A. H. Kung, H. L. Dai, M. R. Berman, and C. B. Moore, in Laser Spectroscopy IV, edited by H. Walther and K. W. Rothe (Springer-Verlag, Berlin, 1979), p.309.

31. R. V. Ambartzumian, Yu. A. Gorokhov, V. S. Letokhov, and G. N. Makarov, Sov. Phys. JETP 42, 993 (1975).

32. D. K. Evans, R. D. McAlpine, and F. K. McClusky, Chem. Phys. 32, 81 (1978).

33. R. D. McAlpine, D. K. Evans, and F. K. McClusky, Chem. Phys. 39, 263 (1979).

34. R. B. Hall and A. Kaldor, J. Chem. Phys. 70, 4027 (1979).

35. M. R. Berman, P. B. Comita, C. B. Moore, and R. G. Bergman, J. Am. Chem. Soc. 102, 5692 (1980).

36. K. E. Lewis, D. F. McMillen, and D. M. Golden, J. Phys. Chem. 84, 227 (1980).

37. H. Reisler, M. Mangir, and C. Wittig, in Chemical and Biochemical Applications of Lasers, Vol. V, edited by C. B. Moore, (Academic Press, New York, 1980) p.139.

38. J. B. Marling and I. P. Herman, Appl. Phys. Lett. 34, 439 (1979).

39. V. N. Bagratashvili, V. S. Doljikov, V. S. Letokhov, and E. A. Ryabov, Appl. Phys. 20, 231 (1979).

40. A. Kaldor, R. B. Hall, D. M. Cox, J. A. Horsley, P. Rabinovitch, and G. M. Kramer, J. Am. Chem. Soc. 101, 4469 (1979).

41. S. W. Benson and H. E. O'Neal, Kinetic Data on Gas Phase Unimolecular Reactions (Nat. Bureau of Standards, U.S. Department of Commerce, Washington, D.C. 1970).

42. P. J. Robinson and K. A. Holbrook, Unimolecular Reactions (Wiley, New York, 1972).

43. J. C. Hassler and D. W. Setser, J. Chem. Phys. 45, 3246 (1966). K. Dees and D. W. Setser, J. Chem. Phys. 49, 1193 (1968).

44. W. L. Hase and D. L. Bunker, Quantum Chemistry Program Exchange Cat. No. QCPE-234.

45. F. A. Miller and F. E. Kiriat, Spectochim. Acta Part A 25, 1363 (1969).

46. M. B. Zughul, Ph.D. Thesis, Department of Chemistry, University of California, Berkeley (1978).

47. Stephen E. Harris, Proceedings of the IEEE 57, 12 (1969).

48. R. L. Byer and R. L. Herbst, in Nonlinear Infrared Generation, edited by Y. R. Shen (Springer-Verlag, New York, 1977), p.81.

49. M. R. Berman, Ph.D. Thesis, Department of Chemistry, University of California, Berkeley (1981).

50. G. Herzberg, Infrared and Raman Spectra of Polyatomic Molecules (Van Nostrand, New York, 1945), p.421.

51. N. Bloembergen, C. D. Cantrell, and D. M. Larsen, in Tunable Lasers and Applications, edited by A. Mooradian, T. Jaeger, and P. Stokseth (Springer-Verlag, Berlin, 1976), p.162.

52. Aa. S. Subdo, P. A. Schulz, Y. R. Shen, and Y. T. Lee, J. Chem. Phys. 69, 2312 (1978), and references therein.

53. J. C. Lyman, J. Chem. Phys. 67, 1868 (1977).

54. J. C. Stephenson, D. S. King, M. F. Goodman, and J. Stone, J. Chem. Phys. 70, 4496 (1978).

55. W. Fuss, Chem. Phys. 36, 135 (1979).

56. D. M. Cox and J. A. Horsley, J. Chem. Phys. 72, 864 (1980).

57. J. R. Barker, J. Chem. Phys. 72, 3686 (1980).

58. R. G. Gordon, W. Klemperer, and J. I. Steinfeld, Ann. Rev. Phys. Chem. 18, 215 (1967).

59. D. C. Tardy and B. S. Rabinovitch, Chem. Rev. 77, 369 (1977).

60. Handbook of Chemistry and Physics, 54th ed. (Chemical Rubber, Cleveland, 1973).

61. P. A. Schulz, Aa. S. Sudbo, E. R. Grant, Y. R. Shen, and Y. T. Lee, J. Chem. Phys. 72, 4985 (1980); P. A. Schulz, Ph.D. Thesis, University of California, Berkeley (1979).

62. C. Reiser and J. I. Steinfeld, Opt. Eng. 19, 2 (1980).

63. D. O. Ham and M. Rothschild, Opt. Lett. 1, 28 (1977).

64. W. H. Louisell, Quantum Statistical Properties of Radiation (Wiley, New York, 1973); E. W. Montroll and K. E. Shuler, J. Chem. Phys. 26, 454 (1957).

65. W. Fuss, J. Hartmann, and W. E. Schmid, Appl. Phys. 15, 297 (1978).

66. J. L. Lyman, W. C. Danen, A. C. Nilsson, and A. V. Nowak, J. Chem. Phys. 71, 1206 (1979).

67. J. Stone, E. Thiele, M. F. Goodman, J. C. Stephenson, and D. S. King, J. Chem. Phys. 73, 2259 (1980).

68. V. N. Bagratashvili, I. N. Knyazev, V. S. Letokhov, and V. V. Lobko, Opt. Commun. 14, 426 (1975).

69. W. Fuss and K. L. Kompa, Ann. Rev. Phys. Chem. (submitted).

70. K. A. Holbrook and J. S. Palmer, Trans. Faraday Soc. 67, 80 (1971); G. J. Martens, M. Godfroid, and J. Ramoisy, Int. J. Chem. Kinetics 2, 123 (1970).

71. K. C. Kim and D. W. Setser, J. Phys. Chem. 78, 2166 (1974).

72. W. A. Guillory, Introduction to Molecular Spectroscopy (Allyn and Bacon, Boston, 1977), Chapter II.

73. R. D. Hudson, Jr., Infrared System Engineering (Wiley, New York, 1969).

74. P. A. Hackett, C. Willis, and M. Gauthier, J. Chem. Phys. 71, 2682 (1979).

75. S. Mukamel and J. Jortner, J. Chem. Phys. 65, 5204 (1976).

76. R. S. Taylor, T. A. Znotins, E. A. Ballik, and B. K. Garside, J. Appl. Phys. 48, 4435 (1977).

77. N. Bloembergen, and E. Yablonovitch, Phys. Today, May 1978, p.23.

78. C. Reiser, F. M. Lussier, C. C. Jensen, and J. I. Steinfeld, J. Am. Chem. Soc. 101, 350 (1979).

79. R. V. Ambartzumyan, Yu. A. Gorokhov, V. S. Letokhov, G. N. Makarov, and A. A. Puretskii, Sov. Phys. JETP 44, 231 (1976).

80. H. L. Dai, A. H. Kung, and C. B. Moore, J. Chem. Phys. 73, 6124 (1980); Phys. Rev. Lett. 43, 761 (1979).

81. D. M. Brenner, J. Chem. Phys. 74, 494 (1981).

82. George W. Flynn, in Chemical and Biochemical Applications of Lasers, Vol. 1, edited by C. B. Moore (Academic Press, New York, 1974); and references therein.

83. A. C. Baldwin and H. van den Bergh, J. Chem. Phys. 74, 1012 (1981).

84. C. C. Jensen, J. I. Steinfeld, and R. D. Levine, J. Chem. Phys. 69, 1432 (1978).

85. R. D. Bates, J. T. Knudtson, G. W. Flynn, and A. M. Ronn, Chem. Phys. Lett. 8, 103 (1971).

86. L. O'Neil, R. S. Brockaw, Phys. Fluids, 6, 1675 (1963).

87. F. Brunner and D. Proch, J. Chem. Phys. 68, 4936 (1978).

88. C. L. O'Connor, J. Acoust. Soc. Am. 26, 361 (1954).

89. Yu. A. Gorokhov, private communication.

90. V. N. Bagratashvili, I. N. Knyazev, V. S. Letokhov, and V. V. Lobko, Opt. Commun. 18, 525 (1976).

91. H. L. Dai, unpublished result. Photolysis of 1,2-dichloropropane with 1.0 J/cm^2 OPO pulses at 2990 cm^{-1}, on the red side shoulder of the Q branch of the strongest CH stretching fundamental, showed that the product ratio of CH_3CClCH_2:trans-$CHClCHCH_3$:cis-$CHClCHCH_3$:$CH_2ClCHCH_2$ was about 1:2:4:16. The dissociation yield of 1,2-dichloropropane was ~0.9%.

92. H. L. Dai and C. B. Moore, to be published.

93. G. Kohlmaier and B. S. Rabinovitch, J. Chem. Phys. 38, 1692 (1963).

94. D. W. Setser and E. E. Seifert, J. Chem. Phys. 57, 3623 (1972).

95. G. Richmond and D. W. Setser, J. Phys. Chem. 84, 2699 (1980).

96. P. J. Marcoux, E. E. Seifert, and D. W. Setser, Int. J. Chem. Kinet. 7, 473 (1975).

97. W. C. Danen, Opt. Eng. 19, 21 (1980).

98. Aa. S. Sudbo, P. A. Schulz, E. R. Grant, Y. R. Shen, and Y. T. Lee, J. Chem. Phys. 68, 1306 (1978).

99. W. Braun and W. Tsang, Chem. Phys. Lett. 44, 354 (1976).

100. D. H. R. Barton, J. Chem. Soc. 148 (1949).

101. T. Teramoto, M. Kitabatake, and T. Onouchi, J. Chem. Soc. Japan, Ind. Chem. Sec. 67, 460 (196

102. W. Kauzmann, Kinetic Theory of Gases (Benjamin, New York, 1966).

103. F. T. Wall, Chemical Thermodynamics (Freeman, San Francisco, 1974).

104. F. M. Lussier, J. I. Steinfeld, and T. F. Deutsch, Chem. Phys. Lett. 58, 277 (1978).

105. N. V. Chekalin, V. S. Dolzhikov, V. S. Letokhov, V. N. Lokhman, and A. W. Shibonov, Appl. Phys. 12, 191 (1977).

106. L. D. Hanton and G. P. Semeluk, Can. J. Chem. 44, 2143 (1962); P. M. Jeffers, J. Phys. Chem. 76, 2829 (1972).

107. J. D. Lambert, Vibrational and Rotational Relaxation in Gases (Oxford University Press, 1977), Chapter 3.

108. W. Kauzmann, Thermodynamics and Statistics: With Applications to Gases (Benjamin, New York, 1967).

109. D. H. R. Barton and P. F. Onyon, J. Am. Chem. Soc. 72, 988 (1950).

110. A. Maccoll, Chem. Rev. 69, 33 (1969).

111. E. S. Swinbourne, in Decomposition and Isomerization of Organic Compounds, edited by C. H. Bamford and C. F. H. Tipper (Elsevier, New York, 1972), Chapter 2; and references therein.

112. V. N. Kondratiev, Rate Constants for Gas Phase Reactions Reference Book, translated by L. J. Holtschlag and edited by R. M. Fristrom (National Bureau of Standard, Washington, D.C., 1972).

113. K. W. Egger and A. T. Cocks, in The Chemistry of The Carbon-Halogen Bond, Part 2, edited by S. Patai (Wiley, New York, 1973).

114. C. Cillien, P. Goldfinger, G. Huybrechts, and G. Martens, Trans. Faraday Soc. 63, 1631 (1967).

115. C. Cheng and P. Keehn, J. Am. Chem. Soc. 99, 5808 (1977); D. Garcia and P. Keehn, J. Am. Chem. Soc. 100, 6111 (1978).

116. Ref. 50, p.167.

117. T. Y. Wu, Vibrational Spectra and Structure of Polyatomic Molecules (Edwards, Ann Arbor, Mich., 1946) p.356; J. C. Evans and H. J. Bernstein, Canadian J. Chem. 33, 1746 (1955).